UNIVERSITY OF CALIFORNIA

Santa Barbara

Anthropogenic disturbances in the marine environment: effects on microbial physiology and community structure

Dissertation submitted in partial satisfaction of the requirements

for the degree Doctor of Philosophy in Marine Science

by

Tanika Ladd

Marine Science

Committee:

Prof. M. Débora Iglesias-Rodríguez, Chair

Prof. Mark Brzezinski

Dr. Uta Passow, Researcher

December 2021

The dissertation by Tanika Marie Ladd is approved.

_____

Mark Brzezinski

_____

Uta Passow

_____

M. Débora Iglesias-Rodríguez, Committee Chair

September 2021

AKNOWLEDGEMENTS

This dissertation and the completion of my PhD would not have been possible without the support from many people that I have had the privilege to work with and build friendships with throughout my time at UCSB. I greatly appreciate my advisor, Debora Iglesias-Rodriguez, for her constant support, long discussions about science, and for always pushing me to become a better scientist. I am very fortunate to have had an amazing mentor to look up to. I thank my committee members Uta Passow and Mark Brzezinski for their advice, guidance, time, and contribution to the work presented in this dissertation and for always being available and supportive. I appreciate the mentorship and friendship of Helene Gardner who has made me a better teacher. I am immensely grateful for the Interdepartmental Graduate Program in Marine Science (IGPMS) and all of the faculty, students, and staff that have made UCSB a wonderful place to learn, work, and call home for the past several (more than several, really…) years. I also thank my collaborators and co-authors at NOAA and other universities for making it possible to do awesome research.

I lovingly thank my family and friends. My husband, Danny Goertz, deserves much of the credit for my PhD because he has continuously encouraged, supported, and loved me throughout this journey while he has listened to me blab about science, teaching, and all the struggles that come with doing a PhD. My parents Carol and Mike Ladd, my sister Taylor Ladd, my in-laws Sonia and Brian Goertz and all the Goertz brothers and wives, my grandparents, aunts, uncles, and cousins have provided endless love and support. The wonderful friends I have maintained during my PhD and gained throughout this time have made this all possible and without them I would never have made it this far. I thank Nick Baetge, Mike Maniscalco, Logan Kozal, Dylan Catlett, and Ellen McNicoll for always being

there for me and making life fun. I want to thank all the current and past members of the Iglesias-Rodriguez lab that I have been fortunate enough to get to know on this journey. I have particularly appreciated the advice, collaborations, and friendships I have gained from Paul Matson, Ellie Halewood, Jessica Bullington, Sylvia Kim, and Zoe Welch. I am also thankful for the amazing friends I have met while playing softball on the SB Biohazards and C&S auto teams.

Lastly, I am extremely appreciative of the financial support I have received during my time at UCSB. I thank the UCSB Coastal Fund, UCSB Graduate Division, North Pacific Research Board, National Science Foundation, Simons Foundation, and SBC-LTER for making the work presented in this dissertation possible.

VITA OF TANIKA MARIE LADD

September 2021

EDUCATION

Ph.D. Candidate, Marine Science, University of California, Santa Barbara, Advisor: Débora Iglesias-Rodríguez, October 2014 – Present (expected December 2021)

Bachelor of Science, Mathematics *Magna Cum Laude*, Minors: **Chemistry**, **Environmental Science**, and **Physics**, Western Washington University, 2010 – 2014

College of Arts & Sciences, University of Colorado, Boulder, 2009 - 2010

PROFESSIONAL EMPLOYMENT

Teaching Assistant, University of California, Santa Barbara, 2015 – 2021
Courses: **Introductory Biology Laboratory** (2015, 2019, 2020 – Head TA), **Environmental Processes in Ocean and Lakes** (2015, 2017, 2018), **Environmental Chemistry** (2020, 2021)

Graduate Student Researcher, Mentor: Debora Iglesias-Rodriguez, University of California, Santa Barbara, 2014 – 2020

Course Lecturer, Ecology, Evolution, and Marine Biology Department, University of California, Santa Barbara, Spring quarter 2019

PUBLICATIONS

(Submitted) **Ladd, T.M.,** Catlett, D. Maniscalco, M., Kim, S.K., Kelly, R.L., John, S.G., Carlson, C.A., and Iglesias-Rodriguez, M.D., Wildfire ash deposition fertilizes coastal marine ecosystems.

Matson, P.G., Washburn, L., Fields, E.A., Gotschalk, C., **Ladd, T.M.**, Siegel, D.A., Welch, Z.S., and Iglesias-Rodriguez, M.D. (2019) Formation, development, and propagation of a rare coastal coccolithophore bloom. Journal of Geophysical Research: Oceans, 124, 3298-3316

Ladd, T.M., Bullington, J., Matson, P.G., Kudela, R.M., Iglesias-Rodriguez, M.D. (2018) Exposure to oil from the 2015 Refugio spill alters the physiology of a common coastal harmful algal bloom species, *Pseudo-nitzschia australis*, and the ubiquitous coccolithophore, *Emiliania huxleyi*. Marine Ecology Progress Series 603: 61-78

Matson, P.G., **Ladd, T.M.,** Halewood, E.R., Sangodkar, R.P., Chmelka, B.F. and Iglesias-Rodriguez, M.D. (2016) Intraspecific differences in biogeochemical responses to thermal change in the coccolithophore *Emiliania huxleyi*. PLoS ONE 11(9): e0162313

GRANTS

UCSB Coastal Fund Grant ($13,798.36) – *The effects of Thomas Fire ash on Santa Barbara Channel Phytoplankton communities*, 2019

UCSB Coastal Fund Grant ($9,474.64) – *The Effects of the Refugio Oil Spill on Phytoplankton in the Santa Barbara Channel*, 2016

HONORS & AWARDS

ASLO Ocean Sciences Meeting 2020 Registration Grant, 2020
UCSB Graduate Division Dissertation Fellowship, 2019
North Pacific Research Board - Graduate Student Research Award, 2017-2018
Best Oral Presentation, PICES-2016, 2016
Worster Research Mentorship Award, 2016
Honorable mention, NSF Graduate Research Fellowship Program, 2015
NOAA Hollings Scholarship, 2012 - 2014
Western Washington University Dean's List, 2010 – 2014
University of Colorado Dean's List, 2009 – 2010

PRESENTATIONS

Wildfire ash promotes growth of Santa Barbara Channel phytoplankton communities under low nutrient conditions, Ocean Sciences Meeting, San Diego, CA, 2020

Coccolithophore populations in the Eastern Bering Sea (poster presentation), Alaska Marine Science Symposium, Anchorage, AK, 2019

Coccolithophore populations in the Eastern Bering Sea, Ocean Sciences Meeting, Portland, OR, 2018

Physiological responses of marine phytoplankton to oil exposure in the context of the 2015 oil spill in the Santa Barbara Channel, PICES-2016, San Diego, CA, 2016

The Ocean's Chalk Factory - How Microscopic Plants Control the Earth's Carbon Cycle, University of California, Santa Barbara - Grad Slam Competition, 2015

Modeling the Dynamics of Zooplankton pH Exposure in Puget Sound, Hollings Program Science and Education Symposium, NOAA Headquarters, Silver Spring, MD, 2013

ABSTRACT

Anthropogenic disturbances in the marine environment: effects on microbial physiology and community structure

By

Tanika M. Ladd

This dissertation uses multiple case studies to examine the role of environmental disturbances and human activity on microbial physiology and community composition. In ecological theory, environmental disturbances, which govern species succession, adaptation, and evolution and can shift ecosystem function, are critical components of ecosystems. George Hutchinson postulated the so-called “paradox of the plankton” in which the highly diverse plankton communities present in marine and freshwater systems seemed inconceivable due to the relatively homogenous aquatic environment. The unfathomable spatial and temporal scales of marine microbes in their environments help explain this diversity and the role of relatively small-scale disturbances and gradients in marine ecosystems but it also makes it difficult to understand how a variety of large-scale human induced perturbations may shift the overall composition and function of ecosystems. In the modern world, understanding and being able to predict or anticipate how our actions will influence the inherent nature and diversity of the environment as well as how ecosystem services will be altered is extremely important for the survival of the human species and a sustainable future for the Earth. This far-reaching and broad topic is of considerable focus in

the research community and is being addressed at both large and small spatiotemporal scales. In this dissertation, I explore three distinct cases in which environmental disturbance and anthropogenic impacts influence marine microbes. (1) The first case study explores the impacts of an oil spill in the marine environment on phytoplankton physiology. Through laboratory experimentation on representatives of two important phytoplankton groups, the coccolithophore, *Emiliania huxleyi*, and the diatom, *Pseudo-nitzschia australis*, results showed that oil exposure negatively impacted the growth of these species though *E. huxleyi* appeared to be more tolerant of oil exposure than *P. australis*. Additionally, exposure to oil increased cellular transparent exopolymer particle (TEP) production by both species, while the toxin production of *P. australis* cells increased and the formation of calcium carbonate liths by *E. huxleyi* appeared abnormal. (2) The second chapter investigates a novel connection between land and ocean through wildfire ash deposition in the marine environment and the effects on marine protist communities. Experimentation on natural microbial communities and the use of 18S rRNA sequencing and chemical analyses revealed significant enrichment of nutrients due to leaching of wildfire ash in seawater that promoted the growth of microbes. The variety of nutrients appeared to simultaneously enhance the growth of a diverse microbial assemblage rather than selecting for distinct groups. (3) Lastly, the third chapter focuses on microbial community dynamics in a rapidly changing and culturally and economically important sub-Arctic ecosystem. During two years with distinct sea ice influences in the eastern Bering Sea (EBS), physical and chemical conditions and protist communities were drastically different with the warmer, low sea ice year associated with a large fraction of putative parasites while the relatively cooler, average sea ice year was associated with a larger proportion of phytoplankton to non-phytoplankton protists. These

results suggest that as the climate continues to warm and alter the EBS ecosystem, protist communities should be considered as they are likely major drivers of ecosystem function with significant impacts on higher trophic levels.

TABLE OF CONTENTS

Introduction and dissertation summary

The overarching goal of this dissertation is to gain a better understanding of the role of environmental disturbances in altering microbial physiology and community structure. In 1961, George Hutchinson postulated the "paradox of the plankton" in which the diversity of planktonic communities posed the problem of "how it is possible for a number of species to coexist in a relatively isotrophic or unstructured environment all competing for the same sorts of materials" (Hutchinson 1961). This coexistence has since been well studied and multiple mechanisms have been proposed to explain the high biodiversity and lack of competitive exclusion including but not limited to environmental fluctuation, niche diversification, and coevolution (e.g., Wilson 2011). Environmental disturbances both abrupt and short-lived (e.g., pollution events and natural disasters) or gradual and long-lived (e.g., climate change, resource extraction, and development) help maintain coexistence by continually varying the conditions in which organisms must survive and thrive. However, due to this biodiversity and the complex interactions among organisms, it is often difficult to predict or fully understand how communities and the functionality of ecosystems will respond to any given disturbance.

Marine protists, or single-celled eukaryotic plankton, are extraordinarily diverse and ubiquitous microbes that are critical components of marine food webs and biogeochemical cycles. Protists may be autotrophic and/or heterotrophic, with cell sizes that span several orders of magnitude. Oceanic primary production, producing roughly half of the global oxygen, is largely carried out by photoautotrophic protists in addition to photosynthetic bacteria and therefore these communities support the base of marine food webs. Additionally, heterotrophic protists that consume other organisms to meet nutritional requirements provide

a vital trophic link between small protists and bacteria to higher trophic levels. Globally, microzooplankton, most of which are protists, consume about 49% to 77% of the primary production depending on region (Schmoker et al. 2013). Further, the variety of nutritional modes including mixotrophy or the flexibility to alter nutritional strategy, various types of symbioses (including parasitism, commensalism, and mutualism), osmotrophy (assimilation of dissolved organic matter), and saprotrophy (external digestion of organic matter) complicate classical food web dynamics and highlights the complex network of interactions microbes experience in the natural world. The composition and behavior of marine protists not only structures marine food webs but determines how carbon and other elements flow through marine systems. For instance, the efficiency of the biological carbon pump, which controls the transport and storage of carbon in the ocean and hence Earth's climate, is impacted by processes such as the sinking rate of particulate organic matter, production of dissolved organic matter, and the consumption and remineralization of organic material at different ocean depths all of which are altered as protist communities shift.

The recent widespread application of genomic techniques has uncovered an incredibly diverse and complex microbial world across the vast marine environment, but there is still much to learn about novel, uncultured organisms, interactions among microbes, and abiotic and biotic factors influencing community structure and function. A significant body of research is focused on modeling and quantifying the impacts of climate change or other anthropogenic disturbances on marine ecosystems (e.g., Le Quéré et al. 2005, Ainsworth et al. 2011, Rose & Allen 2013, Nabe-Nielsen et al. 2018). However, recent progress in the understanding of protist diversity and ecological flexibility from the rapid advances in bioinformatic and statistical approaches complicates modeling methods (Stec et

al. 2017). For example, it has become clear that the traditional view of separate phytoplankton and zooplankton functional groups is not a realistic depiction of protist physiology and including mixotrophy in modeling of marine food webs better depicted trophic community structure and elemental stoichiometry (Ward & Follows 2016). Additionally, biotic interactions among microbes appear to be extremely important for structuring communities with abiotic factors only able to explain a relatively small amount of the variation in community composition (Lima-Mendez et al. 2015), suggesting that these processes should be included in food web and biogeochemical models. The ability to better observe and analyze complex microbial communities, including protists, has shown that it is imperative to continue to use these methods to increase knowledge of this diverse assemblage of organisms and explore important processes controlling food web dynamics and global biogeochemical cycles.

Disturbances in the marine environment are known to alter community composition, organismal physiology, and the biotic interactions within communities with implications for the functionality of ecosystems. Marine ecosystems provide vital resources for humans through their provisioning (e.g., fisheries), regulating (e.g., carbon sequestration), supporting (e.g., critical habitat and genetic diversity), and cultural services (e.g., tourism and recreation) (MEA 2005). However, with the enormous global human population and the resulting stress applied to the marine environment, it is imperative to better understand anthropogenic influences on ecosystems so that management of our important oceanic resources and services will have a sustainable future. In this dissertation, I use multiple case-studies to elucidate microbial responses to anthropogenic disturbances and the resulting consequences for marine ecosystems. This work uses a combination of physiological,

molecular and oceanographic approaches through lab and field sampling and experimentation to explore each case in depth.

Chapter 1. Exposure to oil from the 2015 Refugio spill alters the physiology of a common coastal harmful algal bloom species, *Pseudo-nitzschia australis*, and the ubiquitous coccolithophore, *Emiliania huxleyi* (Manuscript, published in Marine Ecology Progress Series)

Chapter 2. Wildfire ash deposition fertilizes coastal marine ecosystems

Chapter 3. Fall protist communities reveal high variability between recent years with differential sea ice influence in the eastern Bering Sea

Literature cited:

Ainsworth CH, Samhouri JF, Busch DS, Cheung WWL, Dunne J, Okey TA (2011) Potential impacts of climate change on Northeast Pacific marine foodwebs and fisheries. ICES J Mar Sci 68:1217–1229

Hutchinson GE (1961) The Paradox of the Plankton. Am Nat 95:137–145

Lima-Mendez G, Faust K, Henry N, Decelle J, Colin S, Carcillo F, Chaffron S, Ignacio-espinosa JC, Roux S, Vincent F, Bittner L (2015) Determinants of community structure in the grobal plankton interactome. Ocean Plankt 348:1262073

Millennium Ecosystem Assessment (MEA) (2005) Ecosystems and human wellbeing: Wetlands and water synthesis. World Resources Institute, Washington, DC

Nabe-Nielsen J, van Beest FM, Grimm V, Sibly RM, Teilmann J, Thompson PM (2018) Predicting the impacts of anthropogenic disturbances on marine populations. Conserv Lett 11:e12563

Le Quéré C, Harrison SP, Prentice IC, Buitenhuis ET, Aumont O, Bopp L, Claustre H, Da Cunha LC, Geider RJ, Giraud X, Klaas C, Kohfeld KE, Legendre L, Manizza M, Platt T, Rivkin RB, Sathyendranath S, Uitz J, Watson AJ, Wolf-Gladrow D (2005) Ecosystem dynamics based on plankton functional types for global ocean biogeochemistry models. Glob Chang Biol 11:2016–2040

Rose KA, Allen JI (2013) Modeling marine ecosystem responses to global climate change: Where are we now and where should we be going? Ecol Modell 264:1–6

Schmoker C, Hernández-León S, Calbet A (2013) Microzooplankton grazing in the oceans: Impacts, data variability, knowledge gaps and future directions. J Plankton Res 35:691–706

Stec KF, Caputi L, Buttigieg PL, D'Alelio D, Ibarbalz FM, Sullivan MB, Chaffron S, Bowler C, Ribera d'Alcalà M, Iudicone D (2017) Modelling plankton ecosystems in the meta-omics era. Are we ready? Mar Genomics 32:1–17

Ward BA, Follows MJ (2016) Marine mixotrophy increases trophic transfer efficiency, mean organism size, and vertical carbon flux. PNAS 113:2958–2963

Wilson JB (2011) The twelve theories of co-existence in plant communities: The doubtful, the important and the unexplored. J Veg Sci 22:184–195

Chapter 1

Exposure to oil from the 2015 Refugio spill affects phytoplankton physiology and increases the toxin content of a common coastal harmful algal bloom species

Tanika M Ladd[1], Jessica A Bullington[1], Paul G Matson[1], Raphael M Kudela[2], and M Débora Iglesias-Rodríguez[1]

[1]Marine Science Institute and Department of Ecology, Evolution, and Marine Biology, University of California, Santa Barbara, CA 93106

[2]Ocean Sciences Department, University of California, Santa Cruz, CA 95064

This chapter is an adapted re-publication of the Marine Ecology Progress Series Article with the citation as seen below.

Citation: Ladd TM, Bullington JA, Matson PG, Kudela RM, Iglesias-Rodríguez MD (2018) Exposure to oil from the 2015 Refugio spill alters the physiology of a common harmful algal bloom species, *Pseudo-nitzschia australis*, and the ubiquitous coccolithophore, *Emiliania huxleyi*. Mar Ecol Prog Ser 603:61-78. https://doi.org/10.3354/meps12710

1.1 Abstract

Short term oil exposure impacts on the harmful algal bloom (HAB) species, *Pseudo-nitzschia australis*, and the coccolithophore species, *Emiliania huxleyi*, were studied by investigating physiological responses in growth, production of transparent exopolymer

particles (TEP), *P. australis* domoic acid (DA) content, and *E. huxleyi* calcification with the goal of better understanding the potential effects of the 2015 Refugio oil spill in the Santa Barbara Channel (SBC). While oil exposure negatively impacted growth of both species, *P. australis* appeared to be more sensitive to oil exposure compared to *E. huxleyi*. Increased cellular TEP (both species) and DA (*P. australis*), and abnormal calcification (*E. huxleyi*) were observed in the presence of oil. The physiological changes detected in these locally important phytoplankton species have implications for other ecosystem processes, human health, and the fate of the spilled oil. The results from this study enhance our understanding of the repercussions of oil pollution events while further research is necessary to explore ecosystem-wide impacts and chronic or long-term effects of oil.

1.2 Introduction

The annual release of oil from all sources worldwide into the marine environment has been estimated to exceed one million tonnes (NRC 2003). Major oil spills are not the most significant source of oil into the ocean; natural seeps and other chronic sources (e.g., land runoff) are more significant due to the long timescales of input, but large spills can have more dramatic impacts due to highly localized and concentrated pollution (NRC 2003). After oil spill events, much of the ecosystem assessment focuses on marine mammals, birds, and other locally important macrofauna because of the observable impacts such as strandings and deaths of oil-coated organisms. However, although phytoplankton are at the base of the marine food web and key to ocean biogeochemical processes, they are relatively understudied in the context of oil pollution. In the limited but growing number of studies on the effects of oil exposure on individual phytoplankton species or natural phytoplankton

assemblages, enormous variability in physiological responses has been demonstrated. Generally, growth and primary production appear to decrease or be inhibited during oil exposure (e.g., Østgaard et al. 1984, González et al. 2009, Brussaard et al. 2016), but some studies have found that at low oil concentrations, growth or primary production can remain unchanged (e.g., Batten et al. 1998, González et al. 2013, Li et al. 2017) or even increase (e.g., Parsons et al. 1976, Vargo et al. 1982, Hu et al. 2011). Both individual and community-level studies have shown that species-specific phytoplankton sensitivity to crude oil and oil exposure can result in a change in the community composition (González et al. 2009, Ozhan et al. 2014a, Ozhan et al. 2014b). However, there is no apparent general trend in how oil exposure affects the structure of phytoplankton communities as many factors operate simultaneously, including the initial community structure (González et al. 2009, Huang et al. 2011), oil concentration and type (Hsiao et al. 1978), nutrient concentrations (Ozhan & Bargu 2014b), and water temperature (Huang et al. 2011).

On May 19th, 2015, an underground pipeline near Refugio State Beach, about 20 miles west of Santa Barbara, CA, leaked between 101,000 to 140,000 gallons of oil with approximately 21,000 gallons entering the ocean (http://www.refugioresponse.com/go/doc/7258/2588430/). Although not a large spill compared to others in the marine environment, this event was the largest accidental release of crude oil into the Santa Barbara Channel (SBC) since the historic 1969 oil well blowout. The release, and subsequent flow of oil from the land to the ocean and the timing of the spill also make the 2015 event unique in the context of marine spills. Notably, the spill occurred at a time of high phytoplankton primary productivity in the SBC and the dominance of the toxic coastal pennate diatom *Pseudo-nitzschia* spp.

(http://www.sccoos.org/data/habs/history.php?location=Stearns%20Wharf). This diatom genus is known for its production of domoic acid (DA), a neurotoxin transferred through the marine food web that causes sickness or death in marine mammals, birds, and humans (Lefebvre et al. 2002). The species *Pseudo-nitzschia australis*, one of the most prolific DA producers and the main perpetrator of the extensive 2015 blooms along the entire North American west coast (McCabe et al. 2016), typically blooms in warm water off the central and southern California coast (e.g., Fritz et al. 1992, Schnetzer et al. 2006, Sekula-Wood et al. 2011) and has been documented to form massive blooms with high DA production in the SBC (Anderson et al. 2006). The production of DA by *Pseudo-nitzschia* spp. varies dramatically, and even strains of the same species can produce different amounts of DA depending on environmental conditions (e.g., Maldondo et al. 2002, Kudela et al. 2008, Thorel et al. 2014). This makes predictions of toxic events difficult, therefore necessitating DA monitoring and the shutting down of local fisheries when required. Weeks after the oil spill, in early June, an unprecedented coccolithophore bloom, mainly composed of the species, *Emiliania huxleyi*, was observed in the SBC (P. Matson unpubl. data). This species is the most abundant and widespread calcareous phytoplanktonic organism in the world's oceans where it commonly forms extensive blooms in high latitudes (Westbroek et al. 1989, Tyrell & Merico 2004). In the SBC, *E. huxleyi* is present year-round and is considered endemic (Grelaud et al. 2009), but with the exception of the 2015 event (Matson et al. 2019), populations in the SBC do not appear to form blooms.

The aim of this study was to explore how a large and abrupt input of oil into a productive coastal marine ecosystem can impact phytoplankton physiology and morphology, including growth, DA cellular content, and calcium carbonate ($CaCO_3$) production. A limited

number of studies have explored the effect of oil pollution on phytoplankton communities that include *Pseudo-nitzschia* or coccolithophores (e.g., Ignatiades & Mimicos 1977, Ozhan and Bargu 2014b) as well as individual toxic phytoplankton taxa (not including any DA-producer) (e.g., Ozhan & Bargu 2014a) but this is the first study to test the effect of oil exposure on the physiology of either *E. huxleyi* or *P. australis*, or any representative of either coccolithophores or *Pseudo-nitzschia* spp. individually. Additionally, this is the first study to explore oil impacts on phytoplankton in regards to the SBC, a location with significant offshore oil production, natural hydrocarbon seeps, and a highly productive coastal ecosystem. We used two species representing the functionally distinct phytoplankton groups dominating the SBC phytoplankton community at the time of the spill. We discuss the implications of this study on phytoplankton succession, harmful algal bloom dynamics, and the fate of the spilled oil.

1.3 Materials and methods

1.3.1 Water accommodated fraction preparation and analysis

The oil used for the experiments included crude oil from offshore Platform Holly (34.389º N, 119.906º W) collected in 2012 (0.915 g mL^{-1}, calculated API = 23º) and crude oil from the Plains All American Line 901 collected during the oil spill in May 2015 (0.946 g mL^{-1}, calculated API = 18º [Passow et al. 2017]). Although the focus of this study was to test oil originating from the Refugio oil spill, the Refugio spill oil was not available until more than 6 months after the spill occurred. Therefore, we used Platform Holly oil to conduct initial tests and to provide comparisons to other oil present in SBC waters. The Platform Holly oil used was similar to the spilled oil (a fraction of the spilled oil originated from

Platform Holly) and the use of this crude oil gives this study a broader context and insight into whether the Refugio oil had any unique impacts on physiology that may not have been measured directly (such as additives in the oil to improve transportation performance within the pipelines). The water accommodated fraction (WAF) of crude oil was prepared for each experiment separately according to the protocol outlined by Aurand and Coelho (2005). Briefly, 6-7 L of prepared culture medium were poured into ~8L borosilicate glass bottles leaving approximately 20-25% headspace. Crude oil (~2-5 g L^{-1}) was added using a syringe, the bottle was covered to prevent light exposure and the mixture was stirred at 200 rpm for 24 hours at 16 ± 1 °C. Immediately after removing from the stir plate, the WAF was drained from a spigot at the bottom of the bottle and aliquoted into 1 L culture vessels either undiluted or diluted with fresh uncontaminated medium (50% WAF, 50% medium) to a final volume of 800 mL. Samples for initial oil chemistry were taken directly from the WAF bottle before aliquoting into the culture vessels and stored in 1 L amber glass bottles at 4°C for analysis of total petroleum hydrocarbon (TPH) (C9 – C44) (U.S. EPA Method 8015D (SW-846), 2003), polycyclic aromatic hydrocarbon (PAH) (U.S. EPA Method 8270D (SW-846), 2014), and saturated hydrocarbon (SH) (U.S. EPA Method 8015D (SW-846), 2003) analyses by gas chromatography with flame ionization detection (GC-FID) and gas chromatography mass spectrometry (GC/MS) (Alpha Analytical, Inc., Mansfield, MA).

1.3.2 Culture conditions

To explore the effects of oil exposure on the dominant phytoplankton present around the time of the Refugio oil spill, four separate batch culture experiments were conducted with two strains of *Pseudo-nitzschia australis*, one strain of *Emiliania huxleyi*, and two different oil sources. The two strains of *P. australis* were isolated in March 2015 from Monterey

wharf (HAB 207) and Santa Cruz wharf (HAB 197) while the *E. huxleyi* strain (150604 A9) was isolated in June 2015 from the SBC. Multiple *P. australis* strains were used due to the loss of strain HAB 207 in culture after experiment 3 was conducted, which allowed for comparisons between strains with inherently different cellular DA content. Experiments are described as follows: 1) *E. huxleyi* only, exposed to 1.105 and 2.21 mg L^{-1} TPH from Platform Holly oil; 2) *E. huxleyi* only, exposed to 0.72 and 1.44 mg L^{-1} TPH from the Refugio pipeline spill; 3) *P. australis* (HAB 207) only, exposed to 1.39 and 2.78 mg L^{-1} TPH from the Refugio pipeline spill; and 4) *E. huxleyi* and *P. australis* (HAB 197) using the same WAF, exposed to 1.185 mg L^{-1} TPH from the Refugio pipeline spill (Table 1). The goal of experiment 4 was to compare the response of the two species tested under the same WAF (and nutrient) concentrations but due to sampling time, culture volume, and space limitation, intensive sampling was staggered by one day between *E. huxleyi* and *P. australis* (*P. australis* cultures were monitored for one day longer than *E. huxleyi*) and only one concentration of WAF was tested. Clonal batch cultures were inoculated from exponentially growing cultures and maintained in modified f medium (supplemented with 100 µM nitrate, 6.24 µM phosphate, and f/2 concentrations of trace metals and vitamins [e.g., Langer et al. 2006, Iglesias-Rodriguez et al. 2008]) for *E. huxleyi* only experiments (1,2) or f/2 supplemented medium (Guillard & Ryther 1962) for the *P. australis* only experiment (3) and the *P. australis* and *E. huxleyi* experiment using the same WAF (4) prepared with filter-sterilized (0.22 µm Steritop filtration units – EMD Millipore, USA) SBC seawater (Andersen et al. 2005). The modified f medium was used because *E. huxleyi* has a relatively low nutrient requirement and high phosphate concentrations have been shown to impact calcification (e.g., Paasche 1998). Silicate was not added or measured in experiments 1 or 2.

Cultures were maintained at 16 ± 1 ºC under a 12:12 h light:dark cycle at ~120 µmol photons m^{-2} s^{-1} (EnviroGro T5 Hydrofarm, USA). Experimental parameters were monitored in triplicate cultures of each treatment for 4 or 5 days to test short term exposure in early exponential phase growth (to avoid additional stressors due to nutrient, light, or carbon limitation).

1.3.3 Cell density, growth rates, and nutrient utilization

Cell densities of each culture were determined every day of the experiments (except on day 1 for *P. australis* in experiment 4) by light microscopy using a Sedgewick-Rafter counting chamber. Growth rates (µ, d^{-1}) for each replicate culture were determined by calculation of the slope of a linear fit of the natural log of cell density (cells mL^{-1}) versus day of the experiment. Time points that were not linear (suggesting a lag phase or approaching stationary phase) were removed from the fit and not used to calculate experiment-wide growth rates. Nutrient concentrations (nitrate + nitrite, phosphate, ammonium, and silicate [not measured in experiments 1 or 2]) were monitored throughout the experiments by sampling ~20 mL from each culture, filtering through 0.45 µm syringe filters, and storing at -20°C until flow injection analysis (QuikChem 8000, Zellweger Analytics). This work was conducted at the UCSB Marine Science Institute Analytical Laboratory.

1.3.4 Dissolved and cellular domoic acid content

Dissolved DA (dDA) samples were collected daily by filtering 2 mL aliquots through 0.45 µm syringe filters into cryovials, immediately flash frozen in liquid nitrogen, and stored at -80 ºC until analysis. Particulate DA (pDA) samples were taken at three time points (initial, middle, and final) throughout the experiment by filtering 50-100 mL aliquots onto 25 mm glass fiber filters (EMD-Millipore), collecting the filters in 2 mL cryovials, flash

freezing in liquid nitrogen, and storing at -80 ºC until analysis. Both dDA and pDA samples were analyzed in the Kudela lab at the University of California, Santa Cruz using well established methods. Briefly, DA analysis was conducted using an Agilent 6130 LC-MS system with an Agilent Zorbax Rapid Resolution column using an 8-point dilution series of CRM DA-f DA standards (National Research Council Canada) for calibration. Sample preparation followed Wang et al. (2007). The LC-MS was operated with a gradient elution of acidified water (0.1% formic acid) and acidified acetonitrile (0.1% formic acid). DA was identified by the presence of a 312 amu peak in positive Scanning Ion Mode (SIM) with concentration determined by signal integration of the peak area and back-calculations based on the standard curve. Cellular DA, expressed in pg DA $cell^{-1}$, was determined by normalizing pDA to *P. australis* cell abundance.

1.3.5 Transparent exopolymer particle analysis

Duplicate or triplicate 20 mL aliquots were sampled for transparent exopolymer particle (TEP) analysis. Samples were filtered through 0.4 µm polycarbonate filters (Isopore, EMD Millipore) under gentle vacuum, stained with 0.5 mL of pre-calibrated Alcian Blue dye, and stored in 15 mL tubes at -20 ºC until analysis. Samples were analyzed colorimetrically as described by Passow and Alldredge, 1995. Briefly, 5 mL of 80% sulfuric acid were added to the tubes containing the filter and allowed to sit for longer than 2 hours with occasional gentle mixing. Samples were then transferred into cuvettes and the absorbance at 787 nm was measured on a Genesys 10S Vis spectrophotometer. Absorbance values were converted to Gum Xanthan equivalents (determined by calibration with the Alcian Blue dye) and expressed as Gum Xanthan equivalents $cell^{-1}$ (GXeq $cell^{-1}$) after normalization by *E. huxleyi* or *P. australis* cell abundance.

1.3.6 Coccolith morphology and cellular $CaCO_3$

Scanning electron microscopy (SEM) was used to observe coccolith morphology. SEM samples were collected at the beginning and the end of each experiment by filtering 3-7 mL of culture onto a 13 mm 0.4 µm polycarbonate filter (Isopore, EMD-Millipore) and allowing filters to dry overnight at room temperature. Each filter was mounted on an aluminum stub and sputter-coated with gold prior to being observed with a Zeiss EVO 40 XVP scanning electron microscope at the Santa Barbara Museum of Natural History (CA, USA). For each replicate filter, a minimum of 50 coccospheres (cells with surrounding coccoliths) were imaged for analysis of coccolith morphology. Coccospheres were counted and recorded as either normal (containing ≤ 1 incomplete or malformed coccolith [e.g., Langer et al. 2011]) or abnormal (containing > 1 incomplete or malformed coccoliths [e.g., Langer et al. 2011]).

Samples for cellular $CaCO_3$ were collected and processed following Iglesias-Rodriguez et al. (2008). Briefly, 100 mL aliquots were filtered through 47 mm 0.2 µm polycarbonate filters (Isopore, EMD-Millipore), rinsed with a dilute ammonium hydroxide solution (pH ~9), and stored at -20 ºC before further processing. Approximately 50 mL of 0.1 M HNO_3 were added to the frozen filters and left for 24 hours at room temperature to dissolve the $CaCO_3$ on the filter. The solution was then filtered through 0.45 µm syringe filters and analyzed for Ca^{2+} and Na^{2+} concentrations on a Perkin- Elmer Optima 7300DV inductively coupled plasma – optical emission spectrometer (ICP-OES) at the University of California, Riverside Environmental Sciences Research Laboratory. Sodium concentrations were used to correct for seawater contamination. Cellular $CaCO_3$ was determined by normalizing $CaCO_3$ concentration to *E. huxleyi* cell abundance.

1.3.7 Flow cytometry analysis

Aliquots of 9 mL were preserved with a buffered formaldehyde/glutaraldehyde solution (1% formaldehyde, 0.05% glutaraldehyde final concentration) and stored at -20 ºC until processing on a BD Influx Flow Cytometer (BD Biosciences) in the Iglesias-Rodriguez lab at the University of California, Santa Barbara. Identification of *E. huxleyi* cells and detached coccoliths (non-living calcified particles) were identified using chlorophyll fluorescence (cells only), polarization-sensitive detectors, and forward scatter signals (as in von Dassow et al. 2012). The ratio of detached coccoliths to cells was calculated for each culture replicate. Coccosphere and cell sizes were estimated by concurrently running size standard beads (Sphero^{TM} particle size standard kit; Spherotech) and quality control beads (Ultra Rainbow Beads; Spherotech) with acidified (addition of dilute HCl) and unacidified samples. Cell volume estimates assumed cells were spherical in shape and biovolumes were calculated by multiplying *E. huxleyi* cell volume by the culture cell density.

1.3.8 Bacterial abundance

Bacterial cell densities were measured through epifluorescence microscopy each day throughout the four experiments. Briefly, aliquots of 9 mL were preserved with formalin and stored at 4 ºC for less than 48 hours, then filtered onto Irgalan Black stained 47 mm 0.2 µm polycarbonate filters (Isopore, EMD-Millipore). Addition of 0.5 mL of the nucleic acid stain, DAPI (4, 6-Diamidino-2-Phenylindole, Dihydrochloride) (5 µg mL^{-1} solution) to each filter followed and was allowed to sit for 3 minutes before filtering the remaining volume. Filters were subsequently mounted onto microscope slides with immersion oil and stored in the dark at -20 ºC before counting cells with epifluorescence microscopy.

1.3.9 Statistical analyses

Several statistical tests were used to examine both within experiment responses and across experiment responses to oil exposure. Analyses were performed using R software (version 3.4.2) and JMP Pro 12 software. Data were initially examined for homogeneity of variances and normality of residuals to determine if parametric or non-parametric tests were necessary. If the assumptions of a parametric test were met, one-way ANOVAs, repeated measures ANOVAs, linear regression analyses, or logistic regression analyses were implemented to examine differences between treatments at each time point measured. As necessary, the false discovery rate (FDR) post hoc test (best compromise between type I and type II errors) was used to identify significant differences (reported as *q* values [FDR adjusted *p* values]) between each treatment. To compare trends across experiments, measurements of physiological parameters were normalized through division by the mean of the control replicates at each time point in each experiment and then averaged across all time points sampled. Normalized values were grouped by control or oil treatments and compared using nonparametric confidence intervals for the median. Overall differences between control and oil groups were considered significant if the confidence intervals did not overlap at the 95% confidence level. Significant differences are reported as *p* values.

1.4 Results

1.4.1 Phytoplankton growth and oil chemistry

Across all experiments, growth rates (μ, d^{-1}) of *Pseudo-nitzschia australis* and *Emiliania huxleyi* were negatively affected by exposure to crude oil in the form of WAF (Figs. 1 & 2, Table 1). In all experiments, oil exposure completely inhibited the growth of *P.*

australis (strains HAB 207 and HAB 197) ($\mu \leq 0$ d^{-1}). Growth rates of exponentially growing *E. huxleyi* cultures significantly decreased as TPH ($p < 0.0001$, $R^2 = 0.660$), PAH ($p < 0.0001$, $R^2 = 0.633$), and SH ($p < 0.0001$, $R^2 = 0.672$) concentrations increased. Growth of *E. huxleyi* was completely inhibited during exposure to Platform Holly crude oil WAF at high concentrations ([TPH] = 2.21 mg L^{-1}, [PAH] = 0.0531 mg L^{-1}, [SH] = 0.017 mg L^{-1}). Under the same initial WAF concentrations using Refugio spill oil in experiment 4, *E. huxleyi* cultures grew exponentially while *P. australi*s (HAB 197) growth was inhibited. Nutrients were replete throughout the course of each experiment so growth was not limited by availability of inorganic nutrients (Table A1).

Cell volumes of *E. huxleyi* were measured and culture biovolumes were calculated on days 2 and 4 of experiments 1, 2, and 4 and compared across treatment (Figs. A1 & A2, Table A2). In experiment 1, cell volumes of the growth-inhibited high oil treatment were on average more than 16 μm^3 (day 2) ($q = 0.001$) and 33 μm^3 (day 4) ($q = 0.003$) larger than cells in the control treatment while the low oil treatment had cells that were more than 10 μm^3 larger than the control on day 2 ($q = 0.0002$), but similar cells sizes to those in the control treatment on day 4 ($q = 0.85$). For experiment 2, *E. huxleyi* cells in both oil treatments were consistently larger than those in the control treatment with cells in the high oil treatment and low oil treatment being more than 3 μm^3 ($q = 0.003$) and 2 μm^3 ($q = 0.005$) larger than control cells on day 2 and on average 4.5 μm^3 ($q = 0.002$) and 3.9 μm^3 ($q = 0.002$) larger than control cells by day 4. On the other hand, experiment 4 did not show significant differences between the oil and control cell volumes at either day 2 ($p = 0.12$) or day 4 ($p = 0.080$). Although significant differences were not detected during all time points in all

experiments, across all 3 *E. huxleyi* experiments cell volumes in oil-exposed treatments were shown to be on average (median) 16% greater than control treatments ($p < 0.004$).

Biovolume calculations show that although cell size is larger in oil-exposed treatments, the culture biovolume is still generally lower in oil-exposed treatments compared to control treatments (Fig. A2, Table A2). Specifically, control *E. huxleyi* cultures in experiment 1 had on average more than 1.4 ($q < 0.020$) and 3 ($q < 0.0029$) times more biovolume than the low and high oil treatments on days 2 and 4 respectively. In experiment 2, the control treatment had more than 1.3 times more biovolume than the high oil and low oil treatments on day 2 ($q = 0.010$) and 1.6 times more than the high oil treatment on day 4 ($q = 0.015$). The control treatment in experiment 4 had consistently more biovolume than the oil treatment with 1.8 times and 3.4 times more on days 2 ($p = 0.024$) and 4 ($p = 0.015$) respectively. Normalized culture biovolumes calculated throughout all experiments confirm that on average (median) culture biovolumes of oil-exposed treatments are 49% lower than control treatments ($p < 0.004$).

The initial WAF chemistry for the four experiments is shown in Table 1 and Figures S3 and S4. The TPH ($p = 0.619$), PAH ($p = 0.326$), and SH ($p = 0.100$) concentrations did not appear to be correlated with the initial mass of oil added to make the WAF. The relative concentrations of measured compounds also varied between experiments even when using the same source oil, but naphthalene (parent compound + alkylated homologs) was always the dominant PAH, making up approximately 94-96% of the total measured PAH concentration.

1.4.2 Dissolved and cellular domoic acid content in *P. australis* cultures

Dissolved DA normalized to cell abundance and cellular DA were compared across treatments at each sampled time point for both *P. australis* strains (Fig. 3 & 4, Table A2). For *P. australis* strain HAB 207 (experiment 3), dissolved DA was below the limit of detection (0.52 ng mL^{-1}) at the start of the experiment (T_0) but had measurable dissolved DA ranging from 1.60 to 2.04 ng mL^{-1} in all treatments for days 1-4. One replicate in the control treatment on day 2 as well as one replicate in the low oil treatment on day 3 had dissolved DA concentrations below the detection limit and were not included in the analyses (substitution of values below the detection limit were avoided to limit bias [Helsel 2006]). On day 1, the control treatment had approximately 3 times higher dissolved DA per cell than the oil treatments ($q = 0.028$) while by days 3 and 4, the oil treatments had on average more than 4 ($q < 0.0012$) and 20 ($q = 0.010$) times higher dissolved DA concentrations per cell than the control respectively. In *P. australis* strain HAB 197 (experiment 4), dissolved DA concentrations were not detected until day 4 in both the control and oil treatments and when normalized to cell abundance, dissolved DA $cell^{-1}$ was approximately 11 and 72 times higher in the oil treatment than the control on days 4 ($p = 0.0019$) and 5 ($p = 0.0018$), respectively. Across both experiments, using 2 different strains of *P. australis*, nonparametric confidence intervals for normalized dissolved DA $cell^{-1}$ suggest that oil-exposed treatments of *P. australis* had on average (median) 10 times more dissolved DA $cell^{-1}$ compared to control treatments ($p < 0.03$).

Cellular DA in *P. australis* HAB 207 (experiment 3) did not differ significantly between treatments except on day 4 where the low oil treatment was on average more than 6 times higher than the control or high oil treatments ($p = 0.045$), although pairwise comparisons did not show significant differences between any two individual treatments. In

P. australis HAB 197 (experiment 4), cellular DA in the oil treatment was 4.5 times higher than in the control treatment on day 5 ($p = 0.020$). Across both experiments, nonparametric confidence intervals constructed with normalized cellular DA show that on average (median) cellular DA in oil-exposed treatments is 2.6 times higher than in control treatments ($p < 0.03$). The consistent effect of treatment across experiments using multiple strains shows that oil exposure increases cellular DA in *P. australis* under growth-inhibiting conditions.

1.4.3 Transparent exopolymer particle content in *P. australis* and *E. huxleyi* cultures

The concentration of cellular TEP in both *P. australis* and *E. huxleyi* was compared across treatments at multiple time points throughout the four experiments (Figs. 5 & 6, Table A2). Cellular TEP in *P. australis* HAB 207 (experiment 3) in oil-exposed treatments was more than 16 times higher than the control treatment on day 4 ($q = 0.015$) in contrast with day 2 when no significant differences were observed ($p = 0.37$). For *P. australis* HAB 197 (experiment 4), cellular TEP in the oil-exposed treatment was approximately 7 times and 50 times higher on days 3 ($p = 0.016$) and 5 ($p = 0.0036$) respectively compared to the control treatment. Across both *P. australis* experiments, normalized cellular TEP in oil-exposed treatments was overall on average (median) 11 times higher than control treatments ($p < 0.03$).

For *E. huxleyi* in experiment 1, cellular TEP in the growth-inhibiting high oil treatment was more than 1.8 times higher compared to the control treatment on day 2 ($q = 0.022$) and more than 7 times higher than the control ($q = 0.013$) and low oil treatment on day 4 ($q = 0.013$) of the experiment respectively. Cellular TEP in exponentially growing *E. huxleyi* cultures did not significantly differ between the oil and control treatments at most

time points during the three experiments. The only significant difference between exponentially growing *E. huxleyi* cultures was on day 2 during experiment 2 when the high oil treatment was 1.4 times higher than the control treatment ($q = 0.041$). Although statistical differences in *E. huxleyi* cellular TEP were not observed at every time point, nonparametric confidence intervals for normalized cellular TEP across all *E. huxleyi* experiments showed that on average (median), oil treatments had 35% higher cellular TEP than control treatments ($p < 0.004$) and even when excluding the growth-inhibited high oil treatment from experiment 1, significant differences are apparent at the 95% confidence level.

1.4.4 Cellular $CaCO_3$, coccolith morphology, and shedding of coccoliths by *E. huxleyi*

The amount of $CaCO_3$ per cell in *E. huxleyi* was measured in the three *E. huxleyi* experiments and compared across treatments (Fig. 7, Table A2). The growth-inhibited high oil treatment in experiment 1 had more than 3 and 8 times higher $CaCO_3$ $cell^{-1}$ than the low oil and control treatments on days 2 ($q = 0.0002$) and 4 ($q = 0.0005$) of the experiment respectively. The other experiments did not show significant differences in $CaCO_3$ per cell except for day 2 of experiment 2 when the oil treatments appeared to have more $CaCO_3$ per cell than the control ($p = 0.038$) but pairwise comparisons did not show significant differences between any treatments. Across all experiments $CaCO_3$ per cell was found to be on average (median) 44% greater in oil-exposed treatments compared to control ($p < 0.04$) but when the growth-inhibited treatment is excluded from analysis, a difference between oil and control treatments is not apparent at the 95% confidence level. Quantification of abnormal coccosphere morphology (determined as coccospheres that contained 2 or more incomplete or malformed coccoliths) using SEM revealed that at the end of each *E. huxleyi* experiment, the proportion of abnormal coccospheres increased with increasing TPH

concentration ($p < 0.001$) (Fig. 8). The number of detached coccoliths per cell also appeared to be different between control and oil treatments at some time points throughout the *E. huxleyi* experiments (Fig. A5, Table A2). Specifically, on day 2 of experiment 1 using Platform Holly oil, the low oil treatment had the highest number of detached coccoliths per cell with 1.1 more detached coccoliths per cell than the control ($q = 0.020$) and 1.4 more detached coccoliths per cell than the high oil treatment ($q = 0.0015$). In experiment 4 using Refugio spill oil, the *E. huxleyi* treatment exposed to oil had 2.4 and 1.7 more detached coccoliths per cell than the control treatment at days 2 ($p = 0.026$) and 4 ($p = 0.018$) respectively. Normalized coccolith:cell measurements across all experiments show that on average (median), oil-exposed treatments have 10% higher coccolith to cell ratios than control treatments ($p < 0.04$).

1.4.5 Bacterial abundance

Across all four experiments, bacterial abundances did not differ significantly between treatments (Fig. A6, Table A2). For the first experiment (*E. huxleyi* with Platform Holly oil), a repeated measures ANOVA failed to detect differences in bacterial abundances between treatments ($p = 0.58$) but there was a significant change over time ($p = 0.019$). Independent analysis of each time point showed that bacterial abundances were comparable between treatments at any time point (Table A2). In experiment 2 (*E. huxleyi* with Refugio spill oil), repeated measures ANOVA revealed no differences in bacterial abundances between treatments throughout the experiment ($p = 0.99$) but in agreement with the first experiment (with Platform Holly oil), bacterial abundance changed over time ($p = 0.0002$). For each day, this trend was consistent as there were no significant differences between treatments at any time point (Table A2). A repeated measures ANOVA for experiment 3 with *P. australis* and

Refugio spill oil showed that bacterial abundances did not significantly differ either across treatments ($p = 0.82$) or through time ($p = 0.074$). Analysis at each time point was consistent with the results of the repeated measures ANOVA (Table A2). For experiment 4 (conducted with both *E. huxleyi* and *P. australis*), bacterial abundances were not significantly different between the oil and control treatments for either phytoplankton tested (*E. huxleyi:* $p = 0.18$, *P. australis:* $p = 0.80$) but both appeared to have a significant change in bacterial abundance over time (*E. huxleyi:* $p = 0.0021$, *P. australis:* $p = 0.0015$). Analysis of each day separately showed that for *P. australis* there were no differences in bacterial abundance at any time during the experiment but for *E. huxleyi*, at the initial time point, the oil treatment appeared to have on average 2.4 times more bacteria than the control while bacterial abundance did not differ at any other time point (Table A2).

1.5 Discussion

The results of the four independent experiments conducted in this study indicate short-term impacts of oil exposure on the physiology and morphology (*E. huxleyi*) of the two dominant phytoplankton species blooming in the SBC around the time of the Refugio oil spill. Although, extrapolating laboratory experiments to the natural environment is challenging due to the many interacting and complex factors governing physiology in natural phytoplankton populations, this study provides insight into the physiological responses of two ecologically and biogeochemically important species that were highly abundant during the Refugio oil spill.

1.5.1 Short-term responses of phytoplankton growth to oil exposure

Overall, we observed a decrease and/or inhibition of growth in *Emiliania huxleyi* and *Pseudo-nitzschia australis* during exposure to oil in the form of WAF. Although increases in cellular size have the potential to offset decreases in growth rates in terms of biomass, biovolume measurements in *E. huxleyi* cultures suggest that even though cell sizes increased in the presence of oil, the overall biovolume of the population was still significantly lower in oil-exposed cultures compared to control cultures. Observations that bacterial densities in the cultures were not significantly different in oil-exposed treatments suggests that indirect effects on phytoplankton physiology due to growth of bacterial populations were unlikely to have significantly impacted our results. In addition, a follow-up study on *E. huxleyi* culture bacterial communities during oil exposure revealed that bacterial community composition did not appear to differ significantly between oiled and control treatments within the first 5 days of oil exposure (J. Bullington unpubl. data). Our results agree with many others that have shown a decrease in phytoplankton growth in the presence of oil (e.g., Østgaard et al. 1984, González et al. 2009, Brussaard et al. 2016) which may suggest that phytoplankton growth in spill impacted areas of the SBC was depressed with repercussions for food web dynamics and upper trophic levels. However, due to the fact that in some cases, especially at low oil concentrations, growth can increase (e.g., Parsons et al. 1976, Siron et al. 1991, Huang et al. 2011) or remain unaffected (e.g., Batten et al. 1998, González et al. 2013, Li et al. 2017), it is possible that on longer timescales, using different types of oil, and at different oil concentrations, the responses to oil exposure could differ. Also, due to the abundance of natural hydrocarbon seeps in the SBC, locally adapted phytoplankton may respond differently to oil compared to strains from other locations.

It is common to observe a shift in phytoplankton community structure in mesocosm and microcosm experiments exposed to oil pollution (González et al. 2013, Brussaard et al. 2016, Li et al. 2017) as well as the few field studies that have available information on phytoplankton communities before and after oil pollution events (Brussaard et al. 2016, Parsons et al. 2015). Differential sensitivities of phytoplankton groups or species have also been demonstrated in experiments on individual phytoplankton populations (e.g., Echeveste et al. 2010, Hook & Osborn 2012, Ozhan & Bargu 2014a). Here, we found that at the same oil concentrations (the same WAF), *E. huxleyi* cultures showed growth while *P. australis* cultures did not. Our results are consistent with other studies that have found that diatoms tend to be more sensitive to oil exposure than other groups (e.g., Harrison et al. 1986, Siron et al. 1991, Nomura et al. 2007) while smaller phytoplankton taxa are more resistant (Huang et al. 2011, González et al. 2009). On the other hand, some studies have revealed contradictory results to these general trends. For example, Sargian and colleagues (2007), found that smaller phytoplankton (picophytoplankton) were more sensitive to oil exposure than larger nanophytoplankton, and Echeveste et al. (2010) showed that phytoplankton with larger cell sizes had higher toxicity thresholds to PAH exposure than smaller sized cells. Additionally, some studies have suggested that diatoms can be more resistant to oil exposure than other groups (e.g., González et al. 2009, Ozhan & Bargu 2014b) and Ozhan and Bargu (2014b) showed that under nutrient limited conditions in microcosm experiments, *Pseudo-nitzschia* spp. were more tolerant to crude oil than other pennate diatoms. Although many other factors are likely to influence shifts in the phytoplankton community structure, our results suggest that in the presence of oil, *E. huxleyi* could have a competitive advantage over *P. australis* and we cannot discard the possibility that the oil spill may have created a

competitive niche for *E. huxleyi* in the SBC, where it formed the only reported *E. huxleyi* bloom just two weeks after the spill. However, 2015 proved to be an anomalous year for oceanic conditions in the California Current system with the influence of the 'warm blob' (Bond et al. 2015) and El Niño and therefore other factors also likely influenced *E. huxleyi* success (Cavole et al 2016, McCabe et al 2016, Zaba & Rudnick 2016). A shift in the phytoplankton community from toxic diatoms to smaller calcified coccolithophores has implications for the local ecosystem including decreasing the productivity of an important HAB species in the California Current (while simultaneously increasing DA cellular content) and the alteration of food web dynamics.

1.5.2 Variability of phytoplankton responses to oil exposure

The chemistry and concentrations of WAF as well as the methods of oil addition have been shown to be important factors for phytoplankton responses to oil exposure. The decrease in *E. huxleyi* growth with increasing TPH concentrations observed in our study is in agreement with results for other phytoplankton taxa (e.g., Adekunle et al. 2010, Ozhan et al. 2014a, Li et al. 2017). Overall concentrations of PAHs and SHs showed a similar trend with lower *E. huxleyi* growth at higher concentrations, but for the *E. huxleyi* experiment using Platform Holly oil (experiment 1), the SH concentration in the growth-inhibiting high oil treatment was lower than in the other experiments that supported exponential growth in *E. huxleyi*. This suggests that SHs are unlikely to be solely responsible for the overall toxicity of the WAF and other components of the oil may have greater impacts on the decrease or inhibition of phytoplankton growth. As a group of compounds, PAHs have been suggested to be particularly toxic due to their strong adsorption affinity for particulate material, DNA damaging properties (Gelboin 1980) and interaction with cellular membranes (Neff 1979).

The WAF made with Platform Holly oil used in the first experiment on *E. huxleyi* had five additional high molecular weight PAH compounds that were not detected in the experiments conducted with Refugio spill oil (Fig. A3). It is therefore possible that these compounds may have caused the observed inhibition of growth by *E. huxleyi* in the high oil treatment. However, the overall PAH concentration and naphthalene (parent compound + alkylated homologs), as the dominant PAH measured in all WAFs, were also higher in the Platform Holly WAF, while the *E. huxleyi* growth trends were otherwise comparable across experiments using different oil. This suggests that there may have also been a PAH (or naphthalene) concentration threshold beyond which growth was inhibited. There was no correlation between the amount of oil added to make the WAF and the WAF chemistry (e.g., TPH, PAH, or SH concentrations) (Table 1). This is consistent with findings by Hook and Osborn (2012) who suggest that although the individual hydrocarbon compounds do not seem to be saturated, the total hydrocarbon capacity of the seawater may be saturated. Our values of TPH differ across experiments even with the same oil type and therefore unmeasured hydrocarbon compounds (e.g., volatile, low molecular weight compounds) or other factors (potentially small differences in stirring speed and time, WAF bottle headspace, and temperature across experiments) may have influenced the solubility of the hydrocarbons measured in our study. Interestingly, Hook and Osborn (2012) found that phytoplankton growth did not correlate with TPH or PAH concentrations but rather with the oil loading concentration. They suggest that the observed toxicity in their study must be due to unidentified compounds within the WAF rather than the PAHs or overall TPHs. This is in contrast to the results of this study where it appears that the measured groups of hydrocarbon compounds, especially the TPHs and PAHs, are controlling the toxicity of the WAF.

Unfortunately, seawater oil chemistry measurements could not be taken in the field during the time of the Refugio oil spill and so direct comparisons to the magnitude, extent, and overall time of oil exposure in the SBC is not possible. However, information on *in-situ* TPH and PAH concentrations is available for other oil spill scenarios, which can help provide guidance for our study. In this study, concentrations of TPHs and PAHs ranged from 0.72 – 2.78 mg L^{-1} and 18 – 53 µg L^{-1} respectively, which is higher than field observations for some spills such as the *Prestige* spill (max PAH = 5.8 µg L^{-1}) (González et al. 2006), the *Baltic Carrier* spill (max PAH = 1.45 µg L^{-1}) (Pécseli et al. 2003), and the *Exxon Valdez* spill (max PAH < 1.0 µg L^{-1}) (Neff and Stubblefield, 1995), but within the observed concentrations for other spills such as the *Volgoneft-248* spill (max TPH = 2.17 mg L^{-1}) (Tas et al. 2011), the *North Cape* spill (max TPH = 3.94 mg L^{-1}, max PAH = 115 µg L^{-1}) (Reddy & Quinn 1999), and the Deepwater Horizon (Macondo) oil spill (max TPH = 11400 mg L^{-1}, avg TPH = 202 mg L^{-1}, max PAH = 1231 µg L^{-1}, avg PAH = 47 µg L^{-1}) (Sammarco et al. 2013). Additionally, dissolution and solubility of oil in seawater varies due to many factors such as water temperature, pH, salinity, oil type (e.g., viscosity), and physical processes (e.g., mixing and wave action) (Rice et al. 1976), making it difficult to estimate or compare seawater concentrations across oil spill scenarios. Both the Refugio and Platform Holly oil originating from the Monterey Formation are relatively heavy (calculated API gravity = 23º [Refugio] or 18º [Platform Holly]) and are therefore less soluble in seawater than lighter oils such as the Macondo oil (API gravity = 37º [SL Ross Environmental Research 2010]). However, the oil from the *Prestige* and *Volgoneft-248* spills were both heavy oils with API gravity around 11º (Otay & Yenigun 2000, Castanedo et al. 2006) and given that the concentrations used in this study are comparable to some measured in the field, it is possible

that in some areas near the spill, phytoplankton in the SBC were exposed to concentrations relevant to this study during the Refugio oil spill.

1.5.3 Dissolved and cellular domoic acid content in *P. australis* cultures

This is the first study to explore the effect of oil exposure on DA content in *P. australis* cultures and here we showed that two *P. australis* strains with inherently different cellular DA content generally appeared to produce more DA per cell in growth-inhibited cultures exposed to oil than when growing in the absence of oil (Figs. 3 & 4). In a study by Ozhan and Bargu (2014a), the effects of oil exposure on toxin production in dinoflagellates and a raphidophyte revealed that low oil levels enhanced intracellular toxin concentrations, although when growth was inhibited by high oil concentrations, intracellular toxin concentrations were lower or not significantly different than the control. DA production in *Pseudo-nitzschia* spp. has generally been shown to increase with decreasing growth rates (Pan et al. 1998, Thorel et al. 2014) associated with nutrient limitation (specifically phosphate, silicate, and iron) (e.g., Pan et al. 1998, Maldonado et al. 2002, Santiago-Morales & Garcia-Mendoza 2011) and increasing pH (Lundholm et al. 2004). Different sources of organic and inorganic nitrogen have also been shown to affect both growth rate and DA cellular content but growth rates were not correlated with cellular DA (Martin-Jézéquel et al. 2015). Here, nutrients were not limited in any culture throughout the experiments but growth was inhibited by oil exposure and as others have suggested, this may have contributed to increased DA cellular content due to excess photosynthetic energy from arresting cell division (e.g., Pan et al 1998, Mos 2001). It is also possible that oil addition altered the seawater chemistry directly (e.g., adding organic sources of nitrogen) or indirectly (e.g., bacteria remineralization and respiration) so that DA content was indirectly affected.

Whether cellular and dissolved DA content might differ in exponentially growing *P. australis* cultures is unclear, but our results revealed that even though growth was inhibited by oil exposure, *P. australis* cells appear to continue to produce domoic acid. Although inhibition of growth and competition by other phytoplankton species may have reduced the SBC *Pseudo-nitzschia* populations at the time of the Refugio spill, oil exposure could have resulted in a short-term increase in DA concentrations in the field, particularly if populations with high cell densities were present immediately preceding or at the time of the spill. A closure in commercial and recreational fisheries was enacted immediately following the Refugio spill and the fisheries remained closed for 6 weeks due to potential toxicity from the oil directly (https://www.noozhawk.com/article/santa_barbara_county_fishery_closures_lifted_after_refugio_oil_spill). However, shortly after the Refugio spill, high levels of DA also caused the closure of bivalve shellfish, anchovy, sardine, and crab fisheries in Santa Barbara County from July 3, 2015 to November 13, 2015 (bivalves and small finfish) or December 31, 2015 (Dungeness and rock crab) (California Ocean Science Trust 2016). Elevated levels of DA have historically been an issue in the SBC (Anderson et al. 2006, Anderson et al. 2008, Sekula-Wood et al. 2011) and 2015 also proved to be an anomalous year for the entire U.S. West Coast with unprecedented *Pseudo-nitzschia* blooms and DA production from California to Alaska (McCabe et al. 2016). However, from our study, it is not possible to determine the extent to which the oil impacted overall DA production in the SBC and the resulting fishery closures.

1.5.4. Transparent exopolymer particle content in *E. huxleyi* and *P. australis* cultures

Transparent exopolymer particles (TEP) have been shown to be important components of carbon pools in marine and freshwater environments where they can play a large role in biogeochemical cycling and the structuring of food webs (Passow 2002). Due to the sticky nature of TEP, they are efficient facilitators of particle aggregation. Production by phytoplankton was suggested as one of the possible mechanisms for the formation of large amounts of oil-incorporated marine snow observed after the Deepwater Horizon oil spill (Passow et al. 2012). Here we showed that overall, cellular TEP for both *P. australis* and *E. huxleyi* across all experiments appeared to increase in oil-exposed treatments. This is consistent with other findings showing that cellular TEP, as a carbon overflow mechanism, increases as growth rates decrease (Engel et al. 2002) while it has been suggested to be a response to physiological stress (e.g., Passow & Alldredge 1995, Moriceau et al. 2007, Kahl 2008). Given that TEP is known to enhance sedimentation and export of matter to the sea floor (Passow et al. 2001, Seebah et al. 2014), an increase in the amount of phytoplankton-derived TEP during the Refugio oil spill may have influenced the fate of the spilled oil. Specifically, high abundances of phytoplankton cells combined with sticky TEP could have been aggregated with oil droplets (as in Passow et al. 2012), allowing oil to sink out of the surface ocean where it could eventually be deposited onto the ocean floor.

1.5.5 Production, morphology, and shedding of $CaCO_3$ by *E. huxleyi*

Calcification in coccolithophores is of great significance for the carbon cycle through both the formation of coccoliths and the role of the high density $CaCO_3$ for transporting organic matter to depth. The formation of 'white waters' as a result of the production and shedding of coccoliths has also been suggested to impact higher marine trophic levels. For example, *E. huxleyi* blooms in the Eastern Bering Sea have coincided with widespread

seabird mortality (Baduini et al. 2001) and poor salmon runs (Vance et al. 1998), while visual predators and zooplankton grazers seem to avoid bloom areas (Eisner et al. 2005). Here we showed that although the amount of $CaCO_3$ per *E. huxleyi* cell did not vary significantly between exponentially growing cultures, exposure to oil impacted the appearance and shedding of *E. huxleyi* coccoliths. Specifically, oil exposure increased the relative abundance of cells that had abnormal (containing malformed and/or incomplete coccoliths) coccospheres and the relative number of detached coccoliths per cell. This suggests that oil exposure is interfering with the cellular process of calcification while not inhibiting coccolith formation. Malformed coccoliths have been proposed to be detrimental to the overall fitness of the cell (Rosas-Navarro et al. 2016) but because it is unclear whether the process of calcification, the product of calcification, or both are important for coccolithophore fitness, it is difficult to determine how malformation of coccoliths may impact the cell overall. Coccolith shedding or detachment is also known to vary across *E. huxleyi* strains and environmental conditions where it has been shown to be dependent on growth rates and growth phase (e.g., Balch et al. 1993, Chow et al. 2015, Matson et al. 2016). The detachment of coccoliths in the field can have a large influence on particle aggregation and flux as well the optical properties of the water column. Due to the small size of individual coccoliths, detachment allows the free-floating coccoliths to remain suspended in the surface ocean for longer than if they were attached to cells. This leads to the accumulation of these tiny calcite particles in the surface ocean and an increase in turbidity with implications for visual predators. The accumulation of coccoliths in the surface ocean also increase the probability of particle aggregation. Any aggregates that incorporate enough of the dense $CaCO_3$ particles

will be efficiently exported to depth with implications for the fate of the oil and the impacts on other organisms throughout the water column.

1.6 Conclusions

It is incredibly difficult to determine the effects of an unexpected oil pollution event in the marine environment due to the clear dependence on, among other factors, the physical conditions at the time of the spill, timing of the spill, initial microbial communities present, and the amount and method of oil addition. However, it is important to gain a better understanding of biological responses to these events so that management, clean-up, and future prevention can be optimized. This study focused on the two dominant phytoplankton species present around the time of the Refugio oil spill to elucidate their physiological responses to oil exposure. This is the first study to test a representative DA producer, *P. australis*, or a calcifying, bloom-forming coccolithophore, *E. huxleyi*, in response to oil exposure and our findings provide insight into potential implications of oil spills on phytoplankton communities like those in the SBC. Food web structure and function in the SBC was likely impacted as oil appears to disproportionately decrease growth of the tested phytoplankton species potentially leading to a decline in productivity and shifts in the phytoplankton community composition. Other physiological changes observed in DA content, calcification, and cellular TEP could also have implications for food web structure and function, ecosystem and human health, and the fate of the spilled oil in the environment. This study highlights the need for more comprehensive research into oil spill effects across ecosystem components and trophic levels because the direct and indirect effects, as well as

the interactions between individual phytoplankton populations and other parts of the ecosystem, are currently unclear. This study also brings to light further questions regarding the possibility for oil spills to select for oil-adapted groups in areas with natural hydrocarbon seeps, and how seep oil may have a chronic impact on phytoplankton communities and their physiology.

1.7 Acknowledgements

This work was supported by the Simons Foundation (#385324) and the University of California, Santa Barbara (UCSB) Associated Students Coastal Fund (#FALL15-14). We thank Prof. David Valentine (UCSB) for supplying oil collected at Platform Holly and NOAA for supplying oil from the Refugio spill. We thank Scott Loranger for providing us with a density measurement for the Platform Holly oil. We thank Andrea Valdez-Schulz and Reina Myers for help in the laboratory and Christoph Pierre and Christian Orsini for seawater collection. We also thank our colleagues, Dr. Uta Passow and Julia Sweet from UCSB, for their assistance with measuring and analyzing TEP and Kendra Hayashi from the University of California, Santa Cruz, for her assistance with domoic acid analysis.

1.8 Literature cited

Adekunle IM, Ajijo MR, Adeofun CO, Omoniyi IT (2010) Response of four phytoplankton species found in some sectors of Nigerian coastal waters to crude oil in controlled ecosystem. Int J Environ Res 4:65–74

Andersen RA (Editor) (2005) Algal culturing techniques. Elsevier Academic Press

Anderson CR, Brzezinski MA, Washburn L, Kudela R (2006) Circulation and environmental conditions during a toxigenic *Pseudo-nitzschia australis* bloom in the Santa Barbara Channel, California. Mar Ecol Prog Ser 327:119–133

Anderson CR, Siegel DA, Brzezinski MA, Guillocheau N (2008) Controls on temporal patterns in phytoplankton community structure in the Santa Barbara Channel, California. J Geophys Res Ocean 113:1–16

Aurand D, Coelho GM (Editors) (2005) Cooperative Aquatic Toxicity Testing of Dispersed Oil and the "Chemical Response to Oil Spills: Ecological Effects Research Forum (CROSERF)." Ecosystem Management and Associates, Inc. Lusby, MD. Technical Report 07-03, 105 pages + Appendices

Baduini CL, Hyrenbach KD, Coyle KO, Pinchuk A, Mendenhall V, Hunt GL (2001) Mass mortality of short-tailed shearwaters in the south-eastern Bering Sea during summer 1997. Fish Oceanogr 10:117–130

Balch WM, Kilpatrick K, Holligan PM, Cucci T (1993) Coccolith production and detachment by *Emiliania huxleyi* (Prymnesiophyceae). J Phycol 29:566–575Batten SD, Allen RJS, Wotton COM (1998) The effects of the Sea Empress oil spill on the plankton of the southern Irish Sea. Mar Pollut Bull 36:764–774

Brussaard CPD, Peperzak L, Beggah S, Wick LY, Wuerz B, Weber J, Arey JS, van der Burg B, Jonas A, Huisman J, van der Meer JR (2016) Immediate ecotoxicological effects of short-lived oil spills on marine biota. Nat Commun 7:11206 doi: 10.1038/ncomms11206

Bond NA, Cronin MF, Freeland H, Mantua N (2015) Causes and impacts of the 2014 warm anomaly in the NE Pacific. Geophys Res Lett 42:3414–3420

California Ocean Science Trust (2016) Frequently Asked Questions: Harmful Algal Blooms and California Fisheries. Oakland, CA

Castanedo S, Medina R, Losada IJ, Vidal C, Méndez FJ, Osorio A, Juanes JA, Puente A (2006) The Prestige Oil Spill in Cantabria (Bay of Biscay). Part I: Operational Forecasting System for Quick Response, Risk Assessment, and Protection of Natural Resources. J Coast Res 226:1474–1489

Cavole LM, Demko AM, Diner RE, Giddings A, Koester I, Pagniello CMLS, Paulsen M, Ramirez-Valdez A, Schwenck SM, Yen NK, Zill ME, Franks PJS (2016) Biological impacts of the 2013–2015 warm-water anomaly in the Northeast Pacific: Winners, losers, and the future. Oceanography 29:273–285

Chow JS, Lee C, Engel A (2015) The influence of extracellular polysaccharides, growth rate, and free coccoliths on the coagulation efficiency of *Emiliania huxleyi*. Mar Chem 175:5–17

Echeveste P, Agustí S, Dachs J (2010) Cell size dependent toxicity thresholds of polycyclic aromatic hydrocarbons to natural and cultured phytoplankton populations. Environ Pollut 158:299–307

Eisner LB, Farley EV, Murphy JM, Helle JH (2005) Distributions of Oceanographic Variables, Juvenile Sockeye Salmon and Age-0 Walleye Pollock in the Southeastern Bering Sea during Fall 2000 – 2003. NPAFC Technical Report No. 6

Engel A, Goldthwait S, Passow U, Alldredge A (2002) Temporal decoupling of carbon and nitrogen dynamics in a mesocosm diatom bloom. Limnol Oceanogr 47:753–761

Fritz L, Quilliam MA, Wright JLC, Beale AM, Work TM (1992) An outbreak of domoic acid poisoning attributed to the pennate diatom *Pseudonitzschia australis*. J Phycol 28:439–442Gelboin HV (1980) Benzo[a]pyrene metabolism, activation, and carcinogenesis: role and regulation of mixed-function oxidases and related enzymes. Physiol Rev 60:1107–1167

González JJ, Viñas L, Franco MA, Fumega J, Soriano JA, Grueiro G, Muniategui S, López-Mahía P, Prada D, Bayona JM, Alzaga R, Albaigés J (2006) Spatial and temporal distribution of dissolved/dispersed aromatic hydrocarbons in seawater in the area affected by the Prestige oil spill. Mar Pollut Bull 53:250–259

González JJ, Figueiras FG, Aranguren-Gassis M, Crespo BG, Fernández E, Morán XAG, Nieto-Cid M (2009) Effect of a simulated oil spill on natural assemblages of marine phytoplankton enclosed in microcosms. Estuar Coast Shelf Sci 83:265–276

González JJ, Fernández E, Figueiras FG, Varela M (2013) Subtle effects of the water soluble fraction of oil spills on natural phytoplankton assemblages enclosed in mesocosms. Estuar Coast Shelf Sci 124:13–23

Grelaud M, Schimmelmann A, Beaufort L (2009) Coccolithophore response to climate and surface hydrography in Santa Barbara Basin, California, AD 1917–2004. Biogeosciences 6:2025–2039

Guillard RRL, Ryther JH (1962) Studies of marine planktonic diatoms, I, *Cyclotella nanna* (Hustedt) and *Detonula convervacea* (Cleve). Can J Microbiol 8:229–239

Harrison PJ, Cochlan WP, Acreman JC, Parsons TR, Thompson PA, Dovey HM, Xiaolin C, (1986) The effect of crude oil and Corexit 9527 on marine phytoplankton in an experimental enclosure. Mar Environ Res 18:93-109

Helsel DR (2006) Fabricating data: How substituting values for nondetects can ruin results, and what can be done about it. Chemosphere 65:2434–2439

Hook SE, Osborn HL (2012) Comparison of toxicity and transcriptomic profiles in a diatom exposed to oil, dispersants, dispersed oil. Aquat Toxicol 124-125:139–151

Hsiao SIC, Kittlet DW, Foy MG (1978) Effects of crude oils and the oil dispersant Corexit on primary production of Arctic marine phytoplankton and seaweed. Environ Pollut 15:209–221

Hu C, Weisberg RH, Liu Y, Zheng L, Daly KL, English DC, Zhao J, Vargo GA (2011) Did the northeastern Gulf of Mexico become greener after the Deepwater Horizon oil spill? Geophys Res Lett 38:1–5

Huang Y, Jiang Z, Zeng J, Chen Q, Zhao Y, Liao Y, Shou L, Xu X (2011) The chronic effects of oil pollution on marine phytoplankton in a subtropical bay, China. Environ Monit Assess 176:517–530

Iglesias-Rodríguez MD, Halloran PR, Rickaby REM, Hall IR, Colmenero-Hidalgo E, Gittins JR, Green DRH, Tyrrell T, Samantha J, von Dassow P, Rehm E, Armbrust EV, Boessenkool KP (2008) Phytoplankton Calcification in a High-$C0_2$ World. Science 320:336–340

Ignatiades L, Mimicos N (1977) Ecological responses of phytoplankton on chronic oil pollution. Environ Pollut 13:109–118

Kahl LA, Vardi A, Schofield O (2008) Effects of phytoplankton physiology on export flux. Mar Ecol Prog Ser 354:3–19

Kudela RM, Lane JQ, Cochlan WP (2008) The potential role of anthropogenically derived nitrogen in the growth of harmful algae in California, USA. Harmful Algae 8:103–110

Langer G, Geisen M, Baumann KH, Klas J, Riebesell U, Thoms S, Young JR (2006) Species-specific responses of calcifying algae to changing seawater carbonate chemistry. Geochemistry, Geophys Geosystems 7:Q09006

Langer G, Probert I, Nehrke G, Ziveri P (2011) The morphological response of *Emiliania huxleyi* to seawater carbonate chemistry changes: an inter-strain comparison. J Nannoplankt Res 32:29–34

Lefebvre KA, Bargu S, Kieckhefer T, Silver MW (2002) From sanddabs to blue whales: The pervasiveness of domoic acid. Toxicon 40:971–977

Li J, Bidigare RR, Laws EA (2017) Effects of Macondo Oil on Phytoplankton from Grand Isle, Louisiana. J Environ Anal Toxicol 07:468. doi: 10.4172/2161-0525.1000468

Lundholm N, Hansen PJ, Kotaki Y (2004) Effect of pH on growth and domoic acid production by potentially toxic diatoms of the genera *Pseudo-nitzschia* and *Nitzschia*. Mar Ecol Prog Ser 273:1–15

Maldonado MT, Hughes MP, Rue EL, Wells ML (2002) The effect of Fe and Cu on growth and domoic acid production by *Pseudo-nitzschia multiseries* and *Pseudo-nitzschia australis*. Limnol Oceanogr 47:515–526

Martin-Jézéquel V, Calu G, Candela L, Amzil Z, Jauffrais T, Séchet V, Weigel P (2015) Effects of organic and inorganic nitrogen on the growth and production of domoic acid by *Pseudo-nitzschia multiseries* and *P. australis* (bacillariophyceae) in culture. Mar Drugs 13:7067–7086

Matson PG, Ladd TM, Halewood ER, Sangodkar RP, Chmelka BF, Iglesias-Rodriguez MD (2016) Intraspecific differences in biogeochemical responses to thermal change in the coccolithophore *Emiliania huxleyi*. PLoS ONE 11(9) doi:10.1371/journal.pone.0162313

Matson PG, Washburn L, Fields EA, Gotschalk C, Ladd TM, Siegel DA, Welch ZS, Iglesias-Rodriguez MD (2019) Formation, development, and propagation of a rare coastal coccolithophore bloom. J Geophys Res Ocean 124 https://doi.org/10.1029/2019JC015072

McCabe RM, Hickey BM, Kudela RM, Lefebvre KA, Adams NG, Bill BD, Gulland FMD, Thomson RE, Cochlan WP, Trainer VL (2016) An unprecedented coastwide toxic algal bloom linked to anomalous ocean conditions. Geophys Res Lett 43:10366-10376

Moriceau B, Garvey M, Ragueneau O, Passow U (2007) Evidence for reduced biogenic silica dissolution rates in diatom aggregates. Mar Ecol Prog Ser 333:129–142

Mos L (2001) Domoic acid: a fascinating marine toxin. Environ Toxicol Pharmacol 9:79–85

Neff JM (1979) Polycyclic Aromatic Hydrocarbons in the Aquatic Environment: Sources, Fates and Biological Effects. Applied Science Publishers Ltd, London, England

Neff J, Stubblefield W (1995) Chemical and Toxicological Evaluation of Water Quality Following the *Exxon Valdez* Oil Spill. In: Wells PG, Butler JN, Hughes JS (eds) *Exxon Valdez* Oil Spill." Fate and Effects in Alaskan Waters. ASTM Spec Tech Publ 1219, American Society for Testing and Materials, Philadelphia, p 141-177

Nomura H, Toyoda K, Yamada M, Okamoto K, Wada M, Nishimura M, Yoshida A, Shibata A, Takada H, Ohwada K (2007) Mesocosm studies on phytoplankton community succession after inputs of the water-soluble fraction of Bunker A oil. La Mer 45:105–116

NRC (National Research Council) (2003) Oil in the Sea III: Inputs, Fates, and Effects. National Academies Press, Washington, DC

Østgaard K, Eide I, Jensen A (1984) Exposure of phytoplankton to Ekofisk crude oil. Mar Environ Res 11:183–200

Otay EN, Yenigun O (2000) Volgoneft-248 oil spill in the Marmara Sea. In: Proceedings of 2nd International Conference on Oil Spills in the Mediterranean and Black Sea Regions. October 31–November 3, 2000, Istanbul, pp. 13–23

Özhan K, Bargu S (2014a) Responses of sympatric Karenia brevis, Prorocentrum minimum, and Heterosigma akashiwo to the exposure of crude oil. Ecotoxicology 23:1387–1398

Özhan K, Bargu S (2014b) Distinct responses of Gulf of Mexico phytoplankton communities to crude oil and the dispersant corexit® Ec9500A under different nutrient regimes. Ecotoxicology 23:370–384

Özhan K, Miles SM, Gao H, Bargu S (2014a) Relative phytoplankton growth responses to physically and chemically dispersed South Louisiana sweet crude oil. Environ Monit Assess 186:3941–3956

Ozhan K, Parsons ML, Bargu S (2014b) How Were Phytoplankton Affected by the Deepwater Horizon Oil Spill? Bioscience 64:829–836

Paasche E (1998) Roles of nitrogen and phosphorus in coccolith foramation in *Emiliania huxleyi* (Prymnesiophyceae). Eur J Phycol 33: 33-42

Pan Y, Bates SS, Cembella AD (1998) Environmental Stress and Domoic Acid Production by *Pseudo-nitzschia*: a Physiological Perspective. Nat Toxins Nat Toxins 6:127–135

Parsons TR, Li WKW, Waters R (1976) Some preliminary observations on the enhancement of phytoplankton growth by low levels of mineral hydrocarbons. Hydrobiologia 51:85–89

Parsons ML, Morrison W, Rabalais NN, Turner RE, Tyre KN (2015) Phytoplankton and the Macondo oil spill: A comparison of the 2010 phytoplankton assemblage to baseline conditions on the Louisiana shelf. Environ Pollut 207:152–160

Passow U, Alldredge AL (1995) Aggregation of a diatom bloom in a mesocosm: The role of transparent exopolymer particles (TEP), Deep-Sea Res. Pt.II 42:99–109

Passow U, Shipe RF, Murray A, Pak DK, Brzezinski MA, Alldredge AL (2001) The origin of transparent exopolymer particles (TEP) and their role in the sedimentation of particulate matter. Cont Shelf Res 21:327–346

Passow U (2002) Transparent exopolymer particles (TEP) in aquatic environments. Prog Oceanogr 55:287–333

Passow U, Ziervogel K, Asper V, Diercks A (2012) Marine snow formation in the aftermath of the Deepwater Horizon oil spill in the Gulf of Mexico. Environ Res Lett 7:1–11

Passow U, Sweet J, Quigg A (2017) How the dispersant Corexit impacts the formation of sinking marine oil snow. Mar Pollut Bull 125:139-145

Pécseli M, Pritzl G, Hansen AB, Christensen JH, Andersen O, Banta G, Johansen K, Sørensen JL (2003) The Baltic Carrier oil spill: Monitoring and assessment of PAC levels in water, sediment and biota. Environment Canada Arctic and Marine Oil Spill Program Technical Seminar (AMOP) Proceedings. 26

Reddy CM, Quinn JG (1999) GC-MS Analysis of Total Petroleum Hydrocarbons and Polycyclic Aromatic Hydrocarbons in Seawater Samples After the North Cape Oil Spill. 38:126–135

Rice SD, Short JW, Karinen JF (1976) Comparative oil toxicity and comparative animal sensitivity. In: Wolf DA (ed) Fate and Effects of Petroleum Hydrocarbons in Marine Ecosystems and Organisms. Proceedings of a Symposium, Seattle, p 78 – 94

Rosas-Navarro A, Langer G, Ziveri P (2016) Temperature affects the morphology and calcification of *Emiliania huxleyi* strains. 2:1–22

Sammarco PW, Kolian SR, Warby RAF, Bouldin JL, Subra WA, Porter SA (2013) Distribution and concentrations of petroleum hydrocarbons associated with the BP/Deepwater Horizon Oil Spill, Gulf of Mexico. Mar Pollut Bull 73:129–143

Santiago-Morales IS, García-Mendoza E (2011) Growth and domoic acid content of *Pseudo-nitzschia australis* isolated from northwestern Baja California, Mexico, cultured under batch conditions at different temperatures and two Si:NO_3 ratios. Harmful Algae 12:82–94

Sargian P, Mostajir B, Chatila K, Ferreyra GA, Pelletier É, Demers S (2005) Non-synergistic effects of water-soluble crude oil and enhanced ultraviolet-B radiation on a natural plankton assemblage. Mar Ecol Prog Ser 294:63–77

Sargian P, Mas S, Pelletier É, Demers S (2007) Multiple stressors on an Antarctic microplankton assemblage: Water soluble crude oil and enhanced UVBR level at Ushuaia (Argentina). Polar Biol 30:829–841

Schnetzer A, Miller PE, Schaffner RA, Stauffer BA, Jones BH, Weisberg SB, DiGiacomo PM, Berelson WM, Caron DA (2006) Blooms of *Pseudo-nitzschia* and domoic acid in the San Pedro Channel and Los Angeles harbor areas of the Southern California Bight, 2003–2004. Harmful Algae 6:372–387

Seebah S, Fairfield C, Ullrich MS, Passow U (2014) Aggregation and sedimentation of *Thalassiosira weissflogii* (diatom) in a warmer and more acidified future ocean. PLoS One 9:1–9

Sekula-Wood E, Benitez-Nelson C, Morton S, Anderson C, Burrell C, Thunell R (2011) *Pseudo-nitzschia* and domoic acid fluxes in Santa Barbara Basin (CA) from 1993 to 2008. Harmful Algae 10:567–575

Siron R, Giusti G, Berland B, Morales-Loo R, Pelletier É (1991) Water-soluble petroleum compounds: chemical aspects and effects on the growth of microalgae. Sci Total Environ 104:211–227

SL Ross Environmental Research, Ltd. (2010) Spill Related Properties of MC252 Crude Oil, Sample ENT-052210-178. Appendix 8 to Oil Budget Calculator: Deepwater Horizon. Technical Documentation. A Report to the National Incident Command, November 2010. 7 pp

Tas S, Okus E, Ünlü S, Altiok H (2011) A study on phytoplankton following the 'Volgoneft-248' oil spill on the north-eastern coast of the Sea of Marmara. J Mar Biol Assoc UK 91:715-725

Tyrell T, Merico A (2004) *Emiliania huxleyi*: bloom observations and the conditions that induce them. In Thierstein HR, Young JR (Eds) Coccolithophores – From Molecular Processes to Global Impact. Springer, New York, pp. 75-97

Thorel M, Fauchot J, Morelle J, Raimbault V, Le Roy B, Miossec C, Kientz-Bouchart V, Claquin P (2014) Interactive effects of irradiance and temperature on growth and domoic acid production of the toxic diatom *Pseudo-nitzschia australis* (Bacillariophyceae). Harmful Algae 39:232–241

U.S. EPA Method 8015D (SW-846) (2003) Nonhalogenated organics using GC/FID https://www.epa.gov/sites/production/files/2015-12/documents/8015d_r4.pdf. (Accessed May 4, 2018)

U.S. EPA Method 8270D (SW-846) (2014) Semivolatile organic compounds by gas chromatography/mass spectrometry https://www.epa.gov/sites/production/files/2015-12/documents/8270d.pdf. (Accessed May 4, 2018)

Vance T, Schumacher J, Stabeno P, Baier C, Wyllie-Echeverria T, Tynan C, Brodeur R, Napp J (1998) Aquamarine waters recorded for first time in Eastern Bering Sea. Eos, Trans Am Geophys Union 79:121–121

Vargo GA, Hutchins M, Almquist G (1982) The effect of low, chronic levels of No. 2 fuel oil on natural phytoplankton assemblages in microcosms. 1. Species composition and seasonal succession. Mar Environ Res 6:245–264

von Dassow P, van den Engh G, Iglesias-Rodriguez MD, Gittins JR (2012) Calcification state of coccolithophores can be assessed by light scatter depolarization measurements with flow cytometry. J Plankton Res 34:1011–1027

Wang Z, King KL, Ramsdell JS, Doucette GJ (2007) Determination of domoic acid in seawater and phytoplankton by liquid chromatography–tandem mass spectrometry. J Chromatogr A 1163:169-176

Westbroek P, Young JR, Linschooten K (1989) Coccolith production (biomineralization) in the marine alga *Emiliania huxleyi*. J Protozool 36:368–73

Zaba KD, Rudnick DL (2016) The 2014-2015 warming anomaly in the Southern California Current System observed by underwater gliders. Geophys Res Lett 43:1241–1248

Table 1.1. Descriptions of four independent oil exposure experiments conducted to test physiological responses of *Emiliania huxleyi* and *Pseudo-nitzschia australis*. Concentrations of total petroleum hydrocarbons (TPHs), polycyclic aromatic hydrocarbons (PAHs), and saturated hydrocarbons (SHs) shown represent the initial measured concentrations in the concentrated (100%) water accommodated fraction (WAF) before any dilution or addition of phytoplankton cells. Growth rates (μ) are displayed as the mean ± standard deviation of triplicate cultures for each treatment. Asterisks represent a statistical difference ($\alpha = 0.05$) in oil treatment growth rates compared to the control for each experiment.

Exp ID	Oil source	Species (strain)	Growth media	Oil added for 100% WAF (g oil L^{-1})	[TPH] 100% WAF (mg L^{-1})	[PAH] 100% WAF (mg L^{-1})	[SH] 100% WAF (mg L^{-1})	μ 100% WAF treatment	μ 50% WAF treatment	μ control treatment
1	Platform Holly 2012	*E. huxleyi* (150604 A9)	mod f	3.80	2.21	0.0531	0.017	-0.1 ± 0.1*	0.70 ± 0.04*	0.99 ± 0.09
2	Refugio pipeline spill	*E. huxleyi* (150604 A9)	mod f	4.25	1.44	0.0351	0.019	0.63 ± 0.07*	0.71 ± 0.07*	0.92 ± 0.04
3	Refugio pipeline spill	*P. australis* (HAB 207)	f/2	3.94	2.78	0.0385	0.027	-0.5 ± 0.2*	-0.3 ± 0.1*	1.0 ± 0.2
4	Refugio pipeline spill	*E. huxleyi* (150604 A9) *P. australis* (HAB 197)	f/2	2.59	2.37	0.0513	0.043	---	0.5 ± 0.3* -0.3 ± 0.1*	1.02 ± 0.01 0.8 ± 0.1

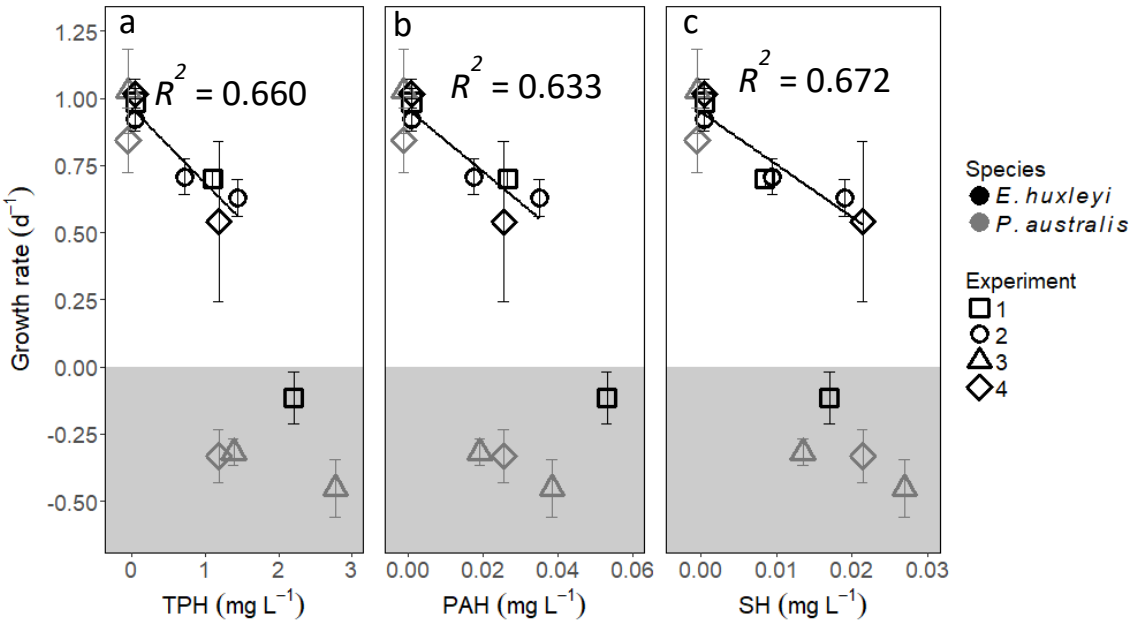

Fig. 1.1. Mean growth rates as a function of initial total petroleum hydrocarbon (TPH) (a), polycyclic aromatic hydrocarbon (PAH) (b), and saturated hydrocarbon (SH) (c) concentrations of triplicate cultures of *E. huxleyi* (black) and *P. australis* (grey) from four independent experiments. Each experiment is denoted by a different symbol: (1) *E. huxleyi* grown in modified f medium with and without Santa Barbara Channel Platform Holly oil added (low oil treatment = ½ dilution of high oil treatment); (2) *E. huxleyi* grown in modified f medium with and without Refugio pipeline spill oil added (low oil treatment = ½ dilution of high oil treatment); (3) *P. australis* (strain HAB 207) grown in f/2 medium with and without Refugio pipeline spill oil added (low oil treatment = ½ dilution of high oil treatment); (4) *P. australis* (strain HAB 197) and *E. huxleyi* grown in f/2 medium with and without Refugio pipeline spill oil added. Control treatments (no oil added) were assumed to have negligible TPH, PAH, and SH concentrations but points are slightly offset to avoid overlapping data points. The grey shaded area represents treatments that had complete inhibition of growth. Linear regression fits (and R^2) of *E. huxleyi* triplicates (individual data points not presented) displaying exponential growth are shown. Error bars are ± 1 standard deviation from the mean (n = 3).

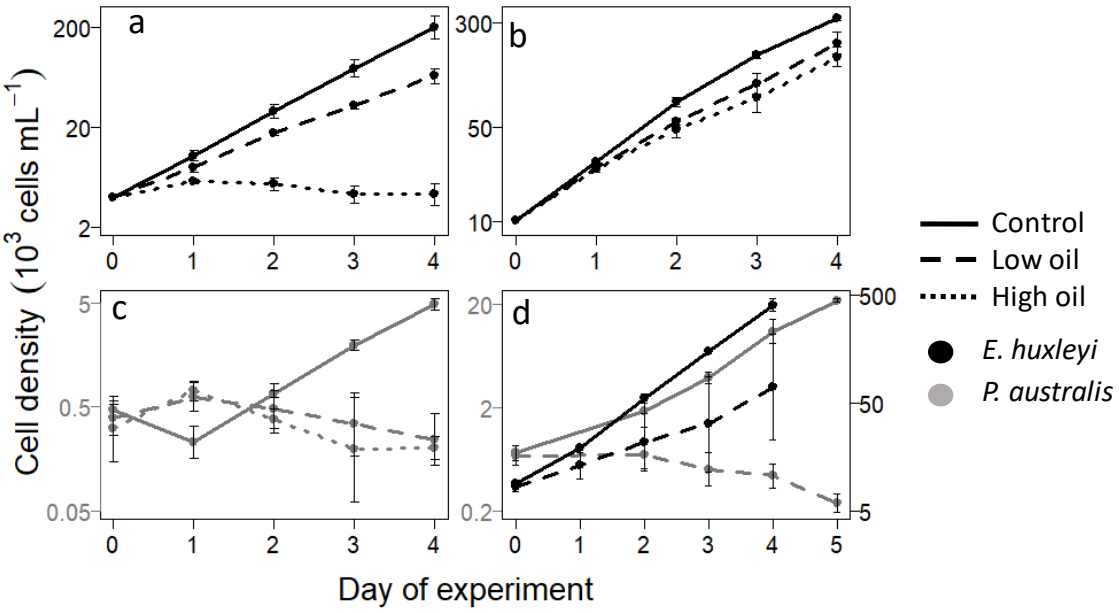

Fig. 1.2. Growth curves (note the log-scale) for the four independent oil exposure experiments conducted. Panels a-d represent experiments 1-4 respectively (refer to legend of Fig. 1 or Table 1 for descriptions of individual experiments). Error bars are ± 1 standard deviation from the mean (n = 3).

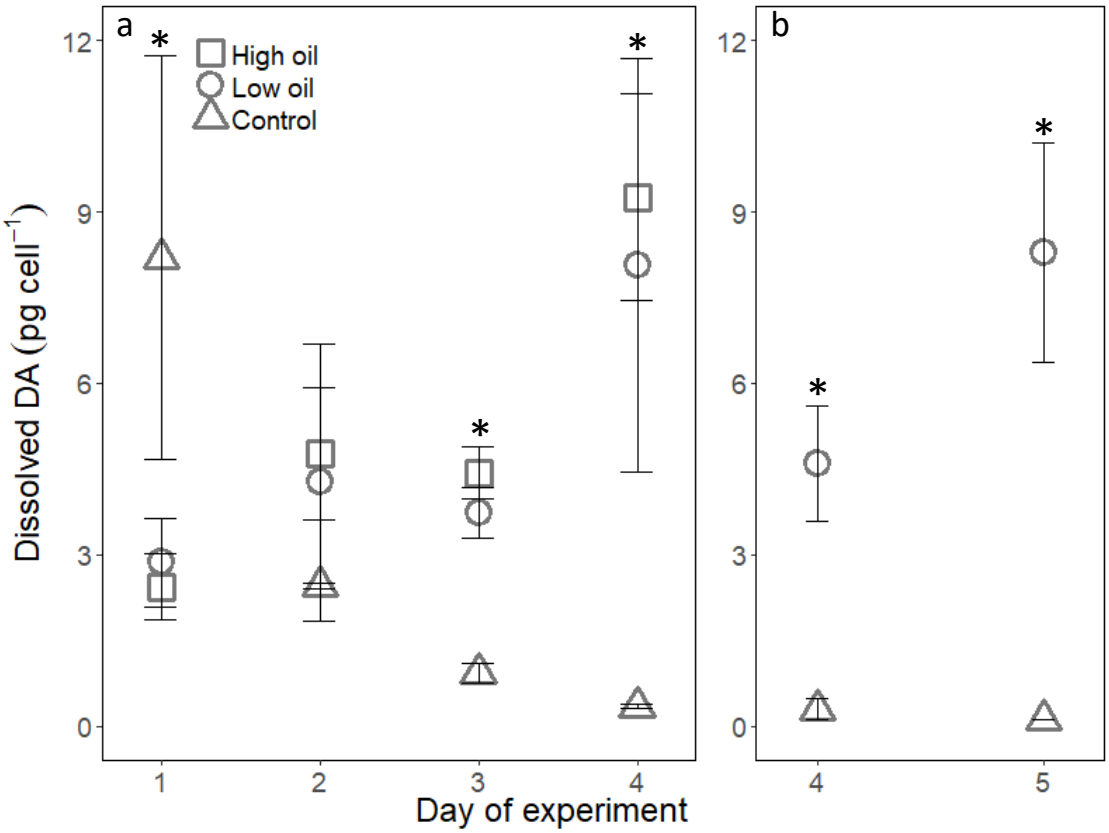

Fig. 1.3. Dissolved domoic acid (DA) normalized to cell abundance measured in the growth media over time in experiments 3 (a) and 4 (b) (refer to legend of Fig. 1 or Table 1 for descriptions of individual experiments). The days for which the data are not shown (day 0 in experiment 3 and days 0-3 in experiment 4) had dissolved DA concentrations below the limit of detection (0.52 ng mL^{-1}). Asterisks represent significant differences among treatments at each time point ($\alpha = 0.05$). Error bars are ± 1 standard deviation from the mean (n = 3 or 2 [below detection limit values removed]).

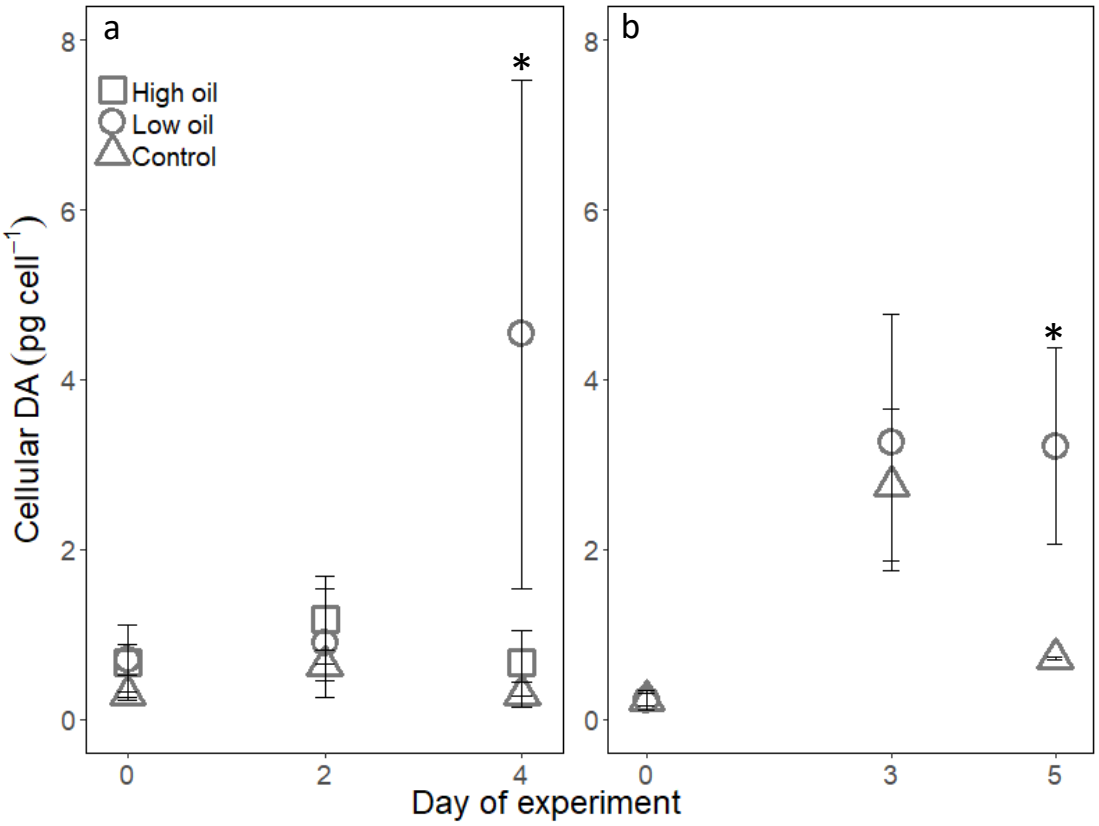

Fig. 1.4. Cellular domoic acid (DA) measured over time in experiments 3 (a) and 4 (b) (refer to legend of Fig. 1 or Table 1 for descriptions of individual experiments). Asterisks represent significant differences among treatments at each time point (α = 0.05). Error bars are ± 1 standard deviation from the mean (n = 3).

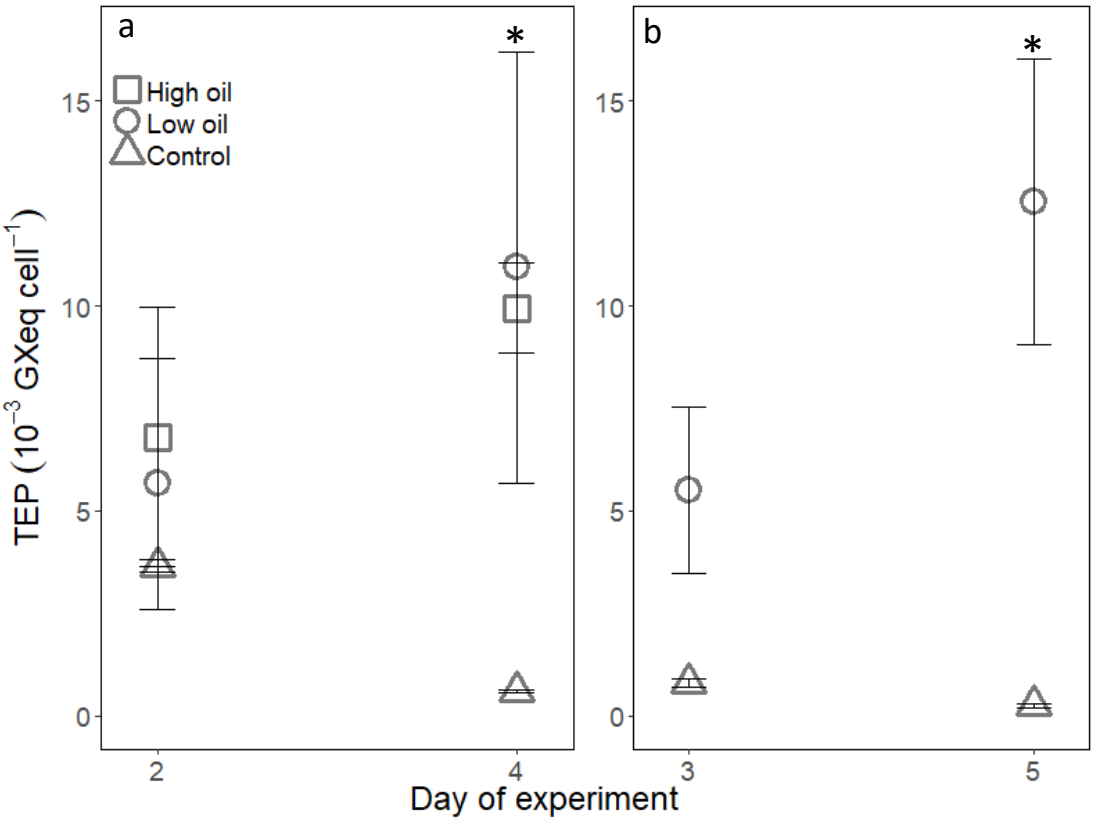

Fig. 1.5. Transparent exopolymer particle (TEP) concentration normalized to *P. australis* cell abundance (Gum Xanthan equivalents per cell) for experiments 3 (a) and 4 (b) (refer to legend of Fig. 1.1 or Table 1.1 for descriptions of individual experiments). Asterisks represent significant differences among treatments at each time point ($\alpha = 0.05$). Error bars are ± 1 standard deviation from the mean (n = 3).

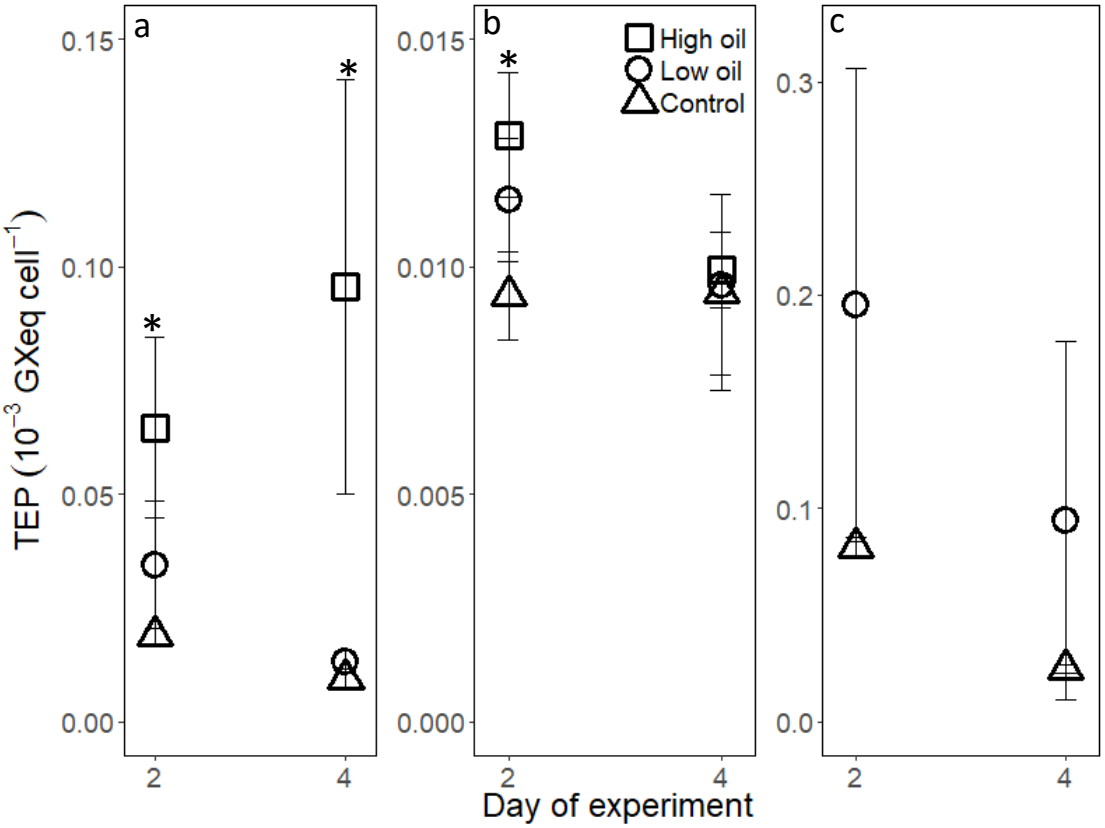

Fig. 1.6. Transparent exopolymer particle (TEP) concentration normalized to *E. huxleyi* cell abundance (Gum Xanthan equivalents $cell^{-1}$) for experiments 1 (a), 2 (b), and 4 (c) (refer to legend of Fig. 1.1 or Table 1.1 for descriptions of individual experiments). Asterisks represent significant differences among treatments at each time point ($\alpha = 0.05$). Error bars are ± 1 standard deviation from the mean (n = 3).

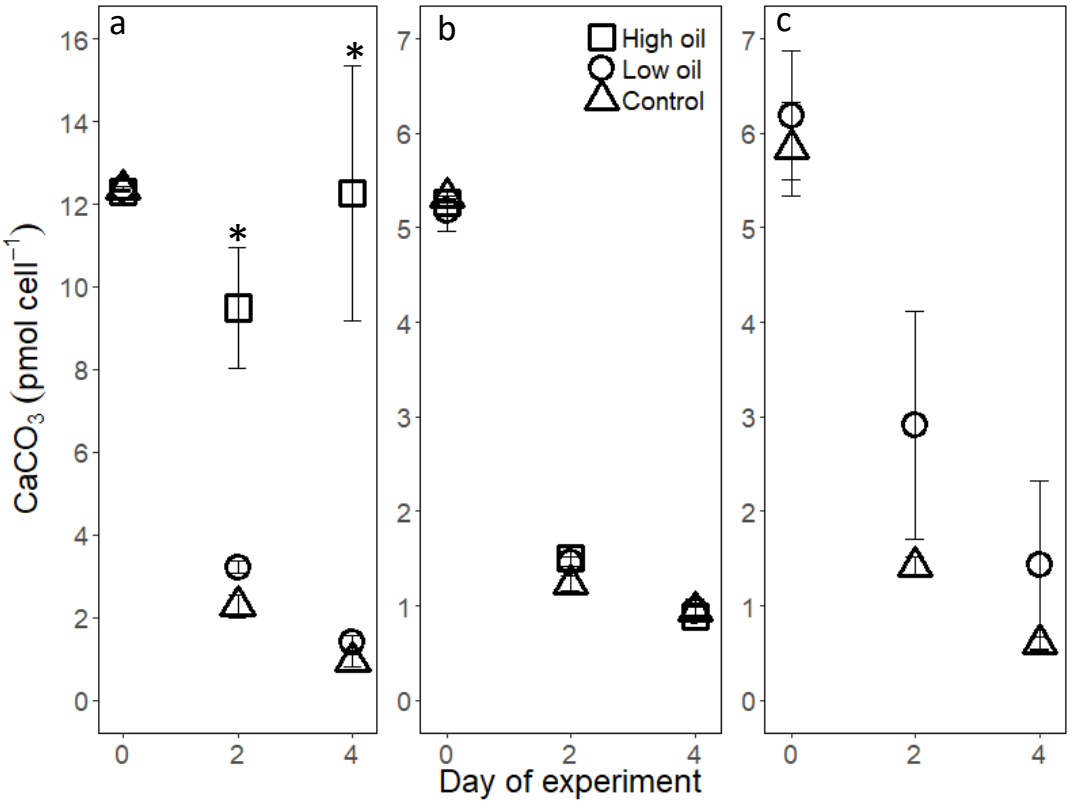

Fig. 1.7. Cellular calcium carbonate ($CaCO_3$) in *E. huxleyi* cultures for experiments 1 (a), 2 (b), and 4 (c) (refer to legend of Fig. 1.1 or Table 1.1 for descriptions of individual experiments). Asterisks represent significant differences among treatments at each time point ($\alpha = 0.05$). Error bars are ± 1 standard deviation from the mean (n = 3).

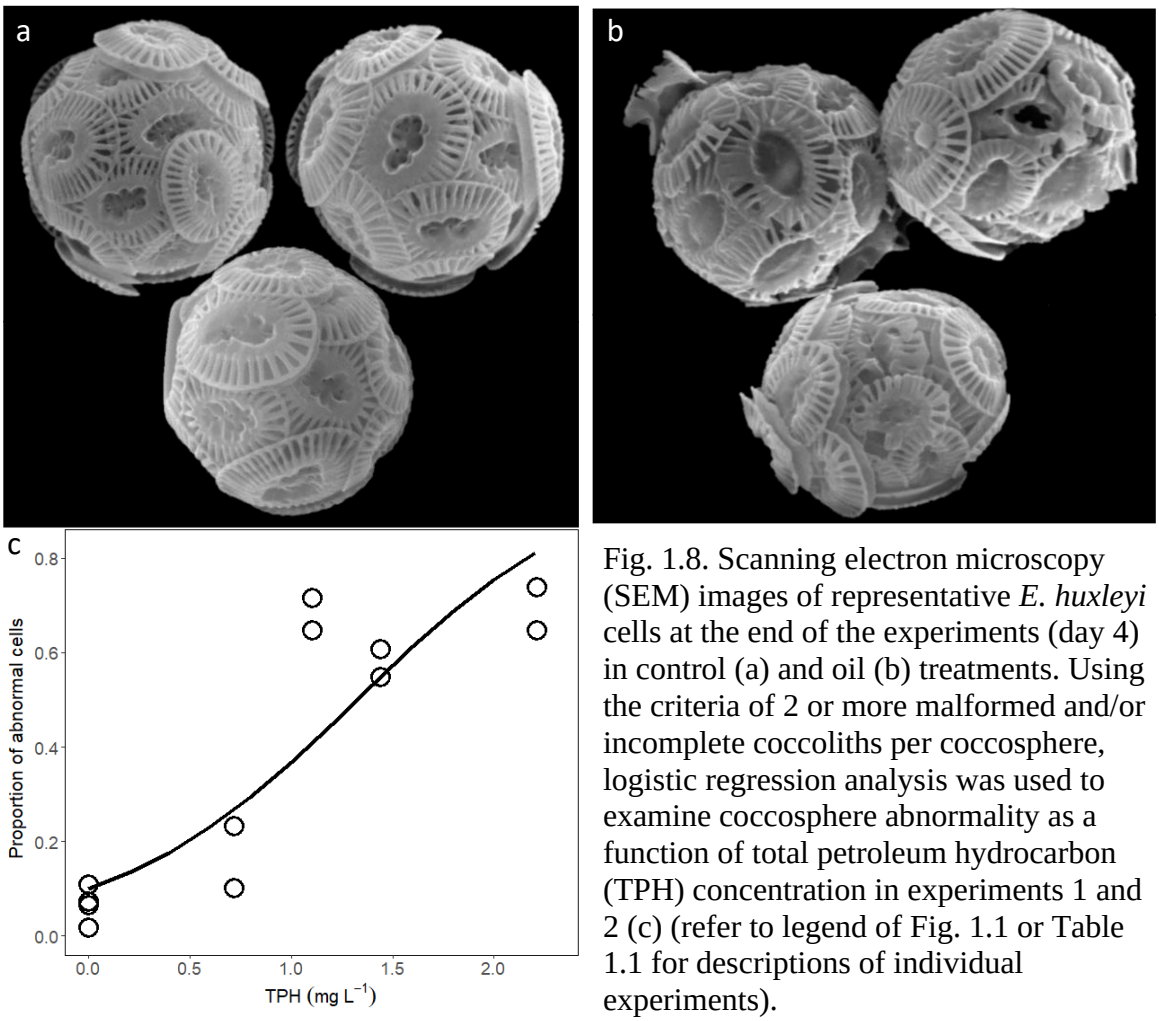

Fig. 1.8. Scanning electron microscopy (SEM) images of representative *E. huxleyi* cells at the end of the experiments (day 4) in control (a) and oil (b) treatments. Using the criteria of 2 or more malformed and/or incomplete coccoliths per coccosphere, logistic regression analysis was used to examine coccosphere abnormality as a function of total petroleum hydrocarbon (TPH) concentration in experiments 1 and 2 (c) (refer to legend of Fig. 1.1 or Table 1.1 for descriptions of individual experiments).

Chapter 2

Wildfire ash deposition fertilizes coastal marine ecosystems

T. M. Ladd[1*], D. Catlett[1], M. A. Maniscalco[1], S. M. Kim[2], R. L. Kelly[3], S. G. John[3], C. A. Carlson[1,2,4], M. D. Iglesias-Rodríguez[2,4]

[1]Interdepartmental Graduate Program in Marine Science, University of California, Santa Barbara, CA, USA.

[2]Marine Science Institute, University of California, Santa Barbara, CA, USA.

[3]Department of Earth Sciences, University of Southern California, Los Angeles, CA, USA.

[4]Department of Ecology, Evolution, and Marine Biology, University of California, Santa Barbara, CA, USA.

2.1 Abstract

Large wildfire events influenced by a changing climate, forest management practices, and human caused ignitions have become more frequent in recent years (Pausas & Keeley 2021). In December 2017, one of the largest wildfires in California history, the Thomas Fire, scorched over 1140 km^2 of coastal California, creating a large smoke and ash plume that extended over the northeastern Pacific Ocean (CalFire 2021a, CalFire 2021b). Despite significant research on wildfire effects in terrestrial systems, the impact of these events on marine ecosystems have rarely been considered. In this study, we explored the implications of wildfire ash deposition on seawater chemistry and microbial communities by conducting experiments off the California coast during the Thomas Fire. Leaching of ash in seawater resulted in significant additions of nutrients that fueled the growth of microbial communities.

We argue that large fire events are important atmospheric sources of nutrients, particularly nitrogen, to coastal marine systems where ash acts as a 'food for all' by promoting the growth of diverse marine protists.

2.2 Introduction

In December 2017, the Thomas Fire became the largest California fire in modern history, though it has since been surpassed by seven other fires (CalFire 2021b). The Thomas Fire ignited in Ventura County (CA, USA) on December 4, 2017 and burned ~1140 km^2 before being fully contained on January 12, 2018 (CalFire 2021a). Satellite imagery showed a large plume of smoke and ash that extended > 1000 km offshore near the Santa Barbara Channel (SBC) and led to persistent but spatially variable ash deposition into the SBC throughout December (Fig. 2.1). Marine environments are likely influenced by nearby fire activity through atmospheric deposition of ash, though the impacts of wildfire ash on marine ecosystems remain largely unknown.

Here, we show that atmospheric deposition of wildfire ash fertilizes coastal marine protist communities and serves as a 'food for all' by leaching a diverse mixture of inorganic nitrogen species and other nutrients when deposited in seawater. Incubation experiments were conducted during a research cruise off the California coast during the Thomas Fire in which wildfire ash leachate was added at high (0.25 g ash L^{-1}) and low (0.08 g ash L^{-1}) concentrations to seawater samples containing natural microbial communities. Initial communities were collected from two locations along the California coast: offshore San Diego (SD) and the SBC (Fig. 2.1). Particulate organic carbon (POC) concentrations (representing approximate community biomass), nutrient (nitrate, nitrite, phosphate, silicic

acid) concentrations, and community composition (18S rDNA metabarcoding) were compared between ash and control (no ash) treatments during 4-day incubations.

2.3 Materials and methods

2.3.1 Environmental setting

Two incubation experiments were conducted on the RV Sally Ride during the ACIDD cruise (Bisson et al. 2020, Kramer et al. 2020), one with water collected offshore San Diego, California (SD) (32.867°, -117.734°) and the other from within the Santa Barbara Channel, California (SBC) (34.250°, -119.906°) (Fig. 2.1). These different water masses were selected to expose microbial communities to surface waters less impacted by recent ash deposition (SD) and waters already exposed to ash deposition from the Thomas Fire (SBC). Each incubation was conducted over 4 days (SD - Dec 16-20, SBC - Dec 17-21) in ~2.3 L polycarbonate bottles within an incubation tank on board the RV Sally Ride deck with flowing seawater and a mesh screen to simulate light at 5 m depth.

2.3.2 Ash collection and leachate

Ash samples were collected from the Santa Barbara, California and Carpinteria, California areas during the Thomas Fire by carefully brushing ash deposited on car windshields into combusted glass jars (4 h at 450 ˚C) with Teflon lined lids. Next, samples were homogenized with mortar and pestle in the laboratory on combusted foil (4 h at 450 ˚C), transferred into new 60 mL EPA certified jars (4 h at 450 ˚C), and stored in the dark at room temperature. Homogenized ash (20 g) was added to 1 L of 0.2 µm-filtered isotonic seawater in an acid washed polycarbonate bottle and left in darkness at 15˚C on a shaker

table rotating at 100 rpm for 24 hours. The mixture was then vacuum filtered through a 0.2 µm polycarbonate filter to remove particulate ash and stored as aliquots in polycarbonate bottles at -20 ºC. An aliquot of the stock leachate was thawed and diluted with filtered seawater (1 mL leachate:14 mL seawater) before being measured in triplicate for inorganic nutrient concentrations (nitrate + nitrite, nitrite, ammonium, phosphate, and silicic acid).

During a follow up study, ash leachate was created by weighing 17-20 g of homogenized ash into a 2 L borosilicate bottle and adding 1.7-2 L of 0.2 µm filtered seawater (for a final concentration of 10 g ash L^{-1}) collected in the SBC from four different times of the year (n=4). The mixture was shaken gently and allowed to sit for an hour before vacuum filtering out the particulate ash (0.2 µm Millipore Steritop filter). The background seawater without added ash was processed in the same way as the ash leachate (double filtered through a 0.2 µm filter and stored in borosilicate bottles). The addition of total and organic macronutrients, organic carbon, and metals due to ash were determined by subtracting the paired filtered seawater sample concentrations for each of the four leachate batches and averaging.

Diluted leachate samples (0.5 g ash L^{-1}) and background filtered seawater for inorganic nutrient (nitrate + nitrite, ammonium, and phosphate) and total dissolved nitrogen (TDN) and phosphorus (TDP) analysis were collected in borosilicate scintillation vials (inorganic nutrients) or HDPE vials (TDN/TDP) and stored at -20 ºC until further processing and analysis. Simultaneous analysis of TDN and TDP was conducted using the alkaline persulfate oxidation method adapted from Valderrama (1981). Briefly, 10 mL of thawed sample was transferred to acid washed and combusted (4 h at 450˚C) glass tubes with Teflon lined caps, 2 mL of oxidation reagent (0.5 M boric acid, 0.2 M potassium persulfate, 0.35 M

sodium hydroxide) was added, and tubes were capped and gently inverted 3-5 times. Oxidation reagent blanks were analyzed to subtract any nitrogen or phosphorus contamination from the oxidation reagent. The tubes were then autoclaved (liquid cycle: 30 minutes, 121 °C, 20 psi), cooled, and stored in the dark at room temperature until flow injection analysis of nitrate + nitrite and phosphate (QuikChem 8000, Zellweger Analytics) at the University of California, Santa Barbara (UCSB) Marine Science Institute (MSI) Analytical Laboratory. Inorganic nutrient samples were analyzed after thawing by flow injection analysis (QuikChem 8000, Zellweger Analytics) at the UCSB MSI Analytical Laboratory and used to calculate dissolved organic nitrogen (DON) and phosphorus (DOP) concentrations by subtracting from the TDN and TDP concentrations (DON = TDN – nitrate – nitrite – ammonium, DOP = TDP – phosphate).

Dissolved organic carbon (DOC) samples (30 mL of 10g L^{-1} leachate or background filtered seawater) were collected in combusted (4 h at 450 °C) 40 mL borosilicate vials and acidified with 50 µL of 4N HCl and stored at 15 °C until high-temperature combustion analysis using a Shimadzu TOC-V in the Carlson lab at UCSB (Carlson et al. 2010).

Samples for trace metal analysis (Fe, Zn, Pb, Ni, Cd, Mn, Co, and Cu) in the concentrated leachate (10 g ash L^{-1}) and the background filtered seawater were collected in 40 mL HDPE vials and stored at -20 ºC until further processing and analysis. Analyses were performed in a class-100 clean room at the University of Southern California. Filtered (<0.2 µm) leachate and background seawater samples were acidified to pH 2 using distilled HCl and stored for >12 months. 15 mL subsamples of the filtered leachate and seawater were aliquoted and amended with 50 µL of an isotope spike (which includes the following: ^{57}Fe, ^{62}Ni, ^{65}Cu, ^{67}Zn, ^{207}Pb, ^{110}Cd). Using a SeaFAST device (Elemental Scientific) spiked

samples were then extracted onto a column with Nobias chelating resin PA-1 (Sohrin et al. 2008) at pH ~ 6 with an ammonium acetate/acetic acid buffer, and the preconcentrated sample was eluted into 0.5 mL 1 M HNO_3 which included 1 ppb In. Final concentrations in all samples were measured on an Element 2 inductively coupled plasma mass spectrometer (ICP-MS, Thermo Fisher Scientific). Concentrations for all elements except Mn and Co were derived using an isotope dilution method (Hawco et al. 2020). Mn and Co concentrations were quantified relative to a 10 ppb multielement standard.

2.3.3 Experiment setup

Each incubation experiment was prepared by collecting water from ~5m depth in Niskin bottles attached to a CTD Rosette. Approximately 60 L of water from multiple Niskin bottles was prefiltered through a 200 µm nylon mesh and combined into a single 60 L bottle and gently mixed. Initial samples (n=3) for protist community composition (DNA metabarcoding) were directly sampled from the 60 L bottle. The remaining water was used to fill three 20 L bottles with a volume of 16 L each (one for each treatment – high (H) ash concentration, low (L) ash concentration, and control (C) (no ash)). Aliquots of 200 mL and 65 mL of the ash leachate (20 g L^{-1}) were added to the H and L treatment vessels respectively for final concentrations of 0.25 g ash L^{-1} (H) and 0.08 g ash L^{-1} (L). The 20 L bottles were gently mixed and samples were collected for particulate organic carbon (POC) and inorganic nutrients (nitrate + nitrite, nitrite, phosphate, and silicic acid). The remaining water from each 20 L bottle was then used to fill six ~2.3 L transparent polycarbonate bottles that were subsequently placed into the incubation tank on deck. Due to the timing of CTD casts and water collection, the two incubations were set up at different times of the day such that the SD and SBC incubations started at 14:30 on December 16 and 09:30 on December 17

respectively. Despite the different initial starting times, sampling occurred every other day for each incubation at 06:00.

2.3.4 Sampling and analysis

After the initial experimental setup and sampling (referred to as "T0" or "day 0" throughout the manuscript), samples were taken for POC, DNA metabarcoding, and inorganic nutrients on days 2 and 4 after each incubation start. Each treatment (H, L, and C) was sampled sacrificially from triplicate bottles.

Samples for POC (500 mL) were vacuum filtered onto pre-combusted glass fiber filters (0.7 µm, 25mm, Whatman) and stored in pre-combusted glass scintillation vials at -20 ºC. Analyses for POC samples were conducted on acidified filters using the Dumas combustion method in an automated elemental analyzer (Model CE-440HA, Exeter Analytical) at the UCSB MSI Analytical Laboratory.

Inorganic nutrient samples were collected by using positive pressure to filter water through a 0.2 µm polycarbonate filter (Isopore, EMD-Millipore). Plastic scintillation vials were rinsed 3 times with the sample before collecting ~15 mL. Samples were frozen at -20 ºC until further processing and analysis. Inorganic nutrients (nitrate + nitrite, nitrite, phosphate, and silicic acid) were analyzed after thawing by flow injection analysis (QuikChem 8000, Zellweger Analytics) at the UCSB MSI Analytical Laboratory.

Samples for DNA metabarcoding (1 L for all samples except SBC initial samples (2 L)) were vacuum filtered onto 1.2 µm polycarbonate filters (Isopore, EMD-Millipore), placed in 4 mL cryovials, and submerged in liquid nitrogen < 15 min after collection. Samples were moved to -80 ºC for longer term storage until DNA extraction. Extraction of

genomic DNA from the filters followed the protocol described by the AllPrep Mini Kit (Qiagen) after lysis of cells by bead beating in lysis buffer (RLT Plus + β-mercaptoethanol; Qiagen). Briefly, filters were transferred to prefilled bead-beating tubes (100 µm acid washed Zirconium Beads, Benchmark Scientific), 800 µL lysis buffer was added, tubes were secured horizontally to a Fisherbrand Scientific Vortex Mixer, and bead-beating was carried out at maximum speed (~ 3200 rpm) for 2 minute increments (x3) with chilling on ice for 2 minutes between each round. The tubes were centrifuged briefly and ~500 µL supernatant was transferred to the AllPrep DNA column. All purification steps were followed according to the manufacturer's instructions. Extracted DNA was stored at -20 °C.

Amplification of the V9 hypervariable region of the 18S rRNA gene and Illumina library preparation followed protocols described by Catlett and colleagues (2020). Briefly, a one-step polymerase chain reaction (PCR) using custom dual-indexed primers (Stoeck et al. 2010, Kozich et al. 2013, Catlett et al. 2020) was carried out using 0.4 µM of each primer and 1x KAPA2G Robust Hotstart ReadyMix (KAPA Biosystems). Samples were amplified in duplicate 25 µL reactions with 1 µL genomic DNA template and thermal cycling conditions as follows: 94 ºC for 3 min; 35 cycles of 94 ºC for 45 s, 65 ºC for 15 s, 57 ºC for 30 s, and 72 ºC for 90 s; 72 ºC for 10 min; 4 ºC until storage at -20 ºC. Duplicate reactions were pooled before proceeding with Illumina library preparation and sequencing. PCR products were first purified and normalized using the SequalPrep Normalization Plate Kit (Applied Biosystems), pooled in equal volumes into a single library, and concentrated with Amicon Ultra-0.5 Centrifugal Filter Devices (Millipore). Concentrated products were then further purified using the Qiagen QIAquick Gel Extraction kit, and concentrated a second time (Amicon Ultra-0.5 Centrifugal Filter Device). The concentration of the final library was

quantified using the Qubit 3.0 dsDNA High Sensitivity kit. Library sequencing was performed using a MiSeq PE150 v2 kit (Illumina) at the DNA Technologies Core of the University of California Davis (UCD) Genome Center.

2.3.5 Processing and analysis of sequencing data

Demultiplexed sequencing data obtained from UCD were processed with the DADA2 pipeline (v1.16.0; Callahan et al. 2016) and followed procedures described by Catlett and colleagues (2020). Briefly, forward and reverse reads were trimmed to 140 nt and 120 nt respectively, then filtered (maxEE = 2, truncQ = 2) and denoised according to the standard DADA2 workflow (https://benjjneb.github.io/dada2/tutorial.html). Paired reads were merged, overhanging sequences were trimmed, and chimeras were removed (method = "consensus"). ASVs shorter than 90 nt or longer than 180 nt (target amplicon is 120-130 nt) were discarded.

Initial taxonomic assignments of amplicon sequence variants (ASVs) were computed with the IDTAXA algorithm (DECIPHER package v2.16.1; Murali et al. 2018) (henceforth, idtaxa), the naive Bayesian classifier implemented in DADA2 (Wang et al. 2007, Callahan et al. 2016) (henceforth, bayes), and the Lowest Common Ancestor algorithm implemented in MEGAN6 (Huson et al. 2007) (henceforth, LCA) using both the Protistan Ribosomal Reference database v4.12.0 (PR2; Guillou et al. 2013) and the SILVA SSU nr reference database v138 (Silva; Quast et al. 2013) available for the DADA2 pipeline (https://benjjneb.github.io/dada2/training.html). The idtaxa and bayes algorithms used a minimum bootstrap confidence threshold of 50%, while the LCA algorithm was implemented using the default settings in MEGAN6.

To maximize the number of ASVs that could be identified as protists and reduce bias from using any single taxonomic assignment derived from a given algorithm and reference database (Catlett et al. 2020), we implemented the recently developed ensembleTax R package (v1.0.2, https://cran.r-project.org/web/packages/ensembleTax/index.html) to compute ensemble taxonomic assignments based on the six independent collections of taxonomic assignments. Taxonomic assignments determined with the Silva reference database and the MEGAN LCA algorithm (which maps all assignments to the NCBI taxonomic nomenclature) were mapped onto the taxonomic nomenclature used by PR2 using the taxmapper algorithm. Where taxonomic names were not able to be mapped, the collection of taxonomic synonyms included with the ensembleTax package was considered (synonym.file = "default", ignore.format = TRUE). Since PR2 does not include bacterial or archaeal sequences, sequences assigned to these domains from the Silva database were retained at the "Kingdom" rank when mapped onto PR2.

Following mapping of all taxonomic assignments onto the PR2 taxonomic nomenclature, ensemble taxonomic assignments were computed for each ASV at each taxonomic rank as the highest frequency assignment predicted by the six individual methods, ignoring non-assignments. In the event that multiple taxonomic assignments were found at equivalent maximum frequencies across the individual methods, those determined using the idtaxa or (if the idtaxa assignment was not one of the highest frequency assignments) the bayes algorithm were prioritized, and the PR2 reference database was prioritized over the Silva database (similar to the approach employed by Catlett and colleagues (2020). Overall, this approach to determine ensemble taxonomic assignments increases the proportion of ASVs with assigned taxonomy at the likely expense of increased false positive annotations.

However, because we focus our analysis on broad taxonomic groupings our analysis should be largely robust to false positive annotations.

To focus our analysis on protists, ASVs classified as Bacteria, Archaea, Metazoa, Fungi, Streptophyta, Rhodophyta, or Ulvophyceae were removed. ASVs with no assigned taxonomy at the Kingdom or Supergroup rank, and those assigned to the Supergroups Opisthokonta or Archaeplastida but not assigned to a Division (or assigned to an ambiguous Division, e.g. "Opisthokonta_X") were also discarded. Finally, ASVs that only appeared in a single sample were removed. Following these pre-processing procedures, sequencing depth varied across the samples considered here (min = 15,818, max = 70,660, mean = 34,995 following the above preprocessing procedures). To mitigate bias arising from uneven sequencing depth, sequences were subsampled without replacement to the minimum library size (15,818 reads per sample).

Finally, to determine whether ash leachate is likely to favor some nutritional strategies over others, we assigned ASVs to trophic functional groups following the guidelines provided by Mitra and colleagues (2016) based on the ensemble taxonomic assignments. ASVs were classified into one of the following groups: phototroph, heterotroph, parasite, constitutive mixotroph, non-constitutive mixotroph, or unknown. Here phototrophs include organisms that meet their energy demands exclusively by photoautotrophy, heterotrophs are consumers that ingest other organisms to meet their energy demands, parasites are heterotrophs where part of their life cycle involves infection of a host organism, and (non-)constitutive mixotrophs are capable of both photoautotrophy and heterotrophy and (do not) have an inherent capacity for photosynthesis. We first compiled a collection of taxonomic names with corresponding trophic functional group(s) based on Adl and

colleagues (2019) and supplemented this with similar data from various other sources (Ramond et al. 2019, Dumack et al. 2020, Schneider et al. 2020). To assign ASVs to functional groups, each ASV's ensemble taxonomic assignment at the lowest assigned rank (e.g. Species if available, otherwise Genus, etc) was mapped to the corresponding functional group. If data was not available to link a particular taxonomic name to a functional group, the assigned taxonomic name at the next lowest rank was used until a match was found or no other taxonomic names were available for the ASV being mapped.

No-template control PCR products (2) and mock community samples (2) (Catlett et al. 2020) were included as negative and positive controls in the sequencing analysis to ensure minimal contamination and precise sequencing results. The no-template control PCR products had only 21 or 1106 total protist sequence reads from 3 or 4 unique protist amplicon sequencing variants (ASVs) in each of the samples. The ASV contributing the majority of the reads in the more contaminated blank (1097/1106 total reads) was not found in any experimental samples. All 22 target ASVs were detected in both mock community replicates in similar proportions to those observed previously (Catlett et al. 2020) although 1 or 2 spurious protist ASVs also contributed a cumulative total of 0.006% and 0.02% of sequence reads in each sample. Two additional spurious protist ASVs that differed from two target ASVs by a single nucleotide at the 3' end were found in one or both of the mock community samples, suggesting that DADA2's denoising approach may have been less effective than previously observed for similar samples (Catlett et al. 2020). However, upon further inspection we found no evidence for similarly differing sequences (a single nucleotide at the 3' end) in experimental samples, suggesting that these denoising errors may be an artifact

arising from the low diversity mock community samples and do not impact our analyses of the experimental samples.

2.3.6 Estimation of protistan group POC variations

To estimate the POC contribution of protistan groups, we scaled the cumulative relative sequence abundances of ASVs within each protistan group considered in our analysis to concurrently determined POC concentrations. Our goal in this analysis was to assess whether the decrease in relative abundances of some protistan groups in response to ash leachate exposure was due to negative impacts of ash leachate on these organisms, or to compositional artifacts. While high variation in 18S rRNA gene copy number obscures the relationships between protistan relative sequence and cell abundances, 18S rRNA gene copy number scales roughly with cell size and biovolume across diverse protistan lineages (Zhu et al. 2005, Godhe et al. 2008) and cellular carbon to biovolume relationships are relatively consistent across taxonomically diverse protist groups (Menden-Deuer & Lessard 2000), suggesting that relative sequence abundances provide an approximation of the POC proportion associated with each protistan group. While the magnitude of POC associated with specific protistan groups is likely biased due to myriad factors, first-order assessments of the variability in protistan group POC concentrations as done here are likely robust assuming the observed variability in POC concentrations in our experiments is driven primarily by (or is directly proportional to) protist community carbon biomass production.

2.3.7 Statistical analysis

Statistical analyses were conducted using R Studio (v1.3.959; base R v4.0.1) and JMP Pro 15. Statistically significant additions ($p<0.05$) of inorganic nutrients due to ash were

determined using a t-test after testing for normality (JMP Pro 15). Statistically significant additions ($p<0.05$) of organic nutrients and metals in the leachate samples were determined using a paired t-test (or paired Wilcoxon signed rank test) after analyzing the distributions for normality (JMP Pro 15). To determine differences in POC or nutrient concentrations between treatments at each time point or across incubations, data were analyzed for normality of residuals and homogeneity of variances before conducting analysis of variance (ANOVA) tests and Tukey HSD post-hoc pairwise comparisons when necessary. For nutrient concentrations measured as below the analytical limit of detection (LOD) (nitrate + nitrite: 0.2 µM, nitrite: 0.1 µM, phosphate: 0.1 µM, ammonium: 0.2 µM, silicic acid 1.0 µM), values were replaced with ½ LOD and only used in statistical analyses when just 1 replicate was below the LOD. Analysis of sequencing data was also done in R Studio using the Phyloseq (v1.32.0), Vegan (v2.5.6), pairwiseAdonis (v0.0.1), and DESeq2 (v1.28.1) packages. For ordinations and analysis of significant differences in community composition, rarefied ASV counts were used to calculate Bray-Curtis dissimilarities, visualized with principal coordinates analysis (PCoA), and significant differences between groups were tested using a permutational multivariate analysis of variance (PERMANOVA) (adonis function, Vegan) and a pairwise PERMANOVA (pairwise.adonis2 function, pairwiseAdonis) (when necessary) after assessing homogeneity of variances (betdisper function, Vegan). Significant differences ($p_{adjusted} < 0.05$) in major taxonomic groups (Division or Class level of the 10 most abundant Divisions across all samples) between treatments at days 2 and 4 were tested with pairwise t-tests or pairwise Alexander-Govern tests (heteroscedasticity, Levene test) for comparisons of interest (H vs. C or L vs. C and differences greater than 1% at day 2 and 2% at day 4) and p-values were adjusted for multiple testing across all tests at a given time point

according to the Benjamini-Hochberg (BH) method. Although the Chlorophyta division was on average greater than 2% more abundant in the high ash treatment compared to the control on day 4 of the SD incubation, the distribution was found to have non-normal residuals (Anderson-Darling goodness of fit test) and was excluded from analysis. Triplicate POC-scaled relative sequence abundances at day 4 (representing estimated POC associated with a given protistan taxonomic group) were $\log_2$ transformed before statistical analysis. Significant differences ($p < 0.05$) in $\log_2$ transformed POC-scaled relative sequence abundance between treatments for each of the major taxonomic groups at day 4 were initially tested with one-way ANOVA or Alexander-Govern (heteroscedasticity, Levene test $p < 0.05$) tests. Pairwise tests (t-tests or Alexander-Govern tests) for significantly different groups were then assessed for comparisons of interest (H vs. C or L vs. C) and p-values were adjusted for multiple testing across all tests according to the BH method ($p_{adjusted} < 0.05$). Differences between ash (H and L) versus control are displayed as approximate $\log_2$ fold changes represented by the difference in the mean $\log_2$ transformed POC-scaled relative sequence abundance of the H or L treatments minus the C treatments for the SD and SBC incubations. Differential relative abundance of individual ASVs in ash treatments (H or L) compared to the control treatment across both days 2 and 4 were analyzed separately for each incubation with DESeq2 (default settings except alpha = 0.05). Before DESeq2 analysis, any ASV that was not present in at least two samples or was never found at more than 0.01% relative abundance from the samples tested was removed to focus the analysis on prevalent and abundant taxa.

2.4 Results and discussion

2.4.1 Nutrient fertilization via wildfire ash deposition and leaching

Addition of ash to seawater caused leaching of nitrate, nitrite, ammonium, and silicic acid (Fig. 2.2a). Thomas Fire ash leached high concentrations of nitrite (7.3 ± 0.1 μmol NO_2^- $g_{(ash)}^{-1}$) and ammonium (6.1 ± 0.2 μmol NH_4^+ $g_{(ash)}^{-1}$) relative to nitrate (2.0 ± 0.1 μmol NO_3^- $g_{(ash)}^{-1}$) and silicic acid (1.2 ± 0.2 μmol $Si(OH)_4$ $g_{(ash)}^{-1}$). However, phosphate concentrations (PO_4^{3-}) were not significantly increased. Subsequent experiments revealed increased concentrations of metals (iron, nickel, cobalt, and copper), dissolved organic nitrogen (DON), and dissolved organic carbon (DOC) following ash leaching in seawater (Tables S1-S2).

The enrichment of inorganic and organic nutrients from the Thomas Fire ash was expected based on similar observations of wildfire ash in freshwater systems (Smith et al. 2011) and deposition of other atmospheric aerosols to marine systems (Jickells & Moore 2015, Mahowald et al. 2017). However, the lack of PO_4^{3-} (Fig. 2.2a) and organic phosphorus (Table S1) leached from Thomas Fire ash was surprising given that wildfires have been shown to increase concentrations of atmospheric phosphorus (Zhang et al. 2002) and dissolved phosphorus in fire impacted watersheds (Spencer & Hauer 1991). Our data suggests that wildfires are not an important source of bioavailable phosphorus to coastal ecosystems although differences in fire conditions, fuel type, and atmospheric transport may alter phosphorus dynamics during different wildfire events (Vicars et al. 2010, Hogue & Inglett 2012). While iron, phosphorus, or other nutrients may sometimes limit primary production, many marine systems, including the California Current System, are considered nitrogen limited (Moore et al. 2013, Deutsch et al. 2021). Indeed, the initial ratios of nitrate + nitrite to phosphate in the control surface seawater from SD and the SBC were approximately

1:1 and 1.5:1 (mol:mol) respectively (Table S3), indicating significant initial nitrogen limitation (N:P < 16:1) at the time of the Thomas Fire, while Thomas Fire ash leachate was nitrogen-rich relative to typical requirements of marine organisms (N:P > 16:1 and N:Fe > 16:0.0075) (Ho et al. 2003) (Fig. 2.2a, Tables S1-S2). Wildfires may thus be more important episodic sources of bioavailable nitrogen to oceanic systems with the potential to relieve local nitrogen limitation compared to other types of atmospheric aerosols such as anthropogenic pollutants, volcanic ash, and desert dust (Fig. 2.3). Although anthropogenic aerosols are also nitrogen-rich, they are often more diffuse than pulses of wildfire ash and therefore may not elicit similarly intense biological responses (Guieu et al. 2014).

Experimental incubations with natural microbial communities exposed to Thomas Fire ash leachate exhibited increased POC concentrations as concentrations of nitrate plus nitrite and phosphate decreased over time (Fig. 2.2bc, Fig. B1), demonstrating that the supplementary nitrogen leached from the ash fueled primary production. Over the first two days of the incubations, the change in POC relative to the control was more than 2-fold higher in the SBC compared to the SD ash treatments, revealing a lagged growth response of the SD microbial communities to ash leachate. We attribute the slower SD POC response to differences in Thomas Fire ash preconditioning. Indeed, satellite images showed that SD communities were outside the area of ash deposition while SBC communities were exposed to ash and smoke for ~13 days prior to sampling (Fig. 2.1). However, by day 4 POC in the SD incubation was 154% and 84.5% greater in high and low ash treatments compared to the control, respectively (Fig. 2.2b). Similar magnitudes of POC increase were observed in the SBC high (126%) and low (59%) ash treatments at day 4 (Fig. 2.2b). Along with inorganic

macronutrients, ash leachate-derived DOC, DON, and micronutrients (e.g., iron) (Tables S1-S2) may have contributed to the observed POC increase in ash treatments.

Upwelling along the central and southern California coast, occurring mainly in spring and early summer, is the largest nitrogen source to coastal surface waters. However, on smaller regional scales, atmospheric deposition and fluvial or wastewater discharge can dominate nitrogen fluxes (Howard et al. 2014). For example, in the nearshore SBC surface waters, atmospheric nitrogen deposition from natural and anthropogenic sources was estimated to account for the largest annually-integrated nitrogen flux (430 kg N km^{-2} yr^{-1}) (Howard et al. 2014). Spatiotemporal complexity of atmospheric aerosol deposition precludes precise quantification of Thomas Fire ash deposition to the SBC; however, based on the area burned (CalFire 2021a), average aboveground live biomass (4.2 kg m^{-2}) (Schrader-Patton & Underwood 2021), and assuming 60% of biomass was lost during combustion (Hogue & Inglett 2012) we estimate that ~1.9 x 10^9 kg of ash was produced by the Thomas Fire. If this ash was deposited throughout the SBC (~100 km x ~40 km) (Winant 2003), our leaching results (15 µM inorganic N $g_{(ash)}^{-1}$; Fig. 2.2a, Table S1) suggest that ~100 kg N km^{-2} (23% of the annually-integrated atmospheric flux) (Howard et al. 2014) would have been added to the SBC surface ocean during the 40 days of the Thomas Fire. Assuming Redfield stoichiometry, this amount of nitrogen addition could stimulate up to ~2.3 x 10^6 kg C of new production which is equivalent to ~3-10 times the estimated new production from large river discharge events in the SBC (Warrick et al. 2005). Based on these estimates, ash deposition from large coastal wildfires is expected to fertilize adjacent marine ecosystems, especially during periods of low nutrient concentrations in surface waters, such as in the absence of upwelling.

2.4.2 Protist community response to ash

Amplicon sequencing of the 18S-V9 rRNA gene revealed significant changes in protist community composition and POC production across protist groups (estimated as the product of POC and relative sequence abundances; see materials and methods) after exposure to Thomas Fire ash leachate (Fig. B2, Fig. 2.4, Fig. 2.5). Although the initial composition of the SD and SBC protist communities varied, we observed several commonalities in the responses of protist groups to ash exposure.

Ash exposure reduced the relative sequence abundance (henceforth, RA) of dinoflagellate (Division Dinoflagellata) amplicon sequence variants (ASVs). After four days of ash exposure, the cumulative RA of ASVs assigned to Dinophyceae and Syndiniales (both within Dinoflagellata) were reduced by 9-13% and 4-8% compared to controls, respectively (Fig. 2.4b). Additionally, 77% (SD) and 93% (SBC) of significantly differentially abundant Dinoflagellata ASVs had lower RA in ash than in control treatments (Fig. 2.5a, Fig. B3). Despite the reduction in dinoflagellate RA, estimated dinoflagellate POC increased (SD) or was not significantly different (SBC) in ash treatments compared to controls at day 4 suggesting that their growth was not inhibited by ash (Fig. 2.4b). Many Dinophyceae species exhibit slower growth rates than similarly sized cells from other taxonomic groups (Banse 1982, Tang & Peters 1995, Stolte & Garcés 2006), potentially explaining their reduced RA without a concomitant decrease in POC in ash treatments (Fig. 2.4). Putative marine parasites belonging to the Class Syndiniales are understudied but apparently ubiquitous and abundant in many marine systems (Guillou et al. 2008, Anderson & Harvey 2020). Counterintuitively, we found that the RA of Syndiniales ASVs decreased in treatments with increased overall

POC and (presumably) greater host density and a higher probability of host encounters. However, positive (possibly parasitic) associations of Syndiniales ASVs with Dinophyceae ASVs have been shown to be more common than with other protist groups (Anderson & Harvey 2020), suggesting that Syndiniales primarily parasitize Dinophyceae species. The reduction in host (Dinophyceae) RA may thus explain the reduced RA of Syndiniales ASVs. As the RA of dinoflagellate ASVs decreased, no single taxonomic group consistently grew to dominate the ash treatments (Fig. 2.4a). Rather, ASVs from 11 different Divisions had significantly higher RAs in ash treatments compared to controls across both incubations (Fig. 2.5a). The lack of a single taxonomic group consistently dominating the ash associated POC increase was unexpected given that diatoms (Class Bacillariophyta) are often the dominant responders to nutrient enrichment with high growth rates (Banse 1982, Furnas 1990) and a propensity to bloom following upwelling events off the coast of California (Wilkerson et al. 2006, Anderson et al. 2008). While diatom POC increased in response to ash exposure in both incubations, the magnitude of increase was comparable to that of Chlorophyta, Cryptophyta, and other groups (Fig. 2.4b), and none of the differentially abundant ASVs in the SD incubation were assigned as Bacillariophyta (Fig. 2.5a). Classification of ASVs to putative trophic strategies revealed that across both the SD and SBC incubations, ASVs with significantly higher RA in ash treatments were more commonly photoautotrophic than ASVs with higher RA in control treatments (Fig. 2.5b). Further, several of the ash-associated phototroph ASVs were identified as putative pico- or nano-phytoplankton (Table B5, Data S1) suggesting that smaller sized phytoplankton were more successful in ash compared to control treatments. Although ash leachate exposure generally favored small phototrophs and decreased dinoflagellate RA, by the end of the incubations the estimated POC of most major

protist groups was higher in ash treatments compared to controls (Fig. 2.4b). We thus propose that deposition of wildfire ash acts as a 'food for all' in coastal marine ecosystems via leaching of a diverse mixture of inorganic nitrogen sources (nitrate, nitrite, and ammonium), silicic acid, metals, and organic compounds.

Ash may serve as a 'food for all' by leaching various chemical forms of nitrogen that promote the growth of multiple protistan taxonomic groups simultaneously since nitrogen metabolism within and across taxonomic groups varies based on the available nitrogen source (Bronk et al. 2006, Kudela et al. 2008, Glibert et al. 2016). For example, diatoms are often considered nitrate opportunists with several physiological and metabolic traits that allow for rapid nitrate uptake, assimilation, and storage (Glibert et al. 2016), while other groups (e.g., chlorophytes, cyanobacteria, dinoflagellates) are associated with more reduced forms of nitrogen (Kudela et al. 2008, Glibert et al. 2016) and become proportionally more abundant when ammonium rather than nitrate is supplied to natural communities (Glibert et al. 2014). Further, the magnitude of nutrient addition by wildfire ash deposition is small relative to nutrient delivery via upwelling. This may also contribute to the lack of a dominant ash-responder as favorable conditions may not persist long enough to maintain high growth rates of a particular group. Other atmospheric deposition sources including anthropogenic pollution, volcanic ash, and desert dust generally provide low concentrations of various nutrients to ocean waters and thus may promote ecosystem responses more akin to those observed here (Fig. 2.3). However, studies of the impacts of other atmospheric deposition sources on marine ecosystems have focused on oligotrophic systems where iron or multiple co-limiting nutrients are required for primary production (Jickells & Moore 2015), making it difficult to compare to the nitrogen limited coastal system considered here. Even with

relatively small nutrient additions some deposition studies report community shifts toward diatom dominance (Romero et al. 2011, Guo et al. 2012, Mélançon et al. 2014, Zhang et al. 2017), though community responses are highly variable (Mills et al. 2004, Lekunberri et al. 2010, Romero et al. 2011, Jickells & Moore 2015). Complex trophic interactions may also be influenced by the magnitude of nutrient addition as seen in dust deposition studies in which bacterial and grazing responses were altered in communities exposed to low or high dust concentrations (Lekunberri et al. 2010, Romero et al. 2011). In our study, putative micrograzers (e.g. radiolarians and ciliates) exhibited POC responses similar to putative phototrophs, suggesting that grazing activity was enhanced in response to the ash-fueled increase in primary and/or bacterial production. The response we observed after wildfire ash addition is thus likely driven by a combination of the various chemical forms of limiting nitrogen and other nutrients leached by wildfire ash in addition to the magnitude of nutrient addition.

2.5 Conclusions

Our findings suggest that large wildfires can be important sources of nitrogen and other nutrients to coastal marine ecosystems, fueling productivity and significantly shifting protistan community structure. Near areas of active burning, wildfire is likely the dominant atmospheric source of nitrogen to coastal areas, and under certain conditions it could contribute significantly to total marine nitrogen inputs, a factor of increasing importance as fire frequency and intensity rises in a changing climate. The trends observed here provide a basic understanding of how marine protist communities respond to wildfire ash while

shedding light on the importance of an understudied mechanism of nutrient delivery to marine ecosystems.

2.6 Acknowledgments

This work resulted from the efforts of many individuals associated with the ACIDD cruise. We thank Nicholas Baetge, Kelsey Bisson, Eleanor Arrington, and David Valentine for cruise planning and assisting with onboard activities. Thanks to the Captain and crew of the *R/V* Sally Ride and other members of the ACIDD science team. Eleanor Arrington collected Thomas Fire ash and supplied it for experimental use. Nicholas Baetge and Eleanor Arrington performed initial leaching tests and made the leachate used for the onboard incubations. Thank you to Keri Opalk for running DOC samples. We thank Monica Pessino for providing us with Fig. 2.3. We appreciate comments from Elizabeth Harvey, John Raven, Nicholas Baetge, and Daniel Goertz. The satellite data products were obtained from the NOAA/NESDIS Center for Satellite Applications and Research (https://www.star.nesdis.noaa.gov/smcd/emb/viirs_aerosol/products_gridded_eps.php) and from the NASA Worldview application (https://worldview.earthdata.nasa.gov), part of the NASA Earth Observing System Data and Information System (EOSDIS). **Funding:** Supported by the University of California's Ship Funds Program, NSF RAPID Grant #1821916, and UCSB's Coastal Fund Grant #FALL18-10. **Author contributions:** T.M.L. and M.A.M. planned and conducted the incubation experiments. T.M.L., D.C., and S.M.K. processed the 18S metabarcoding samples. T.M.L. and S.M.K conducted the nutrient analyses. R.L.K. and S.G.J. processed the metal samples. C.A.C. conducted the DOC analysis. T.M.L., D.C., and M.D.I-R. contributed to data interpretation and figure generation.

T.M.L. wrote the manuscript with contributions from all authors. **Data and materials availability:** The 18S metabarcoding sequence data and ancillary data are deposited in the Sequence Read Archive (National Center for Biotechnology Information) under accension number PRJNA719165.

2.7 Literature cited

Adl SM, Bass D, Lane CE, Lukeš J, Schoch CL, Smirnov A, Agatha S, Berney C, Brown MW, Burki F, Cárdenas P, Čepička I, Chistyakova L, del Campo J, Dunthorn M, Edvardsen B, Eglit Y, Guillou L, Hampl V, Heiss AA, Hoppenrath M, James TY, Karnkowska A, Karpov S, Kim E, Kolisko M, Kudryavtsev A, Lahr DJG, Lara E, Le Gall L, Lynn DH, Mann DG, Massana R, Mitchell EAD, Morrow C, Park JS, Pawlowski JW, Powell MJ, Richter DJ, Rueckert S, Shadwick L, Shimano S, Spiegel FW, Torruella G, Youssef N, Zlatogursky V, Zhang Q (2019) Revisions to the Classification, Nomenclature, and Diversity of Eukaryotes. J Eukaryot Microbiol 66:4–119

Anderson CR, Siegel DA, Brzezinski MA, Guillocheau N (2008) Controls on temporal patterns in phytoplankton community structure in the Santa Barbara channel, California. J Geophys Res Ocean 113:C04038

Anderson SR, Harvey EL (2020) Temporal Variability and Ecological Interactions of Parasitic Marine Syndiniales in Coastal Protist Communities. mSphere 5

Banse K (1982) Cell volumes, maximal growth rates of unicellular algae and ciliates, and the role of ciliates in the marine pelagial. Limnol Oceanogr 27:1059–1071

Bisson KM, Baetge N, Kramer SJ, Catlett D, Girling G, McNair H, Arrington E, Hayes D, Jacobs C, James A, Closset I, Fischer AD, Wagner S, Reading M, Comstock J, Amiri S, Harvey E, Carlson C, Gaube P, Drushka K, Valentine DL (2020) California wildfire burns boundaries between science and art. Oceanography 33:16–19

Bronk DA, See JH, Bradley P, Killberg L (2006) DON as a source of bioavailable nitrogen for phytoplankton. Biogeosciences Discuss 3:1247–1277

Browning TJ, Bouman HA, Henderson GM, Mather TA, Pyle DM, Schlosser C, Woodward EMS, Moore CM (2014) Strong responses of Southern Ocean phytoplankton communities to volcanic ash. Geophys Res Lett 41:2851–2857

CalFire (2021a) Thomas Fire. https://www.fire.ca.gov/incident/?incident=d28bc34e-73a8-454d-9e55-dea7bdd40bee#incident-contacts (accessed 21 May 2021)

CalFire (2021b) Top 20 Largest California Wildfires. https://www.fire.ca.gov/media/4jandlhh/top20_acres.pdf (accessed 3 September 2021)

Callahan BJ, McMurdie PJ, Rosen MJ, Han AW, Johnson AJA, Holmes SP (2016) DADA2: High-resolution sample inference from Illumina amplicon data. Nat Methods 13:581–583

Carlson CA, Hansell DA, Nelson NB, Siegel DA, Smethie WM, Khatiwala S, Meyers MM, Halewood E (2010) Dissolved organic carbon export and subsequent remineralization in the mesopelagic and bathypelagic realms of the North Atlantic basin. Deep Res Part II Top Stud Oceanogr 57:1433–1445

Catlett D, Matson PG, Carlson CA, Wilbanks EG, Siegel DA, Iglesias-Rodriguez MD (2020) Evaluation of accuracy and precision in an amplicon sequencing workflow for marine protist communities. Limnol Oceanogr Methods 18:20–40

Chretiennot-Dinet MJ, Courties C, Vaquer A, Neveux J, Claustre H, Lautier J, Machado MC (1995) A new marine picoeucaryote: Ostreococcus tauri gen. et sp. nov. (Chlorophyta, Prasinophyceae). Phycologia 34:285–292

Deutsch C, Frenzel H, McWilliams JC, Renault L, Kessouri F, Howard E, Liang J-H, Bianchi D, Yang S (2021) Biogeochemical variability in the California Current System. Prog Oceanogr 196:102565

Dumack K, Fiore-Donno AM, Bass D, Bonkowski M (2020) Making sense of environmental sequencing data: Ecologically important functional traits of the protistan groups Cercozoa and Endomyxa (Rhizaria). Mol Ecol Resour 20:398–403

Eikrem W, Throndsen J (1990) The ultrastructure of Bathycoccus gen. nov. and B. prasinos sp. nov., a non-motile picoplanktonic alga (Chlorophyta, Prasinophyceae) from the Mediterranean and Atlantic. Phycologia 29:344–350

Frogner P, Gíslason SR, Óskarsson N (2001) Fertilizing potential of volcanic ash in ocean surface water. Geology 29:487–490

Furnas MJ (1990) In situ growth rates of marine phytoplankton: Approaches to measurement, community and species growth rates. J Plankton Res 12:1117–1151

Glibert PM, Wilkerson FP, Dugdale RC, Parker AE, Alexander J, Blaser S, Murasko S (2014) Phytoplankton communities from San Francisco Bay Delta respond differently to oxidized and reduced nitrogen substrates-even under conditions that would otherwise suggest nitrogen sufficiency. Front Mar Sci 1:1–16

Glibert PM, Wilkerson FP, Dugdale RC, Raven JA, Dupont CL, Leavitt PR, Parker AE, Burkholder JM, Kana TM (2016) Pluses and minuses of ammonium and nitrate uptake and assimilation by phytoplankton and implications for productivity and community

composition, with emphasis on nitrogen-enriched conditions. Limnol Oceanogr 61:165–197

Godhe A, Asplund ME, Härnström K, Saravanan V, Tyagi A, Karunasagar I (2008) Quantification of diatom and dinoflagellate biomasses in coastal marine seawater samples by real-time PCR. Appl Environ Microbiol 74:7174–7182

Guieu C, Aumont O, Paytan A, Bopp L, Law CS, Mahowald N, Achterberg EP, Marañón E, Salihoglu B, Crise A, Wagener T, Herut B, Desboeufs K, Kanakidou M, Olgun N, Peters F, Pulido-Villena E, Tovar-Sanchez A, Völker C (2014) The significance of the episodic nature of atmospheric deposition to Low Nutrient Low Chlorophyll regions. Global Biogeochem Cycles 28:1179–1198

Guillard RRL, Carpenter EJ, Reimann BEF (1974) Skeletonema menzelii sp. nov., a new diatom from the western Atlantic Ocean. Phycologia 13:131–138

Guillou L, Bachar D, Audic S, Bass D, Berney C, Bittner L, Boutte C, Burgaud G, De Vargas C, Decelle J, Del Campo J, Dolan JR, Dunthorn M, Edvardsen B, Holzmann M, Kooistra WHCF, Lara E, Le Bescot N, Logares R, Mahé F, Massana R, Montresor M, Morard R, Not F, Pawlowski J, Probert I, Sauvadet AL, Siano R, Stoeck T, Vaulot D, Zimmermann P, Christen R (2013) The Protist Ribosomal Reference database (PR2): A catalog of unicellular eukaryote Small Sub-Unit rRNA sequences with curated taxonomy. Nucleic Acids Res 41:597–604

Guillou L, Chrétiennot-Dinet MJ, Medlin LK, Claustre H, Loiseaux-de Goër S, Vaulot D (1999) Bolidomonas: A new genus with two species belonging to a new algal class, the Bolidophyceae (Heterokonta). J Phycol 35:368–381

Guillou L, Viprey M, Chambouvet A, Welsh RM, Kirkham AR, Massana R, Scanlan DJ, Worden AZ (2008) Widespread occurrence and genetic diversity of marine parasitoids belonging to Syndiniales (Alveolata). Environ Microbiol 10:3349–3365

Guo C, Yu J, Ho TY, Wang L, Song S, Kong L, Liu H (2012) Dynamics of phytoplankton community structure in the South China Sea in response to the East Asian aerosol input. Biogeosciences 9:1519–1536

Hawco NJ, Yang SC, Foreman RK, Funkey CP, Dugenne M, White AE, Wilson ST, Kelly RL, Bian X, Huang KF, Karl DM, John SG (2020) Metal isotope signatures from lava-seawater interaction during the 2018 eruption of Kīlauea. Geochim Cosmochim Acta 282:340–356

Herut B, Rahav E, Tsagaraki TM, Giannakourou A, Tsiola A, Psarra S, Lagaria A, Papageorgiou N, Mihalopoulos N, Theodosi CN, Violaki K, Stathopoulou E, Scoullos M, Krom MD, Stockdale A, Shi Z, Berman-Frank I, Meador TB, Tanaka T, Paraskevi P (2016) The potential impact of Saharan dust and polluted aerosols on microbial populations in the East Mediterranean Sea, an overview of a mesocosm experimental

approach. Front Mar Sci 3:226

Hill DRA (1991) A revised circumscription of Cryptomonas (Cryptophyceae) based on examination of Australian strains. Phycologia 30:170–188

Ho TY, Quigg A, Finkel Z V., Milligan AJ, Wyman K, Falkowski PG, Morel FMM (2003) The elemental composition of some marine phytoplankton. J Phycol 39:1145–1159

Hogue BA, Inglett PW (2012) Nutrient release from combustion residues of two contrasting herbaceous vegetation types. Sci Total Environ 431:9–19

Howard MDA, Sutula M, Caron DA, Chao Y, Farrara JD, Frenzel H, Jones B, Robertson G, McLaughlin K, Sengupta A (2014) Anthropogenic nutrient sources rival natural sources on small scales in the coastal waters of the Southern California Bight. Limnol Oceanogr 59:285–297

Huson DH, Auch AF, Qi J, Schuster SC (2007) MEGAN analysis of metagenomic data. Genome Res 17:377–386

Ichinomiya M, Dos Santos AL, Gourvil P, Yoshikawa S, Kamiya M, Ohki K, Audic S, De Vargas C, Noël MH, Vaulot D, Kuwata A (2016) Diversity and oceanic distribution of the Parmales (Bolidophyceae), a picoplanktonic group closely related to diatoms. ISME J 10:2419–2434

Jickells T, Moore CM (2015) The Importance of Atmospheric Deposition for Ocean Productivity. Annu Rev Ecol Evol Syst 46:481–501

Jones MT, Gislason SR (2008) Rapid releases of metal salts and nutrients following the deposition of volcanic ash into aqueous environments. Geochim Cosmochim Acta 72:3661–3680

Kozich JJ, Westcott SL, Baxter NT, Highlander SK, Schloss PD (2013) Development of a dual-index sequencing strategy and curation pipeline for analyzing amplicon sequence data on the MiSeq Illumina sequencing platform. Appl Environ Microbiol 79:5112–5120

Kramer SJ, Bisson KM, Fischer AD (2020) Observations of Phytoplankton Community Composition in the Santa Barbara Channel During the Thomas Fire. J Geophys Res Ocean 125:1–16

Kudela RM, Lane JQ, Cochlan WP (2008) The potential role of anthropogenically derived nitrogen in the growth of harmful algae in California, USA. Harmful Algae 8:103–110

Laza-Martínez A, Arluzea J, Miguel I, Orive E (2012) Morphological and molecular characterization of Teleaulax gracilis sp. nov. and T. minuta sp. nov. (Cryptophyceae). Phycologia 51:649–661

Lekunberri I, Lefort T, Romero E, Vázquez-Domínguez E, Romera-Castillo C, Marrasé C, Peters F, Weinbauer M, Gasol JM (2010) Effects of a dust deposition event on coastal marine microbial abundance and activity, bacterial community structure and ecosystem function. J Plankton Res 32:381–396

Mahowald NM, Scanza R, Brahney J, Goodale CL, Hess PG, Moore JK, Neff J (2017) Aerosol Deposition Impacts on Land and Ocean Carbon Cycles. Curr Clim Chang Reports 3:16–31

Marín I, Nunes S, Sánchez-Pérez ED, Txurruka E, Antequera C, Sala MM, Marrasé C, Peters F (2017) Coastal Bacterioplankton Metabolism Is Stimulated Stronger by Anthropogenic Aerosols than Saharan Dust. Front Microbiol 8:2215

Mélançon J, Levasseur M, Lizotte M, Delmelle P, Cullen J, Hamme RC, Peña A, Simpson KG, Scarratt M, Tremblay JÉ, Zhou J, Johnson K, Sutherland N, Arychuk M, Nemcek N, Robert M (2014) Early response of the northeast subarctic Pacific plankton assemblage to volcanic ash fertilization. Limnol Oceanogr 59:55–67

Menden-Deuer S, Lessard EJ (2000) Carbon to volume relationships for dinoflagellates, diatoms, and other protist plankton. Limnol Oceanogr 45:569–579

Mills MM, Ridame C, Davey M, La Roche J, Geider RJ (2004) Iron and phosphorus co-limit nitrogen fixation in the eastern tropical North Atlantic. Nature 429:292–294

Mitra A, Flynn KJ, Tillmann U, Raven JA, Caron D, Stoecker DK, Not F, Hansen PJ, Hallegraeff G, Sanders R, Wilken S, McManus G, Johnson M, Pitta P, Våge S, Berge T, Calbet A, Thingstad F, Jeong HJ, Burkholder JA, Glibert PM, Granéli E, Lundgren V (2016) Defining Planktonic Protist Functional Groups on Mechanisms for Energy and Nutrient Acquisition: Incorporation of Diverse Mixotrophic Strategies. Protist 167:106–120

Moore CM, Mills MM, Arrigo KR, Berman-Frank I, Bopp L, Boyd PW, Galbraith ED, Geider RJ, Guieu C, Jaccard SL, Jickells TD, La Roche J, Lenton TM, Mahowald NM, Marañón E, Marinov I, Moore JK, Nakatsuka T, Oschlies A, Saito MA, Thingstad TF, Tsuda A, Ulloa O (2013) Processes and patterns of oceanic nutrient limitation. Nat Geosci 6:701–710

Murali A, Bhargava A, Wright ES (2018) IDTAXA: A novel approach for accurate taxonomic classification of microbiome sequences. Microbiome 6:140

Pausas JG, Keeley JE (2021) Wildfires and global change. Front Ecol Environ: doi:10.1002/fee.2359

Quast C, Pruesse E, Yilmaz P, Gerken J, Schweer T, Yarza P, Peplies J, Glöckner FO (2013) The SILVA ribosomal RNA gene database project: Improved data processing and web-based tools. Nucleic Acids Res 41:590–596

Ramond P, Sourisseau M, Simon N, Romac S, Schmitt S, Rigaut-Jalabert F, Henry N, de Vargas C, Siano R (2019) Coupling between taxonomic and functional diversity in protistan coastal communities. Environ Microbiol 21:730–749

Romero E, Peters F, Marrasé C, Guadayol Ò, Gasol JM, Weinbauer MG (2011) Coastal Mediterranean plankton stimulation dynamics through a dust storm event: An experimental simulation. Estuar Coast Shelf Sci 93:27–39

Schneider LK, Flynn KJ, Herman PMJ, Troost TA, Stolte W (2020) Exploring the Trophic Spectrum: Placing Mixoplankton Into Marine Protist Communities of the Southern North Sea. Front Mar Sci 7:586915

Schrader-Patton CC, Underwood EC (2021) New Biomass Estimates for Chaparral-Dominated Southern California Landscapes. Remote Sens 13:1581

Simon N, Foulon E, Grulois D, Six C, Desdevises Y, Latimier M, Le Gall F, Tragin M, Houdan A, Derelle E, Jouenne F, Marie D, Le Panse S, Vaulot D, Marin B (2017) Revision of the Genus Micromonas Manton et Parke (Chlorophyta, Mamiellophyceae), of the Type Species M. pusilla (Butcher) Manton & Parke and of the Species M. commoda van Baren, Bachy and Worden and Description of Two New Species Based on the Genetic and . Protist 168:612–635

Smith HG, Sheridan GJ, Lane PNJ, Nyman P, Haydon S (2011) Wildfire effects on water quality in forest catchments: A review with implications for water supply. J Hydrol 396:170–192

Sohrin Y, Urushihara S, Nakatsuka S, Kono T, Higo E, Minami T, Norisuye K, Umetani S (2008) Multielemental determination of GEOTRACES key trace metals in seawater by ICPMS after preconcentration using an ethylenediaminetriacetic acid chelating resin. Anal Chem 80:6267–6273

Spencer CN, Hauer FR (1991) Phosphorus and nitrogen dynamics in streams during a wildfire. J North Am Benthol Soc 10:24–30

Stoeck T, Bass D, Nebel M, Christen R, Jones MDM, Breiner HW, Richards TA (2010) Multiple marker parallel tag environmental DNA sequencing reveals a highly complex eukaryotic community in marine anoxic water. Mol Ecol 19:21–31

Stolte W, Garcés E (2006) Ecological Aspects of Harmful Algal In Situ Population Growth Rates. In: *Ecology of Harmful Algae*, Ecological. Granéli E, Turner JT (eds) Springer Berlin Heidelberg, p 139–152

Tang EPY, Peters RH (1995) The allometry of algal respiration. J Plankton Res 17:303–315

Valderrama JC (1981) The simultaneous analysis of total nitrogen and total phosphorus in natural waters. Mar Chem 10:109–122

Vicars WC, Sickman JO, Ziemann PJ (2010) Atmospheric phosphorus deposition at a montane site: Size distribution, effects of wildfire, and ecological implications. Atmos Environ 44:2813–2821

Wang Q, Garrity GM, Tiedje JM, Cole JR (2007) Naïve Bayesian classifier for rapid assignment of rRNA sequences into the new bacterial taxonomy. Appl Environ Microbiol 73:5261–5267

Warrick JA, Washburn L, Brzezinski MA, Siegel DA (2005) Nutrient contributions to the Santa Barbara Channel, California, from the ephemeral Santa Clara River. Estuar Coast Shelf Sci 62:559–574

Weinbauer MG, Guinot B, Migon C, Malfatti F, Mari X (2017) Skyfall - neglected roles of volcano ash and black carbon rich aerosols for microbial plankton in the ocean. J Plankton Res 39:187–198

Wilkerson FP, Lassiter AM, Dugdale RC, Marchi A, Hogue VE (2006) The phytoplankton bloom response to wind events and upwelled nutrients during the CoOP WEST study. Deep Res Part II Top Stud Oceanogr 53:3023–3048

Winant CD (2003) Characteristic patterns of shelf circulation at the boundary between central and southern California. J Geophys Res 108:3021

Zhang Q, Carroll JJ, Dixon AJ, Anastasio C (2002) Aircraft measurements of nitrogen and phosphorus in and around the Lake Tahoe Basin: Implications for possible sources of atmospheric pollutants to Lake Tahoe. Environ Sci Technol 36:4981–4989

Zhang R, Jiang T, Tian Y, Xie S, Zhou L, Li Q, Jiao N (2017) Volcanic ash stimulates growth of marine autotrophic and heterotrophic microorganisms. Geology 45:679–682

Zhu F, Massana R, Not F, Marie D, Vaulot D (2005) Mapping of picoeukaryotes in marine ecosystems with quantitative PCR of the 18S rRNA gene. FEMS Microbiol Ecol 52:79–92

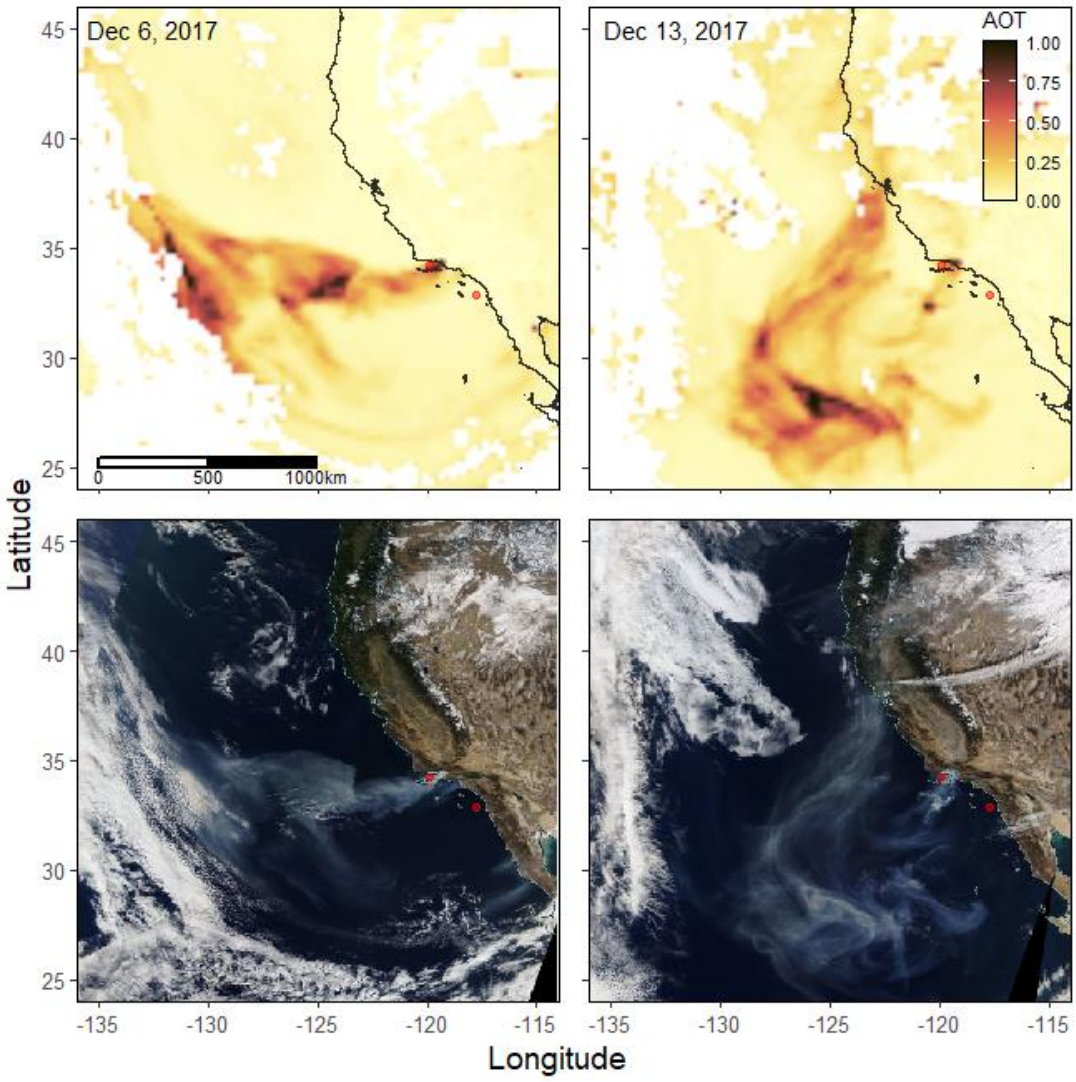

Fig. 2.1. Thomas Fire smoke and ash plume. Aerosol optical thickness (AOT) gridded data (SNPP/VIIRS) and true color imagery (MODIS Terra) of the Thomas Fire plume on December 6 and 13, 2017. The two incubation water collection locations are indicated as red circles with offshore San Diego (SD) (south) and Santa Barbara Channel (SBC) (north) located outside and within the plume, respectively.

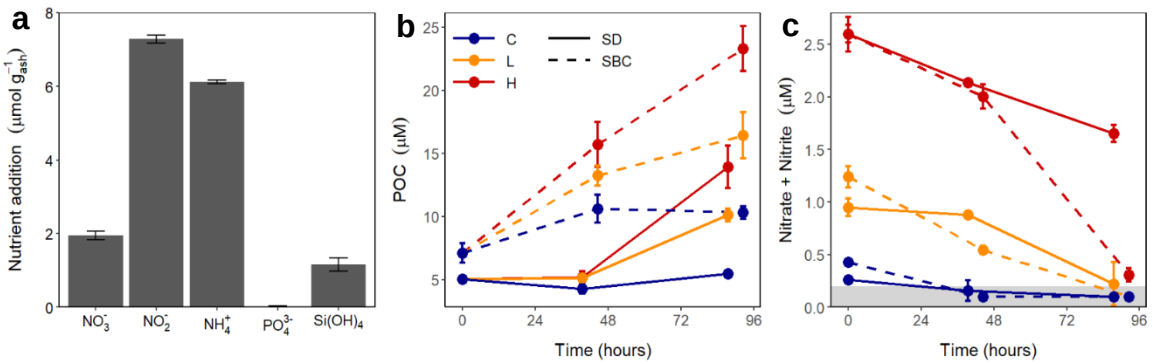

Fig. 2.2. Nutrient and biomass dynamics in response to ash leaching. (a) Mean ± standard deviation additions of nitrate (NO_3^-), nitrite (NO_2^-), ammonium (NH_4^+), phosphate (PO_4^{3-}), and silicic acid ($Si(OH)_4$) (µmol $g_{(ash)}^{-1}$). Significant nutrient additions in the ash leachate (paired t-tests, n=3, $p < 0.05$) were found for all inorganic nutrients except PO_4^{3-}. (b) Mean ± standard deviation (n=3 except n=2 for SD H) concentrations of particulate organic carbon (POC) over time in ash and control treatments of the SD and SBC incubations. Significant increases in POC in high (H) and low (L) ash treatments relative to the control (C) were detected (Tukey HSD $p < 0.05$) at day 4 in the SD incubation and on both days 2 and 4 in the SBC incubation. Differences in the change in POC from days 0 to 2 in ash treatments relative to controls were significantly greater in the SBC than the SD incubation for the H (t-test p = 0.02) and L (t-test p = 0.02) treatments. Between days 2 and 4 differences in the POC change relative to controls were not significantly different between the SD and SBC incubations in either the H (t-test p = 0.4) or L (t-test p = 0.5) treatments. (c) Mean ± standard deviation concentrations of nitrate + nitrite over time in ash and control treatments of the SD and SBC incubations. Measurements are from triplicate bottles (n=3), except at time 0 where values are from a single sample (C) or the average of a single sample and estimated concentrations from the leachate (ash treatments) (N =2). Values in the shaded area represent measurements below the analytical limit of detection (0.2 µM) and are not considered significantly different from zero.

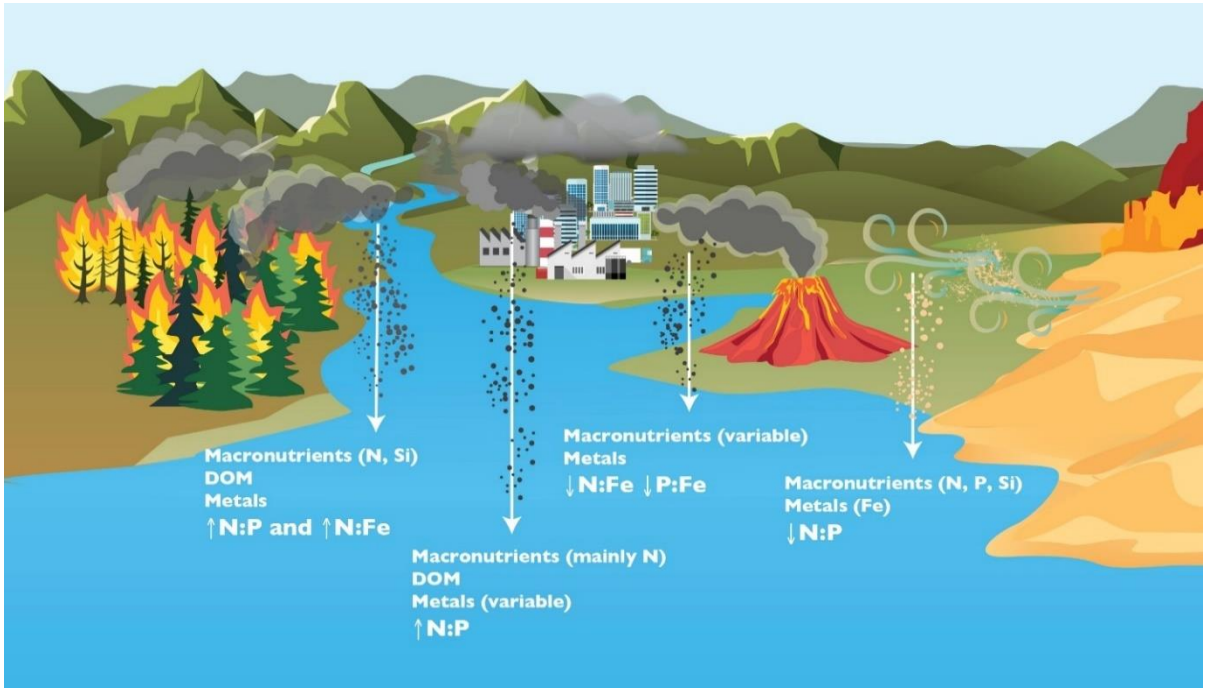

Fig. 2.3. Atmospheric aerosol inputs to the ocean. Sources of atmospheric aerosols and the respective nutrients added to marine ecosystems with estimated impacts of nutrient addition on relative amounts of nitrogen (N), phosphorus (P), and iron (Fe) compared to average biological requirements (N:P:Fe = 16:1:0.0075) (Ho et al. 2003). Estimates of added nutrients and their ratios come from studies that either review biogeochemical impacts of different atmospheric aerosol sources on marine systems (Jickells & Moore 2015, Mahowald et al. 2017, Weinbauer et al. 2017) or measure nutrient concentrations of aerosol (Herut et al. 2016, Marín et al. 2017), volcanic ash (Frogner et al. 2001, Jones & Gislason 2008, Browning et al. 2014), or desert dust (Mills et al. 2004, Lekunberri et al. 2010, Herut et al. 2016) additions to seawater or pure water. Nutrient additions and ratios from the leaching of wildfire ash are from this study.

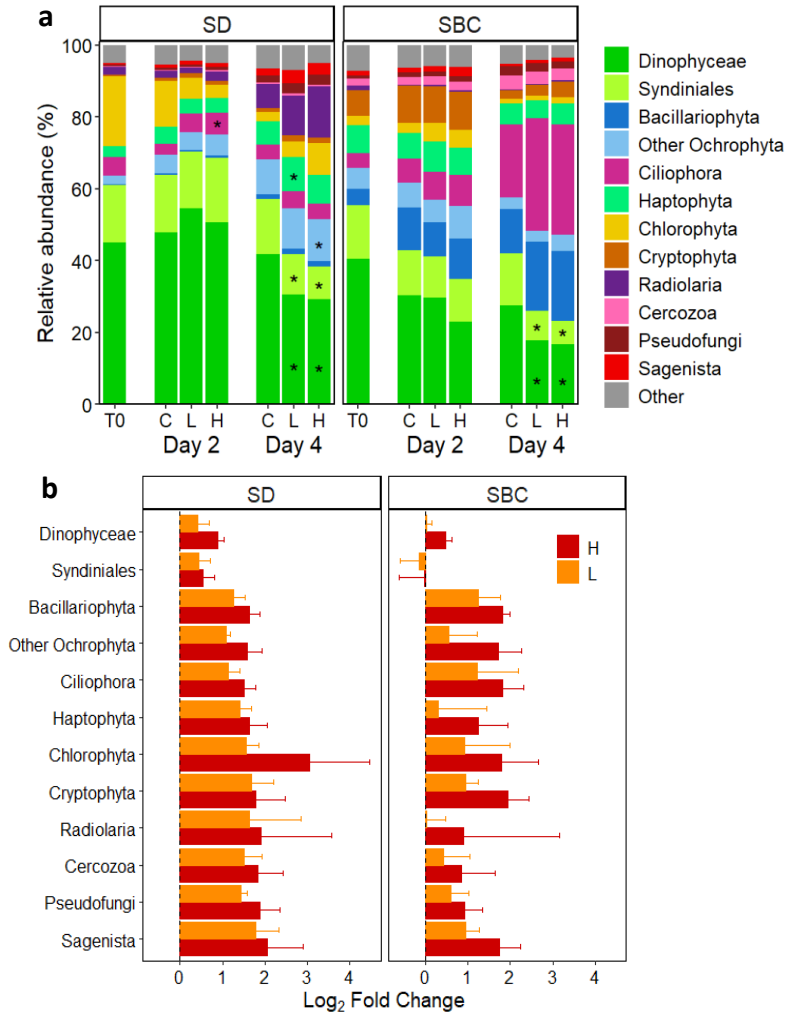

Fig. 2.4. Protist community composition and POC responses to ash exposure. (a) Average relative abundance (RA) of ASVs grouped by Division or Class (n=3) in the SD and SBC incubation experiments at the start of each experiment (T0) and at days 2 and 4 for each treatment; control (C), low ash (L), or high ash (H). Division Dinoflagellata has been divided into Classes Dinophyceae and Syndiniales and Division Ochrophyta was split into Bacillariophyta and other Ochrophyta Classes. The "Other" group represents ASVs from less abundant Divisions/Classes (Telonemia, Katablepharidophyta, Discoba, Opalozoa, Picozoa, Apicomplexa, Choanoflagellida, Centroheliozoa, unassigned Alveolata, unassigned Stramenopiles, Mesomycetozoa, Lobosa, unassigned Amoebozoa, Foraminifera, Conosa, and other Dinoflagellata Classes). Asterisks represent divisions or classes with significantly different RA [pairwise t-tests on differences >1% (day 2) or 2% (day 4), BH adjusted $p < 0.05$] between either the H or L treatments compared to control at day 2 or day 4. (b) Mean ± standard deviation differences in $\log_2$ transformed POC-scaled RA of the major protistan taxonomic groups between the H (red) or L (orange) treatments compared to the controls (n=3 except n=2 for SD H) at day 4 representing approximate $\log_2$ fold changes in protistan POC. Positive values represent increased POC in the ash (H or L) treatments compared to the control while negative values represent increased POC in the control compared to ash treatments.

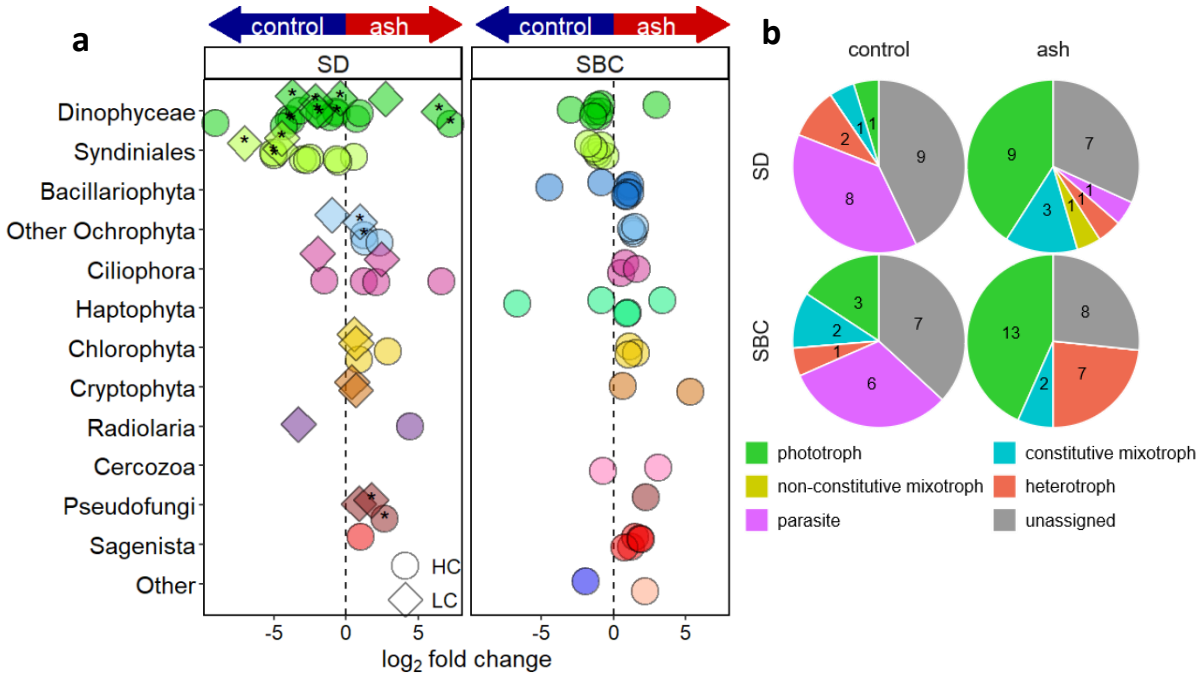

Fig. 2.5. Significant responses of protist ASVs to ash exposure. (a) ASVs that were significantly differentially abundant (DESeq2, $p<0.05$) between ash and control treatments in the SD and SBC incubations. Colors represent each ASV's Division or Class (denoted on the y-axis and colored as in Fig. 2.4b) and the shape of the point represents differentially abundant ASVs in either the high (circles) or low (diamonds) ash treatment relative to the control. A negative (positive) $\log_2$ fold change indicates that an ASV is relatively more abundant in the control (ash) treatment(s). Asterisks represent ASVs that were significantly differentially abundant in both low and high ash treatments. ASVs that are classified as "Other" come from Divisions Telonemia (violet) and Opalozoa (light pink). (b) Putative trophic strategies of ASVs with significantly higher RA in the control or ash treatments for the SD and SBC incubations. Numbers represent the total number of significantly differentially abundant ASVs between either the low or high ash treatments compared to the control (DESeq2, $p<0.05$).

Chapter 3

Fall protist communities reveal high variability between recent years with differential sea ice influence in the eastern Bering Sea

3.1 Abstract

Marine protists in the eastern Bering Sea (EBS) are understudied but constitute an important component of the productive subarctic ecosystem. Protists (single-celled eukaryotes) are a diverse group of microbes that form the base of the marine food web and control biogeochemical cycling within ecosystems. In the EBS, climate change, and particularly the loss of sea ice, is rapidly altering the physical, chemical, and biological landscape making monitoring ever more imperative to the sustainable management of this economically important system. In this study, 18S rRNA gene sequencing was used to explore the protist community composition in the context of drastic changes in sea ice extent experienced in recent years. In 2019 when sea ice extent was anomalously low and retreat was early, warmer fall water temperatures resulted and the protist community was dominated by putative parasites (Division Apicomplexa). In contrast, 2017 experienced relatively average sea ice extent and retreat resulting in comparably cooler fall water temperatures with protist communities that had comparably more phytoplankton compared to non-phytoplankton protists. Several physical and chemical variables changed across years and correlated with the biomass of protist taxonomic groups but there was also evidence that biotic interactions played significant roles in controlling the community structure across years. Future work in the EBS should incorporate monitoring of protist communities while there is a need to further explore the impacts of protistan parasites.

3.2 Introduction

Marine protists, or single-celled eukaryotes, represent a taxonomically and functionally diverse component of marine ecosystems. With cell sizes spanning more than five orders of magnitude and representatives exhibiting a variety of ecological roles including primary production, grazing, and parasitism, protists control the flow of energy and carbon through marine food webs (Sherr et al. 2007, Caron et al. 2012). Ongoing advances in DNA sequence-based approaches for analyzing protist communities and the development of extensive global datasets (e.g., *Tara* Oceans; Pesant et al. 2015) have revealed several new taxonomic lineages, a surprising amount of taxonomic diversity, and often unexpected trends in the relative abundances of protist groups, such as putative parasites (Moreira & López-García 2002, De Vargas et al. 2015, Del Campo et al. 2016, Cleary & Durbin 2016, Del Campo et al. 2019, Clarke et al. 2019). As these methods are increasingly more affordable and are considerably less labor intensive than traditional microscopic community analysis, they have become critical tools for understanding complex microbial dynamics within communities and the responses of protist communities to environmental change.

The eastern Bering Sea (EBS) is an economically and culturally important subarctic ecosystem that supports some of the largest and most productive U.S. fisheries (NMFS 2021). The EBS is characterized by a shallow (up to ~180 m deep) broad shelf that extends ~ 500 km offshore of western Alaska (Stabeno et al. 1999). It is bounded to the north by the Bering Strait and in the south by the Aleutian Island Chain with slow northward flowing currents over the shelf that connect the North Pacific Ocean to the Arctic Ocean (Stabeno et al. 1999, 2016). A key feature of the EBS is the seasonal advance and retreat of sea ice that can have high interannual variability with winter ice covering almost the entire shelf in some

years while only covering the northern shelf in other years (Stabeno & Bell 2019). Due to the long residence time of water on the shelf, winter sea ice dynamics have a strong influence on the physical and chemical properties of the water column over much of the year (Mueter & Litzow 2008, Stabeno et al. 2010, 2012a, 2012b 2016, Mordy et al. 2021). In recent years unprecedented low sea ice extent and early year retreat have been observed (Stabeno & Bell 2019). The winters of 2017/2018 and 2018/2019 may provide a glimpse into the future of this system as shifting wind patterns in this region created conditions that led to the lowest winter sea ice extent on record (2017/2018) followed by a second year with an early sea ice retreat and low extent (2018/2019) (Stabeno & Bell 2019) (Fig. 3.1).

Long term monitoring in the EBS with an ecosystem-wide perspective has been conducted over the last few decades with the goal of managing important fisheries and supporting resilient communities (Sheffield Guy et al. 2014). Despite an extensive research program, marine microbial communities are relatively understudied in this region. A few studies have assessed phytoplankton community composition (Hare et al. 2007, Goes et al. 2014, Zhou et al. 2015, Szymanski & Gradinger 2016), primary production (Moran et al. 2012, Sambrotto et al. 2015, Lomas et al. 2020) or microzooplankton grazing (Olson & Strom 2002, Strom & Fredrickson 2008, Sherr et al. 2013, Stoecker et al. 2014), but measurements of chlorophyll fluorescence or concentration are the only long-term tools used to constrain phytoplankton dynamics while knowledge of many other protists remain unclear. Previous work in the EBS suggests that ‘who’ makes up these microbial communities at the base of the marine food web is important for understanding whole ecosystem processes, especially as warming, sea ice loss, and ocean acidification continue to influence this productive ecosystem (Olson & Strom 2002, Hare et al. 2007, Zhou et al. 2015). For

example, large ice-associated diatoms are an important food source for large copepods, which are the main prey for juvenile and adult walleye pollock, and therefore sea ice extent and timing of retreat impact the availability of this food source and the transfer of energy up the food chain (Durbin & Casas 2014). Generally, larger phytoplankton species are considered more efficient for the transfer of energy and biomass to higher trophic levels due to fewer trophic links and reduced flows through the microbial loop (Azam et al. 1983, Pomeroy et al. 2007, Armengol et al. 2019). Additionally, massive blooms of the coccolithophore, *Emiliania huxleyi*, potentially influenced by warming (Iida et al. 2002, Merico et al. 2004), stratification (Iida et al. 2012, Ladd et al. 2018), and trophic interactions (Olson & Strom 2002, Merico et al. 2004), have been suggested to impair the feeding ability of visual predators (such as seabirds and fish) due to the unique alteration of water optical properties from this phytoplankton species (Vance et al. 1998, Eisner et al. 2003). Toxic phytoplankton species are also a concern in the EBS as seabird die-offs may be linked to algal toxins (Van Hemert et al. 2021), shellfish have been found with high toxin concentrations (Gao et al. 2019), and warming might be exacerbating harmful algal bloom events (Gobler et al. 2017, Natsuike et al. 2017). As this system continues to undergo rapid change, it is imperative to gain a better understanding of the community composition, diversity, and the complex interactions within microbial communities and in relation to abiotic factors.

Here amplicon sequencing of the 18S rRNA gene is used to explore fall protist community dynamics across two years (2017 versus 2019) with dramatic differences in prior winter sea ice extent and timing of retreat (Fig. 3.1). Physical and chemical data obtained concurrently are used to describe biological trends in the context of environmental

conditions. This work sheds light on the necessity for characterizing microbial communities in this important ecosystem.

3.3 Materials and methods

3.3.1 Cruise details

Samples and data for this work were collected on two cruises in the EBS aboard the NOAA ship Oscar Dyson from September 24 through October 4 or September 20 through 29 in 2017 and 2019 respectively. Fig 3.2 only displays locations where 18S rDNA sequencing samples were taken from the surface in each year but to compare physical and chemical properties at similar locations across years, the circled stations from 2019 (see Fig. 3.2) were also sampled for physical and chemical variables in 2017. Conductivity-temperature-depth (CTD) measurements were made with a Seabird SBE 911Plus system at all stations displayed in Fig 3.2 and additionally in 2017 at all circled stations (Fig. 3.2). During the CTD upcast, discrete water samples were collected in Niskin bottles attached to the CTD Rosette. At all stations in Fig 3.2, surface water samples (~3 m depth) were taken for 18S rDNA sequencing, particulate organic carbon (POC), nitrogen (PON), and total particulate phosphorus (TPP), chlorophyll-a concentrations, and dissolved inorganic nutrient concentrations (dissolved inorganic nitrogen (nitrate + nitrite + ammonium), silicic acid, and phosphate). Additionally, samples for dissolved inorganic nutrient concentrations were collected from bottles sampled at ~50 m depth. Dissolved inorganic nutrient concentrations at the surface and 50 m depth were also collected at the circled stations (Fig. 3.2) for in 2017 as well as in 2019. Measurements from the circled stations in Fig 3.2 from each year were

used to compare general physical and chemical conditions across years near the locations of 3 long-term moorings (M2, M5, and M8).

3.3.2 Field sampling and processing

Water samples taken for chlorophyll-a concentration (~300 mL) were filtered onto glass fiber filters (~0.7 μm pore size) and frozen at -80 °C until analysis. Chlorophyll was extracted from filters with 90% acetone at -80 °C in the dark for ~24 hours, then centrifuged before measuring with a Turner TD-700 fluorometer. Dissolved inorganic nutrient samples were syringe filtered through a 0.45 μm cellulose acetate membrane into 30 mL acid washed high-density polyethylene bottles and frozen at -80 °C until analysis. Measurements of phosphate, silicic acid, nitrate, and nitrite were made based on the protocol described by Gordon et al. (1993) for continuous flow automated analysis while ammonium was measured based on a modified indophenol blue method (Mantoura & Woodward 1983). Samples for chlorophyll and nutrients were analyzed by the EcoFOCI program at PMEL.

Surface water samples for POC/PON, and TPP concentrations (200 – 700 mL) were prefiltered through either a 200 μm or 20 μm mesh onto combusted glass fiber filters (0.7 μm, 25mm, Whatman) and stored at -20 °C until analysis. Acidified filters for POC/PON were analyzed at the University of California, Santa Barbara (UCSB) Marine Science Institute Analytical Laboratory using the Dumas combustion method on an automated elemental analyzer (Model CE-440HA, Exeter Analytical). TPP concentrations were analyzed at the University of Maryland Center for Environmental Science Nutrient Analytical Services Laboratory following protocols described by Aspila et al. (1976). Molar ratios of POC to PON or POC to TPP were calculated for the 'whole' protist community

(~0.7 – 200 μm) (POC:PON <200 or POC:TPP <200) or the small size fractions (~0.7-20 μm) (POC:PON <20 or POC:TPP <20).

Samples for 18S rDNA sequencing were collected from surface Niskin bottles (~1-1.2 L) and prefiltered at 200 μm before filtering onto a 1.2 μm pore size polycarbonate membrane (Isopore, EMD-Millipore). Filters were stored at -80 °C until further processing. DNA was extracted from the filters using a modified CTAB (cetyl trimethylammonium bromide) method based on Doyle (1991). Briefly, tubes containing the filters were removed from the freezer and for each sample 100 μL CTAB buffer was added, the tube was dipped in liquid nitrogen, and a pestle was used to disrupt cell contained on the filter. An additional aliquot of CTAB buffer (900 μL) was added and the tube was inverted several times to mix. Samples were incubated at 60 °C for 30 minutes with gentle mixing every 10 minutes. Samples were centrifuged and the supernatant was transferred to new tubes where a chloroform isoamyl alcohol mixture (24:1) was added (750 μL) followed by another round of centrifugation and transfer of the supernatant to new tubes. Cold isopropanol was added (500 μL) and the tube was gently but thoroughly mixed to precipitate the DNA and then incubated for 3 hours at -20 °C. The tubes were centrifuged to isolate the DNA pellet and the supernatant was removed followed by 2 rounds of washing with 70% ethanol and left to dry for ~20 minutes. The DNA pellet was resuspended in DNase free water, incubated at 65 °C for 30 minutes before storing at 4 °C overnight. The extracted DNA concentration was measured (Qubit 3.0 fluorometer, Thermo Fisher) before storage at -20 °C until DNA library preparation.

Amplification of the V9 hypervariable region of the 18S rRNA gene and Illumina library preparation followed protocols described by Catlett and colleagues (2020). Briefly, a

one-step polymerase chain reaction (PCR) using custom dual-indexed primers (Stoeck et al. 2010, Kozich et al. 2013, Catlett et al. 2020) was carried out using 0.4 μM of each primer and 1x KAPA2G Robust Hotstart ReadyMix (KAPA Biosystems). Samples were amplified in duplicate 25 μL reactions with 1 μL genomic DNA template and thermal cycling conditions as follows: 94 ºC for 3 min; 35 cycles of 94 ºC for 45 s, 65 ºC for 15 s, 57 ºC for 30 s, and 72 ºC for 90 s; 72 ºC for 10 min; 4 ºC until storage at -20 ºC. Duplicate reactions were pooled before proceeding with Illumina library preparation and sequencing. PCR products were first purified and normalized using the SequalPrep Normalization Plate Kit (Applied Biosystems), pooled in equal volumes into a single library, and concentrated with Amicon Ultra-0.5 Centrifugal Filter Devices (Millipore). Concentrated products were then further purified using the Qiagen QIAquick Gel Extraction kit and concentrated a second time (Amicon Ultra-0.5 Centrifugal Filter Device). The concentration of the final library was quantified using the Qubit 3.0 dsDNA High Sensitivity kit. Library sequencing was performed using a MiSeq PE150 v2 kit (Illumina) at the DNA Technologies Core of the University of California Davis (UCD) Genome Center.

3.3.3 Processing and analysis of sequencing data

Demultiplexed sequencing data obtained from UCD were processed with the DADA2 pipeline (v1.16.0; Callahan et al. 2016) and followed procedures described by Catlett and colleagues (2020). Briefly, forward and reverse reads were trimmed to 140 nt and 120 nt respectively, then filtered (maxEE = 2, truncQ = 2) and denoised according to the standard DADA2 workflow (https://benjjneb.github.io/dada2/tutorial.html). Paired reads were merged, overhanging sequences were trimmed, and chimeras were removed (method =

"consensus"). ASVs shorter than 90 nt or longer than 180 nt (target amplicon is 120-130 nt) were discarded. Initial taxonomic assignments of amplicon sequence variants (ASVs) were computed with the IDTAXA algorithm (DECIPHER package v2.16.1; Murali et al. 2018) (henceforth, idtaxa), the naive Bayesian classifier implemented in DADA2 (Wang et al. 2007, Callahan et al. 2016) (henceforth, bayes), and the Lowest Common Ancestor algorithm implemented in MEGAN6 (Huson et al. 2007) (henceforth, LCA) using both the Protistan Ribosomal Reference database v4.12.0 (PR2; Guillou et al. 2013) and the SILVA SSU nr reference database v138 (Silva; Quast et al. 2013) available for the DADA2 pipeline (https://benjjneb.github.io/dada2/training.html). The idtaxa and bayes algorithms used a minimum bootstrap confidence threshold of 50%, while the LCA algorithm was implemented using the default settings in MEGAN6.

The ensembleTax R package (v1.0.2, Catlett et al. 2021) was used to compute ensemble taxonomic assignments based on the six independent collections of taxonomic assignments in order to maximize the number of ASVs that could be identified as protists and reduce bias from using any single taxonomic assignment derived from a given algorithm and reference database (Catlett et al. 2020). Taxonomic assignments determined with the Silva reference database and the MEGAN LCA algorithm (which maps all assignments to the NCBI taxonomic nomenclature) were mapped onto the taxonomic nomenclature used by PR2 using the taxmapper algorithm. Where taxonomic names were not able to be mapped, the collection of taxonomic synonyms included with the ensembleTax package was considered (synonym.file = "default", ignore.format = TRUE). Since PR2 does not include bacterial or archaeal sequences, sequences assigned to these domains from the Silva database were retained at the "Kingdom" rank when mapped onto PR2. Following mapping of all

taxonomic assignments onto the PR2 taxonomic nomenclature, ensemble taxonomic assignments were computed for each ASV at each taxonomic rank as the highest frequency assignment predicted by the six individual methods, ignoring non-assignments. In the event that multiple taxonomic assignments were found at equivalent maximum frequencies across the individual methods, those determined using the idtaxa or (if the idtaxa assignment was not one of the highest frequency assignments) the bayes algorithm were prioritized, and the PR2 reference database was prioritized over the Silva database (similar to the approach employed by Catlett and colleagues (2020)). To focus the analysis on protists, ASVs classified as Bacteria, Archaea, Metazoa, Fungi, Streptophyta, Rhodophyta, or Ulvophyceae were removed. ASVs with no assigned taxonomy at the Kingdom or Supergroup rank, and those assigned to the Supergroups Opisthokonta or Archaeplastida but not assigned to a Division (or assigned to an ambiguous Division, e.g. "Opisthokonta_X") were also discarded. To mitigate bias arising from uneven sequencing depth, sequences were normalized by scaling with ranked subsampling (Beule & Karlovsky 2020) to the minimum library size (24,051 reads per sample).

Protist ASVs were further assigned to trophic functional groups following the guidelines provided by Mitra and colleagues (Mitra et al. 2016) based on the ensemble taxonomic assignments. ASVs were classified into one of the following groups: phototroph, constitutive mixotroph, non-constitutive mixotroph, heterotroph, parasite, phytoplankton (unclear), non-phytoplankton (unclear) or unassigned. Here phototrophs include organisms that meet their energy demands exclusively by photoautotrophy, (non-)constitutive mixotrophs are capable of both photoautotrophy and heterotrophy and (do not) have an inherent capacity for photosynthesis, heterotrophs are consumers that ingest other organisms

to meet their energy demands, parasites are heterotrophs where part of their life cycle involves infection of a host organism, phytoplankton (unclear) are either phototrophs or constitutive mixotrophs but it is not clear which, and non-phytoplankton (unclear) are non-constitutive mixotrophs, heterotrophs, or parasites but it is not clear which. A collection of taxonomic names with corresponding trophic functional group(s) based on Adl and colleagues (2019) and supplemented this with similar data from various other sources (Ramond et al. 2019, Dumack et al. 2020, Schneider et al. 2020) was compiled (prepared and provided by Dylan Catlett). To assign ASVs to functional groups, each ASV's ensemble taxonomic assignment at the lowest assigned rank (e.g. Species if available, otherwise Genus, etc) was mapped to the corresponding functional group. If data was not available to link a particular taxonomic name to a functional group, the assigned taxonomic name at the next lowest rank was used until a match was found or no other taxonomic names were available for the ASV being mapped.

To estimate the POC contribution of protistan groups or ASVs, the relative sequence abundances of ASVs (hereafter RA) were scaled to concurrently determined POC concentrations. While high variation in 18S rRNA gene copy number obscures the relationships between protistan relative sequence and cell abundances, 18S rRNA gene copy number scales roughly with cell size and biovolume across diverse protistan lineages (Zhu et al. 2005, Godhe et al. 2008) and cellular carbon to biovolume relationships are relatively consistent across taxonomically diverse protist groups (Menden-Deuer & Lessard 2000), suggesting that relative sequence abundances provide an approximation of the POC proportion associated with protist groups or ASVs (De Vargas et al. 2015). While the magnitude of POC associated with specific protists is likely biased due to various factors

(e.g., detrital particles, biomass associated with bacteria/viruses trapped on the filter), comparisons of protistan POC concentrations across samples as done here are likely robust assuming the observed variability in POC concentrations in these samples is driven primarily by (or is directly proportional to) protist community carbon biomass.

3.3.4 Statistical analysis

All statistical analyses were conducted using R Studio (v1.3.959, base R v4.0.1) and JMP Pro 16. Statistically significant differences ($p<0.05$) in physical and chemical variables across years at locations near three long term moorings (M2, M5, and M8) were conducted with 2-way ANOVAs, pairwise t-tests, or pairwise median tests with adjustment of p-values across multiple tests using the Benjamini-Hochberg (BH) method. If there were significant interaction effects of year and mooring ($p<0.05$), pairwise tests were conducted at each mooring location (n=5 for each mooring). T-tests were conducted for variables that did not have significant heterogeneity of variances (Levene test, $p>0.05$) and residuals were approximately normal (Anderson-Darling test, $p>0.05$) (surface and bottom temperature, surface salinity, turbidity, and stratification intensity). If the assumption of normality was not met, median tests were conducted (surface and 50 m nutrient concentrations and nutrient ratios). For POC, PON, TPP, chlorophyll, and POC:TPP measurements that were collected at varying locations among years, Welch's t-test was used to compare differences across years and p-values were adjusted for multiple testing with the BH method. Comparisons across years in the measurements of POC:PON, the fraction of small POC, and the POC to chlorophyll ratio were done using Wilcoxon rank sum tests with BH adjustment. Comparisons of protist group biomass, and ordination, correlation and network analyses were conducted on the POC-scaled RA data. Principal coordinates analysis (PCoA) on Bray-Curtis

dissimilarities of the POC-scaled RA allowed for visual comparisons of community composition across year and sampling location. A permutational multivariate analysis of variance (PERMANOVA) was conducted to detect significant differences in community composition across years ($p<0.05$). To determine the best subset of environmental factors with maximum correlation to community dissimilarities the bioenv function in R was used. Protist taxonomic group POC differences between years were analyzed using a bootstrap hypothesis testing approach for the difference in protist group POC means between years (10,000 replications) and were adjusted for multiple testing using the BH method. Pairwise Spearman correlations were used to explore the relationship between environmental variables and taxonomic group POC concentrations across both years. Microbial association networks based on the POC-scaled RAs of a subset of ASVs across all samples in both years that made up at least 1% RA in at least 1 sample were constructed for each year separately using the Semi-Parametric Rank-based approach for INference in Graphical model (SPRING) (Yoon et al. 2019).

3.4 Results

3.4.1 Environmental conditions

During cruises conducted in 2017 and 2019 in late September and early October, several physical and chemical characteristics of water masses around mooring locations in the southern (M2), middle (M5), and northern (M8) latitudes of the EBS shelf along the 70 m isobath significantly differed between years (Fig. 3.3, Table 3.1, Table C1). Principal component analysis of environmental variables displayed clear clustering of stations by year

and mooring with separation by year along the first principal axis (PC1) (Fig. 3.3). Salinity, surface and bottom temperature, turbidity, deep water dissolved inorganic nitrogen (DIN) concentrations, deep water silicic acid concentrations, and deep water DIN to phosphate ratios (N:P) had measurements that were on average higher at each mooring location in 2019 compared to 2017 although the magnitude of difference often varied by mooring (Fig. 3.3, Table 3.1, Table C1). Additionally, surface phosphate concentrations had lower average concentrations across all moorings in 2019 compared to 2017. In 2019 after two winters of abnormally low sea ice extent, surface water temperatures and bottom water temperatures were significantly higher at each mooring location but the differences decreased as latitude increased (Fig. 3.3, Table 3.1). At M2, M5, and M8, surface temperatures were on average (mean ± sd) 4.1 ± 0.3 °C, 1.6 ± 0.3 °C, and 0.81 ± 0.08 °C warmer in 2019 versus 2017 while bottom temperatures were on average (mean ± sd) 3.0 ± 0.4 °C, 3.1 ± 0.2 °C, and 2.0 ± 0.4 °C warmer in 2019 versus 2017 (Fig. 3.3, Table 3.1). The mean bottom temperatures at all moorings in 2017 were below 2 °C, the defined cutoff for the ecologically important 'cold pool' (Wyllie-Echeverria & Wooster 1998, Mueter & Litzow 2008, Stabeno et al. 2012a), while in 2019 the mean bottom water temperatures were above this temperature at both M2 and M5. Unlike temperature, surface salinity had larger differences in 2019 versus 2017 around the mid and northern moorings (M5 and M8) than in the south (M2) with average differences ranging from 0.05 PSU at M2 to 0.96 PSU at M8. Although temperature and salinity consistently differed across years at each mooring, mixed layer depths (MLD) did not significantly differ across year or mooring (2-way ANOVA $p > 0.05$) while differences between 2017 and 2019 in the strength of water column stratification (differences in density (sigma-t) between 50 m and 12 m depths) varied across moorings. Surface and 50 m nutrient

concentrations significantly differed between years at most moorings, though the trend in the differences across mooring stations was not consistent for most nutrients (Table C1). Surface concentrations of DIN and silicic acid were significantly higher in 2019 at M5 and M8 while they were on average lower (although not significantly lower for silicic acid) at M2 compared to 2017. Median surface phosphate concentrations were generally 0.2 – 0.4 µmol L^{-1} lower in 2019 compared to 2019 at all moorings but significant differences were not detected at M5. In water below the mixed layer (50 m), DIN concentrations were significantly elevated at all moorings in 2019 compared to 2017 while silicic acid concentrations were generally (but not significantly) higher at all moorings. Ratios of DIN to phosphate or silicic acid suggested that nitrogen was limiting relative to average biological requirements (N:P <16, N:Si < 1) (Redfield 1958, Brzezinski 1985) but the degree of limitation varied across years and moorings (Table C1).

3.4.2 Particulate organic carbon, biomass elemental ratios, and chlorophyll

Microbial community POC, elemental ratios (POC:PON, POC:TPP), and chlorophyll-a concentrations from samples taken at stations displayed in Fig 3.2 showed overall trends between years (Fig. 3.4, Tables C2 and C3). Concentrations of POC (representing biomass) and PON within the size fractions ~ 0.7-200 µm and ~0.7-20 µm did not significantly differ between 2017 and 2019 (Welch's t-test BH adjusted $p > 0.05$) while the TPP within these size fractions was significantly greater in 2019 compared to 2017 (Welch's t-test BH adjusted $p < 0.05$) (Table C2). Additionally, the fraction of POC that was less than 20 µm within each sample was higher in 2017 (median = 0.93) than 2019 (median = 0.80) (Wilcoxon exact test, BH adjusted $p = 0.01$) (Table C3). The elemental ratio of microbial biomass differed across years with larger POC:PON in 2019 compared to 2017 and

lower POC:TPP in 2019 versus 2017 (Wilcoxon exact test or Welch's t-test BH adjusted values < 0.05) (Tables C2 and C3, Fig. 3.4). Although POC did not differ across years, chlorophyll-a concentrations (often used as a proxy for phytoplankton biomass) were larger on average in 2019 (mean ± sd = 2.4 ± 0.8 μg L^{-1}) compared to 2017 (1.6 ± 0.8 μg L^{-1}) (Welch's t-test BH adjusted p = 0.0115) (Table C2).

3.4.3 Protist community composition and relation to environmental variables

Across all samples in both 2017 and 2019, 1555 unique protist amplicon sequence variants (ASVs) were recovered through amplicon sequencing of the V9 hypervariable region of the 18S rRNA gene. Only 34% of these ASVs were present in both 2017 and 2019 while 20% and 45% were unique to either 2017 or 2019. The relative sequence abundance (hereafter RA) of protist ASVs grouped by taxonomic Division or Class (Division Dinoflagellata was separated into Classes Dinophyceae and Syndiniales and Division Ochrophyta was separated into Bacilliarophyta and 'Other Ochrophyta' Classes) or by trophic position displayed general trends in RA across years and stations (Fig. 3.5). In 2019 the RA was dominated by putative Apicomplexan parasites with this group making up an average (mean ± sd) of 48% ± 2% across all samples. There was only a single sample in 2019 in which Apicomplexa did not make up more than 23% RA (TL6, within a coccolithophore bloom patch; Fig. C1) and this station mainly represented (53% RA) by a different putative parasitic group, Syndiniales. Including Apicomplexa, the top five Divisions/Classes with the highest average RA in 2019 were Dinophyceae (18% ± 10%), Chlorophyta (12% ± 7%), Syndiniales (8% ± 11%), and Bacillariophyta (6% ± 7%). In contrast, in 2017 Dinophyceae ASVs were the most relatively abundant group with an average (mean ± sd) RA of 23% ± 7% while the RA of Apicomplexa ASVs had a mean ± sd

of 7% ± 7% (5th highest average RA) across all samples. ASVs belonging to Bacillariophyta (15% ± 12%), Chlorophyta (11% ± 10%), and Haptophyta (8% ± 12%) made up the remaining top five Divisions/Classes in 2017. When ASVs were grouped by trophic position, putative parasites comprised, on average, 12 ± 10% and 55 ± 15% of the communities in 2017 and 2019 respectively and made up the largest trophic fraction in 2019. Putative phototrophic ASVs, making up the largest trophic fraction in 2017, comprised on average 33 ± 11% and 20 ± 11% of the communities in 2017 and 2019 respectively. The overall ratio of phytoplankton ASVs (obligate autotrophs and constitutive mixotrophs) to non-phytoplankton ASVs (non-constitutive mixotrophs, heterotrophs, and parasites) was significantly higher in 2017 compared to 2019 (Wilcoxon rank sum test $p < 0.0001$).

Although the RA of microbes within communities can provide useful information on the relative importance of different taxonomic or functional groups within the microbial community, it obscures differences in absolute abundance or biomass. Since amplicon sequencing data is inherently compositional, the protistan relative sequence abundances were scaled by concurrently determined POC concentrations (~0.7 – 200 µm size fraction) to provide estimates of POC contributions of individual protist ASVs and groups (see materials and methods). Ordination analysis on the POC-scaled RA of protist ASVs by principal coordinates analysis (PCoA) revealed clustering of sampling locations by year and by region (Fig. 3.6). Significant differences in POC-scaled community composition were detected across years (PERMANOVA $p = 0.0001$) and appeared to separate along the first principal coordinate axis which explained ~ 30.7 % of the community variance (Fig. 3.6). The environmental factors that correlated best (bioenv, method = spearman; $\rho = 0.6036$) with community dissimilarities (and were measured at all stations) were surface temperature,

salinity, turbidity, phosphate, and POC in the 0.7 – 20 µm size fraction, although only temperature ($r^2 = 0.832$, $p = 0.001$) and phosphate ($r^2 = 0.316$, $p = 0.003$) were significantly correlated with the first two coordinate axes (envfit function). Additionally, the top 10 ASVs with the highest average POC concentrations in each year differed for 8 of 10 ASVs with only an ASV assigned to the family Cephaloidophoridae (Division Apicomplexa) and an ASV assigned as *Nannochloris sp.* (Division Chlorophyta) contributing to the top 10 in POC concentrations in both years (Table 3.2). In 2017, the top 10 ASVs contained 4 different diatom ASVs (Class Bacillariophyta) and 1 apicomplexan ASV while in 2019 there was only 1 diatom ASV and 3 apicomplexan ASVs in the top 10 (Table 3.2).

Analysis of POC-scaled RA of the top 12 most abundant taxonomic Divisions revealed significant differences in the mean POC concentrations of most taxonomic groups between 2017 and 2019 (Fig. 3.7a). Notably, mean POC concentrations of Mesomycetozoa and Apicomplexa were approximately 21 and 8 times higher in 2019 compared to 2017. On the other hand, Picozoa, Cryptophyta, and Pseudofungi POC concentrations were approximately 11, 8, and 6 times higher in 2017 compared to 2019. In addition to the environmental factors with the highest correlation to overall community dissimilarity, many other variables significantly correlated with Division/Class biomass (pairwise Spearman correlation $p < 0.05$) (Fig. 3.7b). Surface temperature, which was an important factor describing overall community dissimilarity, significantly correlated with taxonomic group POC concentrations for all major taxonomic groups that significantly differed between years plus Division Haptophyta. This was consistent with trends in temperature across years such that groups with significantly higher POC concentrations in 2019 were positively correlated with temperature. Phosphate concentrations also significantly correlated with the POC

concentration of many taxonomic groups as expected based on differences across years. Although the mixed layer depth and stratification are expected to be important variables controlling phytoplankton production, MLD and stratification intensity were only significantly correlated with one or two taxonomic groups. Latitude was also only significantly correlated with two taxonomic groups (Dinophyceae and Bacilliarophyta). Putative parasitic groups including Apicomplexa and Syndiniales both displayed increased group POC with higher surface salinity. Apicomplexa POC additionally showed significant positive correlations with surface temperature and POC:PON <20 and negative correlations with surface phosphate concentrations, POC:TPP in both size fractions, and the fraction of POC less than 20 μm. Syndiniales POC was positively correlated with silicic acid concentration, the DIN to phosphate ratio, and the fraction of POC less than 20 μm.

3.4.4 Protist community networks

Protist community networks based on POC-scaled ASV RA were created for each year to examine differences in co-occurrence patterns between 2017 and 2019. A total of 155 ASVs (≥ 1% RA in at least 1 sample across both 2017 and 2019) with 8 of these ASVs unique to 2017 and 14 ASVs unique to 2019 were used to construct networks for 2017 (# ASVs = 133) and 2019 (# ASVs = 147). The ASVs involved in both networks included representatives from 17 different taxonomic Divisions including the Divisions/Classes in Figs 3.5 and 3.7 plus Radiolaria, Sagenista, Choanoflagellida, Katablepharidophyta, and Telonemia. The greatest number of ASVs included in the networks belonged to the Dinophyceae Class (2017: n = 31, 2019: n = 36) while Bacillariophyta, other Ochrophyta Classes, Syndiniales, and Ciliophora were all represented by 10 – 16 ASVs and all other Divisions had less than 10 ASVs. Even though Apicomplexa dominated the RA of

communities in 2019, only 6 ASVs had greater than or equal to 1% RA in at least 1 sample across both 2017 and 2019 with 1 Apicomplexa ASV unique to 2019. The overall properties of each network differed with the average degree (number of interactions per ASV) equal to 5.6 in 2017 and 6.9 in 2019 and a higher percent of positive interactions in 2019 (78%) compared to 2017 (68%). In 2019, most Divisions/Classes had a greater average degree, although Haptophyta, Opalozoa, Choanoflagellida, and Telonemia had a greater average degree in 2017 and Pseudofungi ASVs had the same average degree across years. ASVs with a large number of interactions may be considered 'hub species' and in 2019 there were 7 ASVs that had more than 10 interactions per ASV while there were no ASVs in 2017 that had more than 9 interactions. Of the 15 most connected ASVs in either 2017 (degree ≥ 8) or 2019 (degree ≥ 10), only three ASVs were hubs in both 2017 and 2019 (identified as an unknown Dinophyceae (NCBI Blast hit to *Azadinium sp.*), an unknown Tintinnidae (Division Ciliophora; NCBI Blast hit to *Salpingella sp.)*, and the dinoflagellate *Levanderina fissa*) while the other 12 ASVs were from a variety of taxonomic Divisions and Classes (Tables C4, C5). Among the 3 'hub species' that were consistent among years, the interactions with other ASVs differed (Fig. 3.8). Additionally, the interactions of ASVs belonging to the highest abundance taxonomic groups often displayed different patterns between years (Figs. 3.9, C2). In particular, chlorophytes had only positive interactions with Bacillariophyta, Syndiniales, other Ochrophyta, Cryptophyta, and Picozoa ASVs, only negative interactions with Haptophyta ASVs, and no interactions within the Chlorophyta Division in 2017 while in 2019 purely positive interactions occurred within the Chlorophyta Division and with Syndiniales, Haptophyta, Cryptophyta, Pseudofungi, and Picozoa ASVs (Fig. 3.9). Haptophyta interactions also varied across years with 50% of the interactions in 2017 being

negative and a significant number of positive interactions among haptophyte ASVs while in 2019 only ~19% of interactions were negative and there were no interactions among haptophyte ASVs (Fig. 3.9).

3.5 Discussion

This study revealed the previously unknown diversity and variability of fall protist communities across years with differential sea ice influence in the EBS. Although trends in protists communities in the context of ongoing anthropogenic climate change cannot be inferred based on only 2 years of data, these results suggest that understanding microbial community trends may be key for interpreting the mechanisms of bottom-up controls on higher trophic levels in the EBS.

3.5.1 Physical and chemical conditions varied across differential sea ice extent years

It is not particularly surprising that several physical and chemical variables significantly differed across years with contrasting prior winter sea ice extent as it is a key feature of the EBS shelf (Stabeno et al. 2010, 2012b). Several studies have demonstrated that winter sea ice extent, concentration, and timing of retreat dictates whether spring through fall temperatures will be warmer or colder than average (Mueter & Litzow 2008, Stabeno et al. 2012a, 2012b). Results from 2017 and 2019 are consistent with lower sea ice extent and early retreat resulting in warmer surface and bottom temperatures in 2019 compared to 2017, although 2017 was not considered a ‘cold year’ (Siddon & Zador 2017). The increased salinity around all mooring locations and lack of a cold pool at M2 and M5 also show the reduced influence of sea ice melt over the shelf in 2019. The decrease in the magnitude of temperature difference and the increasing magnitude of salinity between years with

increasing latitude show the differing spatial influence of sea ice across years. In 2017, maximum sea ice extent reached to M2 while in 2019 the maximum extent only covered M8 (Stabeno & Bell 2019) while residual heat from a warm and low ice winter of 2017/2018 and advection of warm North Pacific waters may have allowed the area around M2 to display significantly warmer surface and bottom temperatures than the more northern locations in 2019 compared to 2017 (Siddon & Zador 2019, Stabeno & Bell 2019) Even though ice covered M8 in both 2017 and 2019, the early sea ice retreat in 2019 created more time for advection and mixing to influence the water column leaving almost no remnant of a freshwater lens in 2019, resulting in much larger differences across years in salinity at M8 compared to more southern locations.

The middle shelf of the EBS (from ~50-100 m depth) in the summer and fall is generally a highly stratified two-layer system that is separated between northern and southern regions with a transition zone (~59-60°) influenced by the seasonal extent of sea ice and differential patterns of advection (Stabeno et al. 2010, 2012a). Several physical and chemical parameters displayed consistent overall trends between 2017 and 2019 at all mooring locations, though in most cases the magnitude of difference and even the direction of difference across years depended mooring location (latitude). This suggests that the southern and northern regions are distinctly influenced by sea ice changes between years. Lower sea ice extent in the north has been shown to result in weaker water column stratification due to the lack of a freshwater lens (Duffy-Anderson et al. 2019, Stabeno & Bell 2019), and the results shown here suggest that fall stratification strength is slightly weaker in the north (significant differences at M5, non-significant difference at M8) in 2019. However, in the south around M2, stratification was stronger in 2019 compared to 2017 which may be

attributed to less stormy conditions in 2019 than usual (Siddon & Zador 2019) and the fact that temperature controls stratification strength more than salinity in this region (Stabeno et al. 2010, Ladd & Stabeno 2012).

Surface DIN and silicic acid concentrations may have been influenced by the differential stratification trends near each mooring as the higher stratification at M2 could have reduced the ability of wind or storms to mix the water column and bring deep water with high nutrients to the surface (Eisner et al. 2016, Gann et al. 2016). Deep water DIN and N:P was higher on average in 2019 which is consistent with general trends between warm and cold years found by Mordy and colleagues (2021) and may be indicative of a younger bottom water age in 2019 due to stronger northward flow in warm years (Stabeno et al. 2016). The lower surface phosphate concentrations in 2019 compared to 2017 across all moorings potentially indicated that, after mixing with deep waters, biological utilization of the higher deep-water N:P allowed for greater depletion of phosphate in 2019 than in 2017. The differential influence of sea ice on different regions of the EBS makes it difficult to predict how the ecosystem will respond overall (Stabeno et al. 2012a) as the southeastern part of the EBS near M2 has been experiencing stanzas of warm and cold years since the early 2000s (Stabeno et al. 2012b, 2016, 2019) but the northern portion of the EBS has almost always been partially ice covered during winter except in more recent years (Duffy-Anderson et al. 2019, Stabeno & Bell 2019). Several questions remain about how the northern EBS will respond to continued warming and decreasing sea ice with recent years displaying unprecedented changes in this region that weren't expected to occur until at least the next decade (Stabeno et al. 2012a, Wang et al. 2012).

3.5.2 Differences in microbial community biomass quality and composition with implications for higher trophic levels

This study revealed that while overall POC did not significantly differ across years, the nutritional quality with respect to nitrogen and phosphorus, the fraction of POC within the nano- and pico-plankton size range (<20 μm), the chlorophyll concentration, the ratio of phytoplankton to non-phytoplankton, and the protist community composition varied across years. Changes in these variables across years have implications for the transfer of carbon, nutrients, and energy through the microbial food web and up to higher trophic levels.

The nutritional quality of biomass (represented here by POC:PON and POC:TPP) is known to impact growth rates, fitness, and reproductive success of zooplankton and higher trophic levels (Sterner and Elser 2002, Malzahn & Boersma 2012, Schoo et al. 2013). Comparisons of POC:PON and POC:TPP between 2017 and 2019 showed that in 2019 the nutritional quality with respect to nitrogen was lower (POC:PON was higher) but the quality with respect to phosphorus was higher (POC:TPP was lower) than 2017. Deficiencies of nitrogen and phosphorus in the diets of copepods have been shown to result in different physiological responses in copepod growth and reproduction (Burian et al. 2018, Bi & Sommer 2020). For example, Burian and colleagues found that the copepod *Arcatia tonsa* reduced growth rates under both N-deficient and P-deficient diets but the copepods responded to P-deficiency by increasing ingestion rates while they responded to N-deficiency by investing in structural fatty acids and depleting unsaturated fatty acids in storage lipids. It is difficult to discern the mechanisms controlling POC:PON or POC:TPP ratios due to high variability of these ratios across individual phytoplankton species (Geider & La Roche 2002, Finkel et al. 2010, Garcia et al. 2018). In fact, decreased lipid storage in juvenile Bering Sea

crabs during a warm year compared to a cold year was attributed to an increased fatty acid source from diatoms (Copeman et al. 2021). Additionally, changes in organic matter during trophic transfer (Talmy et al. 2016), the confounding effect of detritus and other non-living organic matter, and effects of temperature (Toseland et al. 2013, Garcia et al. 2018), irradiance (Finkel et al. 2006), nutrient limitation (Grosse et al. 2017), and carbon dioxide availability (Schoo et al. 2013) have significant impacts on the elemental ratios of biomass. Since nitrogen and phosphorus quality changes differentially across years, it is unclear how zooplankton growth and reproduction might compare between years but reduced lipid storage due to high POC:PON in 2019 might be detrimental to the survival of zooplankton throughout the winter (Lee et al. 2006). Therefore, it is likely that a combination of environmental conditions and protist community composition controlled the nutritional quality between years with implications for trophic transfer of biomass and the health and success of higher trophic levels.

In addition to changes in the nutritional quality of biomass between years, the fraction of POC that was less than 20 μm in size was lower on average in 2019 compared to 2017, potentially indicating that trophic transfer was more efficient or that larger protists were being less efficiently grazed in 2019 (Goering & Iverson 1981, Sommer et al. 2002, Eisner et al. 2016). The high POC:TPP values in 2017 might have increased copepod ingestion rates of the larger protists as was shown by Burian and colleagues (2018). Additionally, chlorophyll concentrations were significantly higher in 2019. Eisner and colleagues (2016) found that chlorophyll concentrations and the fraction of large-sized phytoplankton were increased in late summer/early fall during warm years compared to cold years in the EBS and suggest that lower abundances of larger copepods and euphausiids in warm years (Coyle et al. 2011,

Ressler et al. 2012, Eisner et al. 2014) may exert less grazing pressure on larger phytoplankton. Indeed, 2017 appeared to have higher abundances of euphausiid grazers than 2019 but large copepod abundances were relatively low in 2017 as well as in 2019, while smaller copepods had similar abundances (Siddon & Zador 2019).

Estimates of proportional biomass of phytoplankton to non-phytoplankton from 18S sequencing data appear to contradict the higher chlorophyll concentrations (suggesting higher phytoplankton biomass) observed in 2019 with a lower proportion of POC as phytoplankton in 2019. This apparent discrepancy may be largely due to the differing methodologies and interpretation of these samples. First, while the POC and 18S sequencing samples were pre-filtered at 200 μm, the chlorophyll samples were unfiltered. This may have resulted in increased chlorophyll associated with phytoplankton or mixotrophs that were larger than 200 μm and not analyzed in the POC or DNA fractions which may confound the comparisons between chlorophyll and phytoplankton:non-phytoplankton POC ratios. Additionally, chlorophyll may not be an accurate measure of phytoplankton biomass as the carbon to chlorophyll ratio of individual phytoplankton cells is known to vary dramatically while environmental conditions such as irradiance, nutrient concentrations, and temperature may all influence species specific carbon to chlorophyll ratios (Chan 1978, Falkowski et al. 1985, Geider 1987, Cloern et al. 1995). Therefore, the trends in chlorophyll concentration across years may not reflect differences in phytoplankton biomass but rather differences in community composition or physiological adaptations to differing environmental conditions. There are also biases associated with the estimate of the phytoplankton to non-phytoplankton ratio from 18S sequencing data including that protist 18S rRNA gene copy numbers vary significantly (Gong & Marchetti 2019) and although it has been shown that gene copy

number scales roughly with cell biovolume and hence carbon biomass across diverse protist groups (Menden-Deuer & Lessard 2000, Zhu et al. 2005, Godhe et al. 2008), there are many ASVs and even whole lineages that have not been cultured and remain understudied. There may also be errors in the identification of ASVs and/or assignment to a trophic class (phytoplankton or non-phytoplankton) while there is some fraction of ASVs (~4% on average) (and therefore biomass) whose identity or trophic status could not be determined. For the purpose of this discussion, we assume that the POC-scaled RA of protist ASVs is representative of the protist community < 200 μm in size and therefore conclude that in 2019, despite increased chlorophyll concentrations, non-phytoplankton biomass comprised largely of putative parasites dominated the communities while phytoplankton biomass generally dominated the communities in 2017. This shift to a more heterotrophic community in a warmer year is consistent with mesocosm experiments showing that as temperatures increased, respiratory consumption of organic carbon was accelerated relative to autotrophic production (Wohlers et al. 2009).

Based on 18S sequencing data, protist communities significantly differed across years with putative parasites from the Division Apicomplexa comprising a significant portion of the RA across almost all samples in 2019. Regarding POC contribution of protist taxonomic groups, only two major groups, Apicomplexa and Mesomycetozoa, had higher average POC concentrations in 2019 compared to 2017. With the recent widespread use of DNA metabarcoding methods across diverse environments, putative parasites from groups such as Apicomplexa and Syndiniales have proved to be more diverse, abundant, and ubiquitous than previously thought (Guillou et al. 2008, De Vargas et al. 2015, Mahé et al. 2017, Clarke et al. 2019, Del Campo et al. 2019). Metamycetozoa have historically been represented by mainly

fish parasites, but descriptions of many new species suggest that this taxonomic group may associate with a variety of organisms in various types of symbioses (Glockling et al. 2013). Gregarines, constituting the majority of apicomplexan ASVs identified here, are an understudied group of putative invertebrate parasites that have been suggested to play a significant role in marine ecosystems (Leander 2008, Del Campo et al. 2019). Gregarines have been shown infect a variety of crustacean hosts (Théodoridès 1989, Rueckert et al. 2011), including copepods (Théodoridès 1989, Rueckert et al. 2011) and euphausiids (Théodoridès 1989, Takahashi et al. 2009, Wallis et al. 2017). Additionally, Takahashi and colleagues (2009, 2011) investigated the impacts of gregarine infection on host ecology and found that heavy parasite infestation impacted krill digestion without causing death of the host. Although the Apicomplexa lineage is suggested to be parasitic, implying harm to host organisms, the understudied nature of many apicomplexans including marine gregarines leave numerous questions about the host-parasite association for many representatives within this diverse taxonomic group (Rueckert et al. 2019). The dominance of apicomplexans in 2019 is noteworthy, but since the ecological role of this group is not entirely clear, it is difficult to speculate on the implications of this trend and further work is necessary to examine the role of these putative parasites in the EBS.

In 2017 the biomass of diatoms (Bacillariophyta), other ochrophytes, ciliates, and lesser abundant Divisions (Cercozoa, Cryptophyta, Pseudofungi, Picozoa, and Opalozoa) was higher on average compared to 2019. In the EBS, large diatoms are often considered an important base of the marine food web by being a more efficient link to higher trophic levels than other small phytoplankton and providing adequate food to benthic communities due to fast sinking rates (Springer et al. 1996, Grebmeier et al. 2006, Eisner et al. 2016). Although

large diatoms may typically represent an efficient food chain, the most abundant diatom ASVs in 2017 were very small diatom species (*Arcocellulus cornucervis* (< ~3.5 μm in size; Balzano et al. 2017) and *Minidiscus sp.* (< ~5 μm in size; Kaczmarska et al. 2009). Therefore, the presence of diatoms here may not create efficient transfer of biomass to higher trophic levels in fall when these communities were dominated by small cells. The smaller phytoplankton cells in 2017 may be supporting the larger biomass of ciliates (Division Ciliophora) which are an important component of the microzooplankton in the EBS during summer and are a critical food source for copepods (Calbet & Saiz 2005, Stoecker et al. 2014). Summer and early fall are not the most productive times of the year in the EBS, but this is a critical time for growth and lipid accumulation of larval and juvenile fish, including walleye pollock, prior to overwintering (Duffy-Anderson et al. 2006, Siddon et al. 2013, Eisner et al. 2016, Sigler et al. 2016). Therefore, the biomass, nutritional quality, and composition of protists communities supporting higher trophic levels in the EBS are incredibly important for managing this ecosystem and the productive fisheries. The implications of shifting communities and the dominance of putative parasites or phytoplankton on higher trophic levels in the EBS remains unknown and warrants further research.

3.5.3 Parasites and other biotic interactions may be influenced by warming and other environmental conditions

Many environmental variables significantly correlated with the biomass of various protist groups. Since conditions across years were very different, it is hard to uncouple

correlation and causation and it is also clear that not only are abiotic factors important in controlling protist communities, but biotic interactions within communities and with other microbes (e.g., bacteria and archaea), zooplankton, and larger metazoa are likely important in structuring the protist community. Temperature appeared to correlate with taxonomic groups that differed across years and thus it is possible that higher temperatures promote the biomass of apicomplexans and mesomycetozoans but it is also possible that temperature has only an indirect effect on these protist groups. At higher temperatures, as host metabolism is increased it might be expected that the feeding, growth, and development of parasites inside hosts is enhanced which may increase damage to the host organism (Fels & Kaltz 2006, Macnab & Barber 2012, Kirk et al. 2018). Although, host-parasite dynamics in response to temperature change are complex and variable across various host-parasite systems, while the timing of parasitic infection and development may also be altered (Kirk et al. 2018, Byers 2021). One of the other major parasitic groups, Syndiniales, did not have significantly increased biomass in 2019 compared to 2017 while Ciliophora, which had higher biomass in 2017, also has representatives that are parasitic and so it is likely that not all parasites respond similarly to temperature changes. Interestingly, in 2019 Syndiniales dominated the single sample that was taken within a well developed coccolithophore bloom where apicomplexan biomass was relatively low and it might be expected that visual predators (possibly including zooplankton) were also in lower abundances (Vance et al. 1998, Eisner et al. 2003) and therefore this protistan infecting parasite may have benefitted from the highly turbid late bloom conditions while grazing was reduced (Olson & Strom 2002). In addition to temperature, other abiotic and biotic factors may influence host-parasite dynamics. For example, high salinities have been associated with increased parasitism (Bricknell et al.

2006, Coffey et al. 2012, Byers 2021) while stress from high temperatures or low oxygen levels may impact the susceptibility of hosts to parasitic infections (Byers 2021). The potential increase in the biomass of putative parasites in 2019 suggest that a changing climate will alter the complex host-parasite interactions with implications for the transfer of carbon and energy throughout the food web and the survival of protists, zooplankton, or even higher trophic levels prior to the onset of winter conditions.

Network analysis of 2017 and 2019 protist communities revealed that the communities were structured differently with 2019 showing more connectedness than 2017 and individual ASVs and taxonomic groups displaying different co-occurrence dynamics across years. This analysis supports the fact that interactions between protists (such as host-parasite interactions) have a complex dependence on abiotic factors as well as other organisms within the community. Biotic interactions may have a larger role than abiotic factors in structuring communities (Lima-Mendez et al. 2015) and in the middle shelf of the EBS the slow currents and a highly stratified water column allow for ample time for interactions and succession to shape these communities. Although this type of analysis can help predict ecological interactions within the environment, these patterns are only hypotheses, and any specific interactions would need to be tested to confirm the trends observed here. Additionally, with these results it cannot be determined how other microbes or higher trophic levels interact with protists, but that would be an important topic for future work, especially because apicomplexan parasites (as well as other putative parasites) are likely to have a major influence on zooplankton communities. Interpreting the observed positive and negative interactions within these communities may not be completely straightforward, but previous work has suggested that positive, co-occurrence interactions

signify taxa that are performing complementary functions, sharing similar niches, or are involved in symbiotic relationships (including parasitism) while negative interactions may represent competing taxa or resource portioning among taxa (Fuhrman & Steele 2008, Berdjeb et al. 2018, Anderson & Harvey 2020). Predator-prey relationships are difficult to infer from snapshots as temporal dynamics impact whether interactions appear as positive or negative with recent work suggesting that both positive and negative associations may represent predation (Anderson & Harvey 2020, Sassenhagen et al. 2020).

As others have observed, positive interactions between Dinophyceae and Syndiniales ASVs appear to be common (Torres-Beltrán et al. 2018, Anderson & Harvey 2020) with the two Dinophyceae hub species found in both years displaying positive interactions with 1-2 Syndiniales ASVs and relatively large fractions of positive Syndiniales interactions occurring with Dinophyceae. Although, Syndiniales ASVs were also shown to have positive interactions with several other taxonomic groups including, but not limited to, Apicomplexa, Bacilliariophyta, other ochrophytes, Chlorophyta, Ciliophora, Haptophyta, and Cercozoa. These interactions may support the fact that Syndiniales is considered an opportunist with low host specificity (Guillou et al. 2008) and are thought to infect a variety of other hosts such as ciliates, diatoms, and cercozoans (Clarke et al. 2019, Sassenhagen et al. 2020, Zamora-Terol et al. 2021). This may also be an indication of shared niche space or indirect predator-prey relationships (e.g., consumption of prey that has been infected).

The network comparisons between 2017 and 2019 revealed that among high biomass groups, even ones that did not significantly differ in biomass across years, interaction patterns diverged. In particular, Divisions Chlorophyta and Haptophyta showed very different interaction trends between years even though their total biomass did not

significantly differ. Therefore, these groups may provide different functions within the ecosystems when abiotic conditions vary. Both chlorophytes and haptophytes are important and ubiquitous contributors to primary production and phytoplankton biomass in the global ocean (Worden et al. 2004, Liu et al. 2009, Tragin & Vaulot 2018). Although, the recognition that mixotrophy is a common occurrence in the marine environment has uncovered several representatives from both groups that exhibit mixotrophy and suggest that they may be important bacterial grazers (Mitra et al. 2016, Anderson et al. 2018). Light levels and nutrient availability have been shown to alter the trophic strategy of several chlorophytes and haptophytes with varying degrees of trophic flexibility across species (McKie-Krisberg et al. 2015, Anderson et al. 2018) which may help explain why these groups show significantly different interaction patterns across years. The biomass of these groups may also significantly depend on bacterial dynamics which was not analyzed here. In particular, *Chrysochromulina sp.*, represented by several ASVs in the networks, has displayed bacterivory across several species and may increase bacterial ingestion under phosphate limitation (Jones et al. 1993, Nygaard & Tobiesen 1993). Therefore, the lower surface phosphate concentrations in 2019 (although phosphate may not have been limiting) may have shifted the trophic strategy of mixotrophs towards increased grazing. The network analysis done here contains a lot of information about the EBS protist community and if expanded to include more spatial and temporal variability combined with laboratory or culture work, these tools have the ability to explore novel interactions, determine important species within communities, and gain a deeper understanding of important host-parasite dynamics.

3.6 Conclusions

This study provides the first snapshot of EBS protist communities in the fall of two years with distinct sea ice influences. Physical and chemical conditions were significantly different during fall near 3 long-term mooring sites with warmer surface and bottom water temperatures and higher surface salinity in 2019 compared to 2017. The significant variability in protist communities between years and the unexpected diversity and abundance of putative parasites suggests that protists likely play key roles in structuring EBS ecosystems and may help explain bottom-up controls on economically and culturally important species. Putative parasites (mostly from Division Apicomplexa) made up a large fraction of the ASV RA in 2019 and the community was in a more heterotrophic state compared to 2017. Although long term trends in community composition cannot be inferred from only two years of data, many environmental variables correlated with protist group POC and may indicate specific abiotic factors that promote various groups. Additionally, network analysis revealed that biotic interactions have significant roles in shaping community composition and specific interactions within protist groups and with other organisms not analyzed here (e.g. mesozooplankton, bacteria) should be further explored. As climate change continues to disrupt this ecosystem, it is imperative to gain information on microbial communities that form the base of the marine food web and drive biogeochemical cycles. The tools used here can expand the understanding of these processes and uncover novel interactions and controls on the EBS ecosystem.

3.7 Acknowledgements

This work would not have been possible without funding from the North Pacific Research Board (NPRB) graduate student research award in 2017. Additionally, the NOAA EcoFOCI program provided cruise berths and data for this project. Specifically, I'd like to

thank Phyllis Stabeno, Peter Proctor, and Geoff Lebon for providing a berth space on the fall mooring cruises during 2017 and 2019 on the NOAA ship Oscar Dyson. Additionally, Shaun Bell and Phyllis Stabeno provided processed CTD and bottle data for use, Colleen Harpold and Janet Duffy-Anderson provided chlorophyll data, and Eric Wisegarver provided nutrient data. I appreciate sampling help and advice from Peter Proctor, Stephanie Grassia, Allison Deary, and Jesse Lamb. Thanks to the captain and crew on the NOAA Oscar Dyson during both cruises. Thank you to Dylan Catlett and Sylvia Kim for helping to process the DNA samples and analyze the data. I greatly appreciate my advisor, Debora Iglesias-Rodriguez, and my doctoral committee, Uta Passow and Mark Brzezinski, for reviewing this work.

3.8 Literature cited

Adl SM, Bass D, Lane CE, Lukeš J, Schoch CL, Smirnov A, Agatha S, Berney C, Brown MW, Burki F, Cárdenas P, Čepička I, Chistyakova L, del Campo J, Dunthorn M, Edvardsen B, Eglit Y, Guillou L, Hampl V, Heiss AA, Hoppenrath M, James TY, Karnkowska A, Karpov S, Kim E, Kolisko M, Kudryavtsev A, Lahr DJG, Lara E, Le Gall L, Lynn DH, Mann DG, Massana R, Mitchell EAD, Morrow C, Park JS, Pawlowski JW, Powell MJ, Richter DJ, Rueckert S, Shadwick L, Shimano S, Spiegel FW, Torruella G, Youssef N, Zlatogursky V, Zhang Q (2019) Revisions to the Classification, Nomenclature, and Diversity of Eukaryotes. J Eukaryot Microbiol 66:4–119

Anderson R, Charvet S, Hansen PJ (2018) Mixotrophy in chlorophytes and haptophytes - Effects of irradiance, macronutrient, micronutrient and vitamin limitation. Front Microbiol 9:1704

Anderson SR, Harvey EL (2020) Temporal variability and ecological interactions of parasitic marine syndiniales in coastal protist communities. mSphere 5:e00209-20

Armengol L, Calbet A, Franchy G, Rodríguez-Santos A, Hernández-León S (2019) Planktonic food web structure and trophic transfer efficiency along a productivity gradient in the tropical and subtropical Atlantic Ocean. Sci Rep 9:2044

Aspila KI, Agemian H, Chau ASY (1976) A semi-automated method for the determination of inorganic, organic and total phosphate in sediments. Analyst 101:187–197

Azam F, Fenchel T, Field JG, Gray JS, Meyer-Reil LA, Thingstad F (1983) The ecological role of water-column microbes in the sea. Mar Ecol Prog Ser 10:257–263

Balzano S, Percopo I, Siano R, Gourvil P, Chanoine M, Marie D, Vaulot D, Sarno D (2017)

Morphological and genetic diversity of Beaufort Sea diatoms with high contributions from the Chaetoceros neogracilis species complex. J Phycol 53:161–187

Berdjeb L, Parada A, Needham DM, Fuhrman JA (2018) Short-term dynamics and interactions of marine protist communities during the spring-summer transition. ISME J 12:1907–1917

Beule L, Karlovsky P (2020) Improved normalization of species count data in ecology by scaling with ranked subsampling (SRS): Application to microbial communities. PeerJ 8:e9593

Bi R, Sommer U (2020) Food quantity and quality interactions at phytoplankton–zooplankton interface: Chemical and reproductive responses in a calanoid copepod. Front Mar Sci 7:274

Bricknell IR, Dalesman SJ, O'Shea B, Pert CC, Luntz AJM (2006) Effect of environmental salinity on sea lice Lepeophtheirus salmonis settlement success. Dis Aquat Organ 71:201–212

Brzezinski MA (1985) The Si:C:N ratio of marine diatoms: Interspecific variability and the effect of some environmental variables. J Phycol 21:347–357

Burian A, Grosse J, Winder M, Boschker HTS (2018) Nutrient deficiencies and the restriction of compensatory mechanisms in copepods. Funct Ecol 32:636–647

Byers JE (2021) Marine Parasites and Disease in the Era of Global Climate Change. Ann Rev Mar Sci 13:397–420

Calbet A, Saiz E (2005) The ciliate-copepod link in marine ecosystems. Aquat Microb Ecol 38:157–167

Callahan BJ, McMurdie PJ, Rosen MJ, Han AW, Johnson AJA, Holmes SP (2016) DADA2: High-resolution sample inference from Illumina amplicon data. Nat Methods 13:581–583

Del Campo J, Guillou L, Hehenberger E, Logares R, López-García P, Massana R (2016) Ecological and evolutionary significance of novel protist lineages. Eur J Protistol 55:4–11

Del Campo J, Heger TJ, Rodríguez-Martínez R, Worden AZ, Richards TA, Massana R, Keeling PJ (2019) Assessing the diversity and distribution of apicomplexans in host and free-living environments using high-throughput amplicon data and a phylogenetically informed reference framework. Front Microbiol 10:2373

Caron DA, Countway PD, Jones AC, Kim DY, Schnetzer A (2012) Marine protistan diversity. Ann Rev Mar Sci 4:467–493

Catlett D, Matson PG, Carlson CA, Wilbanks EG, Siegel DA, Iglesias-Rodriguez MD (2020) Evaluation of accuracy and precision in an amplicon sequencing workflow for marine protist communities. Limnol Oceanogr Methods 18:20–40

Catlett D, Son K, Liang C (2021) EnsembleTax: An R package for determinations of

ensemble taxonomic assignments of phylogenetically-informative marker gene sequences. PeerJ 9:e11865

Chan AT (1978) Comparative physiological study of marine diatoms and dinoflagellates in relation to irradiance and cell size. 1. Growth under continous light. J Phycol 14:396–402

Clarke LJ, Bestley S, Bissett A, Deagle BE (2019) A globally distributed Syndiniales parasite dominates the Southern Ocean micro-eukaryote community near the sea-ice edge. ISME J 13:734–737

Cleary AC, Durbin EG (2016) Unexpected prevalence of parasite 18S rDNA sequences in winter among Antarctic marine protists. J Plankton Res 38:401–417

Cloern JE, Grenz C, Vidergar-Lucas L (1995) An empirical model of the phytoplankton chlorophyll : carbon ratio-the conversion factor between productivity and growth rate. Limnol Oceanogr 40:1313–1321

Coffey AH, Li C, Shields JD (2012) The effect of salinity on experimental infections of a hematodinium sp. in blue crabs, callinectes sapidus. J Parasitol 98:536–542

Copeman LA, Ryer CH, Eisner LB, Nielsen JM, Spencer ML, Iseri PJ, Ottmar ML (2021) Decreased lipid storage in juvenile Bering Sea crabs (Chionoecetes spp.) in a warm (2014) compared to a cold (2012) year on the southeastern Bering Sea. Polar Biol 44:1883–1901

Coyle KO, Eisner LB, Mueter FJ, Pinchuk AI, Janout MA, Cieciel KD, Farley E V., Andrews AG (2011) Climate change in the southeastern Bering Sea: Impacts on pollock stocks and implications for the oscillating control hypothesis. Fish Oceanogr 20:139–156

Doyle J (1991) DNA Protocols for Plants. In: Hewitt GM, Johnston AWB, Young JPW (eds) Molecular Techniques in Taxonomy. NATO ASI Series (Series H: Cell Biology), vol 57. Springer, Berlin, Heidelberg. https://doi.org/10.1007/978-3-642-83962-7_18

Duffy-Anderson JT, Busby MS, Mier KL, Deliyanides CM, Stabeno PJ (2006) Spatial and temporal patterns in summer ichthyoplankton assemblages on the eastern Bering Sea shelf 1996-2000. Fish Oceanogr 15:80–94

Duffy-Anderson JT, Stabeno P, Andrews AG, Cieciel K, Deary A, Farley E, Fugate C, Harpold C, Heintz R, Kimmel D, Kuletz K, Lamb J, Paquin M, Porter S, Rogers L, Spear A, Yasumiishi E (2019) Responses of the Northern Bering Sea and Southeastern Bering Sea Pelagic Ecosystems Following Record-Breaking Low Winter Sea Ice. Geophys Res Lett 46:9833–9842

Dumack K, Fiore-Donno AM, Bass D, Bonkowski M (2020) Making sense of environmental sequencing data: Ecologically important functional traits of the protistan groups Cercozoa and Endomyxa (Rhizaria). Mol Ecol Resour 20:398–403

Durbin EG, Casas MC (2014) Early reproduction by Calanus glacialis in the Northern Bering Sea: The role of ice algae as revealed by molecular analysis. J Plankton Res 36:523–541

Eisner LB, Farley E V, Murphy JM, Helle JH (2003) Distributions of Oceanographic Variables , Juvenile Sockeye Salmon and Age-0 Walleye Pollock in the Southeastern Bering Sea during Fall 2000 – 2003.

Eisner LB, Gann JC, Ladd C, D. Cieciel K, Mordy CW (2016) Late summer/early fall phytoplankton biomass (chlorophyll a) in the eastern Bering Sea: Spatial and temporal variations and factors affecting chlorophyll a concentrations. Deep Res Part II Top Stud Oceanogr 134:100–114

Eisner LB, Napp JM, Mier KL, Pinchuk AI, Andrews AG (2014) Climate-mediated changes in zooplankton community structure for the eastern Bering Sea. Deep Res Part II Top Stud Oceanogr 109:157–171

Falkowski PG, Dubinsky Z, Wyman K (1985) Growth-irradiance relationships in phytoplankton. Limnol Ocean 30:311–321

Fetterer F, Knowles K, Meier WN, Savoie M, Windnagel AK (2017) Sea Ice Index, Version 3. [N_Sea_Ice_Index_Regional_Monthly_Data_G02135_v3.0.xlsx]. Boulder, Colorado USA. NSIDC: National Snow and Ice Data Center. doi: https://doi.org/10.7265/N5K072F8. Accessed 20 July 2021

Fels D, Kaltz O (2006) Temperature-dependent transmission and latency of Holospora undulata, a micronucleus-specific parasite of the ciliate Paramecium caudatum. Proc R Soc B 273:1031–1038

Finkel Z V., Beardall J, Flynn KJ, Quigg A, Rees TA V., Raven JA (2010) Phytoplankton in a changing world: Cell size and elemental stoichiometry. J Plankton Res 32:119–137

Finkel Z V., Quigg A, Raven JA, Reinfelder JR, Schofield OE, Falkowski PG (2006) Irradiance and the elemental stoichiometry of marine phytoplankton. Limnol Oceanogr 51:2690–2701

Fuhrman JA, Steele JA (2008) Community structure of marine bacterioplankton: Patterns, networks, and relationships to function. Aquat Microb Ecol 53:69–81

Gann JC, Eisner LB, Porter S, Watson JT, Cieciel KD, Mordy CW, Yasumiishi EM, Stabeno PJ, Ladd C, Heintz RA, Farley E V. (2016) Possible mechanism linking ocean conditions to low body weight and poor recruitment of age-0 walleye pollock (Gadus chalcogrammus) in the southeast Bering Sea during 2007. Deep Res Part II Top Stud Oceanogr 134:115–127

Gao C, Lin S, Chen M, Hong J, Liu C (2019) Prevalence of phycotoxin contamination in shellfish from the Northern Bering Sea and the Chukchi Sea. Toxicon 167:76–81

Garcia NS, Sexton J, Riggins T, Brown J, Lomas MW, Martiny AC (2018) High variability in cellular stoichiometry of carbon, nitrogen, and phosphorus within classes of marine eukaryotic phytoplankton under sufficient nutrient conditions. Front Microbiol 9:1–10

Geider RJ (1987) Light and temperature dependence of the carbon to chlorophyll a ratio in microalgae and cyanobacteria: Implications for physiology and growth of phytoplankton. New Phytol 106:1–34

Geider RJ, La Roche J (2002) Redfield revisited: Variability of C:N:P in marine microalgae and its biochemical basis. Eur J Phycol 37:1–17

Glockling SL, Marshall WL, Gleason FH (2013) Phylogenetic interpretations and ecological potentials of the Mesomycetozoea (Ichthyosporea). Fungal Ecol 6:237–247

Gobler CJ, Doherty OM, Hattenrath-Lehmann TK, Griffith AW, Kang Y, Litaker RW (2017) Ocean warming since 1982 has expanded the niche of toxic algal blooms in the North Atlantic and North Pacific oceans. Proc Natl Acad Sci 114:4975–4980

Godhe A, Asplund ME, Härnström K, Saravanan V, Tyagi A, Karunasagar I (2008) Quantification of diatom and dinoflagellate biomasses in coastal marine seawater samples by real-time PCR. Appl Environ Microbiol 74:7174–7182

Goering JJ, Iverson RL (1981). Phytoplankton distribution on the southeastern Bering Sea shelf. The eastern Bering Sea shelf: oceanography and resources 2:933-946

Goes JI, Gomes R, Haugen EM, Mckee KT, Sa EJD, Chekalyuk AM, Stoecker DK, Stabeno PJ, Saitoh S, Sambrotto RN (2014) Deep-Sea Research II Fluorescence , pigment and microscopic characterization of Bering Sea phytoplankton community structure and photosynthetic competency in the presence of a Cold Pool during summer. Deep Res Part II 109:84–99

Gong W, Marchetti A (2019) Estimation of 18S gene copy number in marine eukaryotic plankton using a next-generation sequencing approach. Front Mar Sci 6:219

Gordon LI, Joe C, Jennings J, Ross AA, Krest JM (1993) A suggested protocol for continuous flow automated analysis of seawater nutrients (phosphate, nitrate, nitrite and silicic acid) in the WOCE Hydrographic Program and the Joint Global Ocean Fluxes Study. In: WOCE Operations Manual, Vol. 3: The Observational Program, Section 3.2: WOCE Hydrographic Programme, Part 3.1.3: WHP Operations and Methods. WHP Office Report WHPO 91-1; WOCE Report No. 68/91, November 1994, Revision 1, Woods Hole, MA, USA, 52.

Grebmeier JM, Overland JE, Moore SE, Farley E V, Carmack EC, Cooper LW, Frey KE, Helle JH, Mclaughlin FA, Mcnutt SL (2006) A major ecosystem shift in the northern Bering Sea. Science (80-) 311:1461–1464

Grosse J, Burson A, Stomp M, Huisman J, Boschker HTS (2017) From ecological stoichiometry to biochemical composition: Variation in N and P supply alters key biosynthetic rates in marine phytoplankton. Front Microbiol 8:1299

Guillou L, Bachar D, Audic S, Bass D, Berney C, Bittner L, Boutte C, Burgaud G, De Vargas C, Decelle J, Del Campo J, Dolan JR, Dunthorn M, Edvardsen B, Holzmann M, Kooistra WHCF, Lara E, Le Bescot N, Logares R, Mahé F, Massana R, Montresor M, Morard R, Not F, Pawlowski J, Probert I, Sauvadet AL, Siano R, Stoeck T, Vaulot D, Zimmermann P, Christen R (2013) The Protist Ribosomal Reference database (PR2): A catalog of unicellular eukaryote Small Sub-Unit rRNA sequences with curated taxonomy. Nucleic Acids Res 41:597–604

Guillou L, Viprey M, Chambouvet A, Welsh RM, Kirkham AR, Massana R, Scanlan DJ, Worden AZ (2008) Widespread occurrence and genetic diversity of marine parasitoids belonging to Syndiniales (Alveolata). Environ Microbiol 10:3349–3365

Hare CE, Leblanc K, DiTullio GR, Kudela RM, Zhang Y, Lee PA, Riseman S, Hutchins DA (2007) Consequences of increased temperature and CO2 for phytoplankton community structure in the Bering Sea. Mar Ecol Prog Ser 352:9–16

Van Hemert C, Dusek RJ, Smith MM, Kaler R, Sheffield G, Divine LM, Kuletz KJ, Knowles S, Lankton JS, Ransom Hardison D, Wayne Litaker R, Jones T, Burgess HK, Parrish JK (2021) Investigation of algal toxins in a multispecies seabird die-off in the Bering and Chukchi seas. J Wildl Dis 57:399–407

Huson DH, Auch AF, Qi J, Schuster SC (2007) MEGAN analysis of metagenomic data. Genome Res 17:377–386

Iida T, Mizobata K, Saitoh SI (2012) Interannual variability of coccolithophore Emiliania huxleyi blooms in response to changes in water column stability in the eastern Bering Sea. Cont Shelf Res 34:7–17

Iida T, Saitoh SI, Miyamura T, Toratani M, Fukushima H, Shiga N (2002) Temporal and spatial variability of coccolithophore blooms in the eastern Bering Sea, 1998-2001. Prog Oceanogr 55:165–175

Jones HLJ, Leadbeater BSC, Green JC (1993) Mixotrophy in marine species of chrysochromulina (prymnesiophyceae): Ingestion and digestion of a small green flagellate. J Mar Biol Assoc United Kingdom 73:283–296

Kaczmarska I, Lovejoy C, Potvin M, Macgillivary M (2009) Morphological and molecular characteristics of selected species of Minidiscus (Bacillariophyta, Thalassiosiraceae). Eur J Phycol 44:461–475

Kirk D, Jones N, Peacock S, Phillips J, Molnar PK, Krkosek M, Luijckz P (2018) Empirical evidence that metabolic theory describes temperature dependency of within-host parasite dynamics. PLoS One 16:e2004608

Kozich JJ, Westcott SL, Baxter NT, Highlander SK, Schloss PD (2013) Development of a dual-index sequencing strategy and curation pipeline for analyzing amplicon sequence data on the MiSeq Illumina sequencing platform. Appl Environ Microbiol 79:5112–5120

Ladd C, Eisner LB, Salo SA, Mordy CW (2018) Spatial and Temporal Variability of Coccolithophore Blooms in the Eastern Bering Sea. J Geophys Res O 123:9119–9136

Ladd C, Stabeno PJ (2012) Stratification on the Eastern Bering Sea shelf revisited. Deep Res Part II Top Stud Oceanogr 65–70:72–83

Leander BS (2008) Marine gregarines: evolutionary prelude to the apicomplexan radiation? Trends Parasitol 24:60–67

Lee RF, Hagen W, Kattner G (2006) Lipid storage in marine zooplankton. Mar Ecol Prog Ser

307:273–306

Lima-Mendez G, Faust K, Henry N, Decelle J, Colin S, Carcillo F, Chaffron S, Ignacio-espinosa JC, Roux S, Vincent F, Bittner L (2015) Determinants of community structure in the global plankton interactome. Ocean Plankt 348:1262073

Liu H, Probert I, Uitz J, Claustre H, Aris-Brosou S, Frada M, Not F, de Vargas C (2009) Extreme diversity in noncalcifying haptophytes explain a major pigment paradox in open oceans. PNAS 106:12803–12808

Lomas MW, Eisner LB, Gann J, Baer SE, Mordy CW, Stabeno PJ (2020) Time-series of direct primary production and phytoplankton biomass in the southeastern bering sea: Responses to cold and warm stanzas. Mar Ecol Prog Ser 642:39–54

Macnab V, Barber I (2012) Some (worms) like it hot: Fish parasites grow faster in warmer water, and alter host thermal preferences. Glob Chang Biol 18:1540–1548

Mahé F, De Vargas C, Bass D, Czech L, Stamatakis A, Lara E, Singer D, Mayor J, Bunge J, Sernaker S, Siemensmeyer T, Trautmann I, Romac S, Berney C, Kozlov A, Mitchell EAD, Seppey CVW, Egge E, Lentendu G, Wirth R, Trueba G, Dunthorn M (2017) Parasites dominate hyperdiverse soil protist communities in Neotropical rainforests. Nat Ecol Evol 1:0091

Malzahn AM, Boersma M (2012) Effects of poor food quality on copepod growth are dose dependent and non-reversible. Oikos 121:1408–1416

Mantoura RFC, Woodward EMS (1983) Optimization of the indophenol blue method for the automated determination of ammonia in estuarine waters. Estuar Coast Shelf Sci 17:219–224

McKie-Krisberg ZM, Gast RJ, Sanders RW (2015) Physiological responses of three species of Antarctic mixotrophic phytoflagellates to changes in light and dissolved nutrients. Microb Ecol 70:21–29

Menden-Deuer S, Lessard EJ (2000) Carbon to volume relationships for dinoflagellates, diatoms, and other protist plankton. Limnol Oceanogr 45:569–579

Merico A, Tyrrell T, Lessard EJ, Oguz T, Stabeno PJ, Zeeman SI, Whitledge TE (2004) Modelling phytoplankton succession on the Bering Sea shelf: Role of climate influences and trophic interactions in generating Emiliania huxleyi blooms 1997-2000. Deep Res Part I Oceanogr Res Pap 51:1803–1826

Mitra A, Flynn KJ, Tillmann U, Raven JA, Caron D, Stoecker DK, Not F, Hansen PJ, Hallegraeff G, Sanders R, Wilken S, McManus G, Johnson M, Pitta P, Våge S, Berge T, Calbet A, Thingstad F, Jeong HJ, Burkholder JA, Glibert PM, Granéli E, Lundgren V (2016) Defining Planktonic Protist Functional Groups on Mechanisms for Energy and Nutrient Acquisition: Incorporation of Diverse Mixotrophic Strategies. Protist 167:106–120

Moran SB, Lomas MW, Kelly RP, Gradinger R, Iken K, Mathis JT (2012) Seasonal succession of net primary productivity, particulate organic carbon export, and

autotrophic community composition in the eastern Bering Sea. Deep Res Part II Top Stud Oceanogr 65–70:84–97

Mordy CW, Eisner L, Kearney K, Kimmel D, Lomas MW, Mier K, Proctor P, Ressler PH, Stabeno P, Wisegarver E (2021) Spatiotemporal variability of the nitrogen deficit in bottom waters on the eastern Bering Sea shelf. Cont Shelf Res 224:104423

Moreira D, López-García P (2002) The molecular ecology of microbial eukaryotes unveils a hidden world. Trends Microbiol 10:31–38

Mueter FJ, Litzow MA (2008) Sea ice retreat alters the biogeography of the Bering Sea continental shelf. Ecol Appl 18:309–320

Murali A, Bhargava A, Wright ES (2018) IDTAXA: A novel approach for accurate taxonomic classification of microbiome sequences. Microbiome 6:140

NASA Goddard Space Flight Center (2018) Ocean Ecology Laboratory, Ocean Biology Processing Group. Moderate-resolution Imaging Spectroradiometer (MODIS) Aqua Particulate Inorganic Carbon Data; 2018 Reprocessing. NASA OB.DAAC, Greenbelt, MD, USA. doi: data/10.5067/AQUA/MODIS/L3M/PIC/2018. Accessed on 25 November 2019

National Marine Fisheries Service (NMFS) (2021) Fisheries of the United States, 2019. U.S. Department of Commerce, NOAA Current Fishery Statistics No. 2019 Available at: https://www.fisheries.noaa.gov/national/sustainable-fisheries/ fisheries-united-states

Natsuike M, Saito R, Fujiwara A, Matsuno K, Yamaguchi A, Shiga N, Hirawake T, Kikuchi T, Nishino S, Imai I (2017) Evidence of increased toxic Alexandrium tamarense dinoflagellate blooms in the eastern Bering Sea in the summers of 2004 and 2005. PLoS One 12:1–13

Nygaard K, Tobiesen A (1993) Bacterivory in algae: A survival strategy during nutrient limitation. Limnol Ocean 38:273–279

Olson MB, Strom SL (2002) Phytoplankton growth, microzooplankton herbivory and community structure in the southeast Bering Sea: Insight into the formation and temporal persistence of an Emiliania huxleyi bloom. Deep Res Part II Top Stud Oceanogr 49:5969–5990

Pesant S, Not F, Picheral M, Kandels-Lewis S, Le Bescot N, Gorsky G, Iudicone D, Karsenti E, Speich S, Trouble R, Dimier C, Searson S (2015) Open science resources for the discovery and analysis of Tara Oceans data. Sci Data 2:150023

Pomeroy LR, leB Williams PJ, Azam F, Hobbie JE (2007) The microbial loop. Oceanography 20:28–33

Quast C, Pruesse E, Yilmaz P, Gerken J, Schweer T, Yarza P, Peplies J, Glöckner FO (2013) The SILVA ribosomal RNA gene database project: Improved data processing and web-based tools. Nucleic Acids Res 41:590–596

Ramond P, Sourisseau M, Simon N, Romac S, Schmitt S, Rigaut-Jalabert F, Henry N, de

Vargas C, Siano R (2019) Coupling between taxonomic and functional diversity in protistan coastal communities. Environ Microbiol 21:730–749

Redfield AC (1958) The biological control of chemical factors in the environment. Am Sci 46:205–221

Ressler PH, De Robertis A, Warren JD, Smith JN, Kotwicki S (2012) Developing an acoustic survey of euphausiids to understand trophic interactions in the bering sea ecosystem. Deep Res Part II Top Stud Oceanogr 65–70:184–195

Rueckert S, Betts EL, Tsaousis AD (2019) The Symbiotic Spectrum: Where Do the Gregarines Fit? Trends Parasitol 35:687–694

Rueckert S, Simdyanov TG, Aleoshin V V., Leander BS (2011) Identification of a divergent environmental DNA sequence clade using the phylogeny of gregarine parasites (Apicomplexa) from crustacean hosts. PLoS One 6:e18163

Sambrotto RN, Burdloff D, McKee K (2015) Spatial and year-to-year patterns in new and primary productivity in sea ice melt regions of the eastern Bering Sea. Deep Res Part II Top Stud Oceanogr 134:86–99

Sassenhagen I, Irion S, Jardillier L, Moreira D, Christaki U (2020) Protist Interactions and Community Structure During Early Autumn in the Kerguelen Region (Southern Ocean). Protist 171:125709

Schneider LK, Flynn KJ, Herman PMJ, Troost TA, Stolte W (2020) Exploring the Trophic Spectrum: Placing Mixoplankton Into Marine Protist Communities of the Southern North Sea. Front Mar Sci 7:586915

Schoo KL, Malzahn AM, Krause E, Boersma M (2013) Increased carbon dioxide availability alters phytoplankton stoichiometry and affects carbon cycling and growth of a marine planktonic herbivore. Mar Biol 160:2145–2155

Sheffield Guy L, Duffy-Anderson J, Matarese AC, Mordy CW, Napp JM, Stabeno PJ (2014) Understanding climate control of fisheries recruitment in the eastern Bering Sea: Long-term measurements and process studies. Oceanography 27:90–103

Sherr BF, Sherr EB, Caron DA, Vaulot D, Worden AZ (2007) Oceanic protists. Oceanography 20:130–134

Sherr EB, Sherr BF, Ross C (2013) Microzooplankton grazing impact in the Bering Sea during spring sea ice conditions. Deep Res Part II Top Stud Oceanogr 94:57–67

Siddon E, Zador S (2017) Ecosystem Considerations 2017: Status of the Eastern Bering Sea Marine Ecosystem. Alaska Marine Science Center. Available at: https://www.fisheries.noaa.gov/alaska/ecosystems/ecosystem-status-reports-gulf-alaska-bering-sea-and-aleutian-islands Accessed on: 9 September 2021

Siddon E, Zador S (2019) Ecosystem Status Report 2019 Eastern Bering Sea. Available at: https://www.fisheries.noaa.gov/alaska/ecosystems/ecosystem-status-reports-gulf-alaska-bering-sea-and-aleutian-islands Accessed on: 9 September 2021

Siddon EC, Kristiansen T, Mueter FJ, Holsman KK, Heintz RA, Farley E V. (2013) Spatial match-mismatch between juvenile fish and prey provides a mechanism for recruitment variability across contrasting climate conditions in the eastern Bering Sea. PLoS One 8:e84526

Sigler MF, Napp JM, Stabeno PJ, Heintz RA, Lomas MW, Hunt GL (2016) Variation in annual production of copepods, euphausiids, and juvenile walleye pollock in the southeastern Bering Sea. Deep Res Part II Top Stud Oceanogr 134:223–234

Sommer U, Stibor H, Katechakis A, Sommer F, Hansen T (2002) Pelagic food web configurations at different levels of nutrient richness and their implications for the ratio fish production:primary production. Hydrobiologia 484:11–20

Springer AM, Peter McRoy C, Flint M V. (1996) The Bering Sea Green Belt: Shelf-edge processes and ecosystem production. Fish Oceanogr 5:205–223

Stabeno P, Napp J, Mordy C, Whitledge T (2010) Factors influencing physical structure and lower trophic levels of the eastern Bering Sea shelf in 2005: Sea ice, tides and winds. Prog Oceanogr 85:180–196

Stabeno PJ, Bell SW (2019) Extreme Conditions in the Bering Sea (2017–2018): Record-Breaking Low Sea-Ice Extent. Geophys Res Lett 46:8952–8959

Stabeno PJ, Bell SW, Bond NA, Kimmel DG, Mordy CW, Sullivan ME (2019) Distributed Biological Observatory Region 1: Physics, chemistry and plankton in the northern Bering Sea. Deep Res Part II Top Stud Oceanogr 162:8–21

Stabeno PJ, Danielson SL, Kachel DG, Kachel NB, Mordy CW (2016) Currents and transport on the Eastern Bering Sea shelf: An integration of over 20 years of data. Deep Res Part II Top Stud Oceanogr 134:13–29

Stabeno PJ, Farley E V., Kachel NB, Moore S, Mordy CW, Napp JM, Overland JE, Pinchuk AI, Sigler MF (2012a) A comparison of the physics of the northern and southern shelves of the eastern Bering Sea and some implications for the ecosystem. Deep Res Part II Top Stud Oceanogr 65–70:14–30

Stabeno PJ, Kachel NB, Moore SE, Napp JM, Sigler M, Yamaguchi A, Zerbini AN (2012b) Comparison of warm and cold years on the southeastern Bering Sea shelf and some implications for the ecosystem. Deep Res Part II Top Stud Oceanogr 65–70:31–45

Stabeno PJ, Schumacher JD, Ohtani K (1999). The physical oceanography of the Bering Sea. In: Loughlin TR, Ohtani K (eds) A summary of physical, chemical, and biological characteristics, and a synopsis of research on the Bering Sea. North Pacific Marine Science Organization (PICES), University of Alaska Sea Grant, AK-SG-99-03 pp. 1-60

Sterner RW, Elser JJ (2017) Ecological Stoichiometry: The Biology of Elements from Molecules to the Biosphere. Princeton: Princeton University Press. https://doi.org/10.1515/9781400885695

Stoeck T, Bass D, Nebel M, Christen R, Jones MDM, Breiner HW, Richards TA (2010)

Multiple marker parallel tag environmental DNA sequencing reveals a highly complex eukaryotic community in marine anoxic water. Mol Ecol 19:21–31

Stoecker DK, Weigel A, Goes JI (2014) Microzooplankton grazing in the Eastern Bering Sea in summer. Deep Res Part II Top Stud Oceanogr 109:145–156

Strom SL, Fredrickson KA (2008) Intense stratification leads to phytoplankton nutrient limitation and reduced microzooplankton grazing in the southeastern Bering Sea. Deep Res Part II Top Stud Oceanogr 55:1761–1774

Szymanski A, Gradinger R (2016) The diversity, abundance and fate of ice algae and phytoplankton in the Bering Sea. Polar Biol 39:309–325

Takahashi KT, Kawaguchi S, Kobayashi M, Toda T, Tanimura A, Fukuchi M, Odate T (2011) Eugregarine infection within the digestive tract of larval Antarctic krill, Euphausia superba. Polar Biol 34:1167–1174

Takahashi KT, Kawaguchi S, Toda T (2009) Observation by electron microscopy of a gregarine parasite of Antarctic krill: Its histological aspects and ecological explanations. Polar Biol 32:637–644

Talmy D, Martiny AC, Hill C, Hickman AE, Follows MJ (2016) Microzooplankton regulation of surface ocean POC:PON ratios. Global Biogeochem Cycles 30:311–332

Théodoridès J (1989) Parasitology of Marine Zooplankton. Adv Mar Biol 25:117–177

Torres-Beltrán M, Sehein T, Pachiadaki MG, Hallam SJ, Edgcomb V (2018) Protistan parasites along oxygen gradients in a seasonally anoxic fjord: A network approach to assessing potential host-parasite interactions. Deep Res Part II Top Stud Oceanogr 156:97–110

Toseland A, Daines SJ, Clark JR, Kirkham A, Strauss J, Uhlig C, Lenton TM, Valentin K, Pearson GA, Moulton V, Mock T (2013) The impact of temperature on marine phytoplankton resource allocation and metabolism. Nat Clim Chang 3:979–984

Tragin M, Vaulot D (2018) Green microalgae in marine coastal waters: The Ocean Sampling Day (OSD) dataset. Sci Rep 8:14020

Vance T, Schumacher J, Stabeno P, Baier C, Wyllie-Echeverria T, Tynan C, Brodeur R, Napp J (1998) Aquamarine waters recorded for first time in eastern bering sea. Eos, Trans Am Geophys Union 79:121–121

De Vargas C, Audic S, Henry N, Decelle J, Mahé F, Logares R, Lara E, Berney C, Le Bescot N, Probert I, Carmichael M, Poulain J, Romac S, Colin S, Aury J, Bittner L, Guidi L, Horak A, Jaillon O, Lima-Mendez G, Lukeš J, Malviya S, Morard R, Mulot M, Scalco E, Siano R, Vincent F, Zingone A, Dimier C, Picheral M, Searson S, Kandels-Lewis S (2015) Eukaryotic plankton diversity in the sunlit ocean. Science (80-) 348:1261605

Wallis JR, Smith AJR, Kawaguchi S (2017) Discovery of gregarine parasitism in some Southern Ocean krill (Euphausiacea) and the salp Salpa thompsoni. Polar Biol 40:1913–1917

Wang M, Overland JE, Stabeno P (2012) Future climate of the Bering and Chukchi Seas projected by global climate models. Deep Res Part II Top Stud Oceanogr 65–70:46–57

Wang Q, Garrity GM, Tiedje JM, Cole JR (2007) Naïve Bayesian classifier for rapid assignment of rRNA sequences into the new bacterial taxonomy. Appl Environ Microbiol 73:5261–5267

Wohlers J, Engel A, Zöllner E, Breithaupt P, Jürgens K, Hoppe HG, Sommer U, Riebesell U (2009) Changes in biogenic carbon flow in response to sea surface warming. PNAS 106:7067–7072

Worden AZ, Nolan JK, Palenik B (2004) Assessing the dynamics and ecology of marine picophytoplankton: The importance of the eukaryotic component. Limnol Oceanogr 49:168–179

Wyllie-Echeverria T, Wooster WS (1998) Year-to-year variations in Bering Sea ice cover and some consequences for fish distributions. Fish Oceanogr 7:159–170

Yoon G, Gaynanova I, Müller CL (2019) Microbial networks in SPRING - Semi-parametric rank-based correlation and partial correlation estimation for quantitative microbiome data. Front Genet 10

Zamora-Terol S, Novotny A, Winder M (2021) Molecular evidence of host-parasite interactions between zooplankton and Syndiniales. Aquat Ecol 55:125–134

Zhou Q, Wang P, Chen C, Liang J, Li B, Gao Y (2015) Influences of sea ice on eastern Bering Sea phytoplankton. Chinese J Oceanol Limnol 33:458–467

Zhu F, Massana R, Not F, Marie D, Vaulot D (2005) Mapping of picoeukaryotes in marine ecosystems with quantitative PCR of the 18S rRNA gene. FEMS Microbiol Ecol 52:79–92

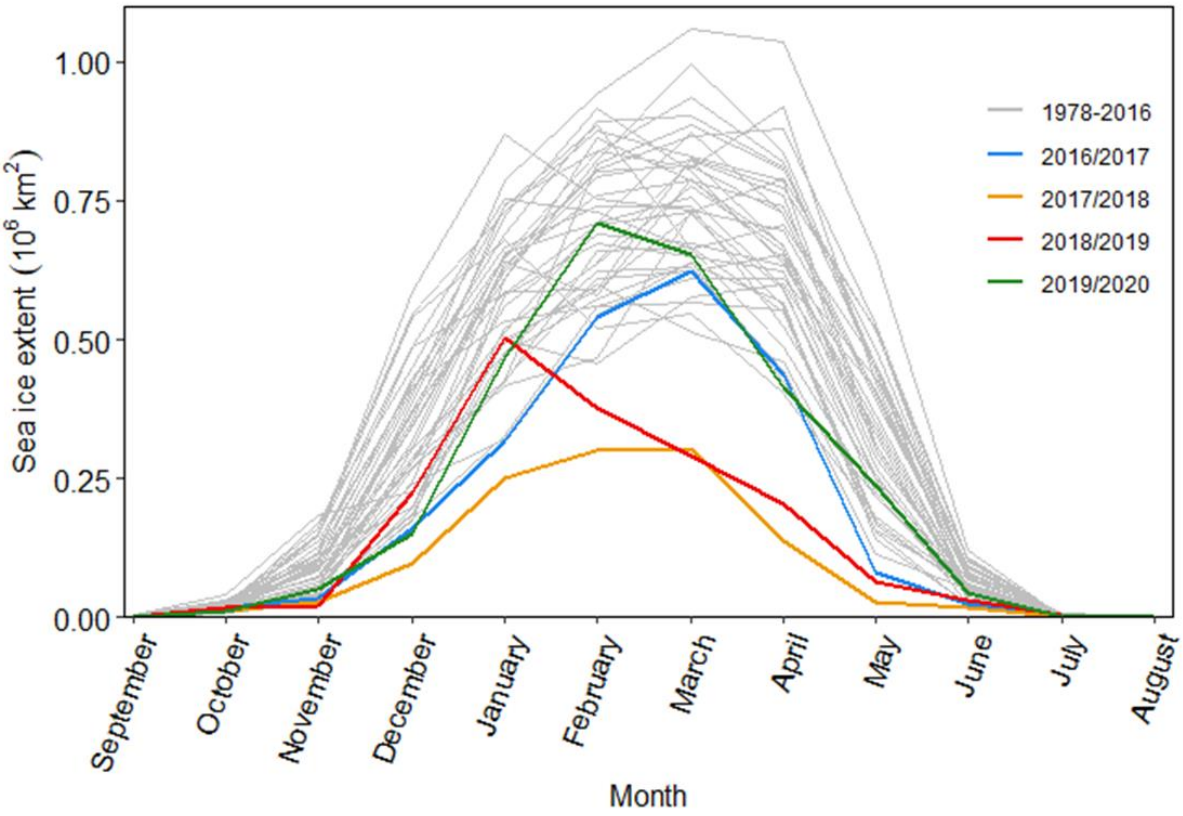

Fig. 3.1. Average monthly sea ice extent in the Bering Sea region for 1978-2020. Most years are in grey, colored lines represent the four winters from 2016-2020. Note that the winter of 2016/2017 (blue) and the winter of 2018/2019 (red) occurred before sampling in the fall of 2017 and 2019, respectively. Data for this figure was obtained from the National Snow and Ice Data Center (Fetterer et al 2017) and was modeled after the figure presented in Stabeno and Bell, 2019.

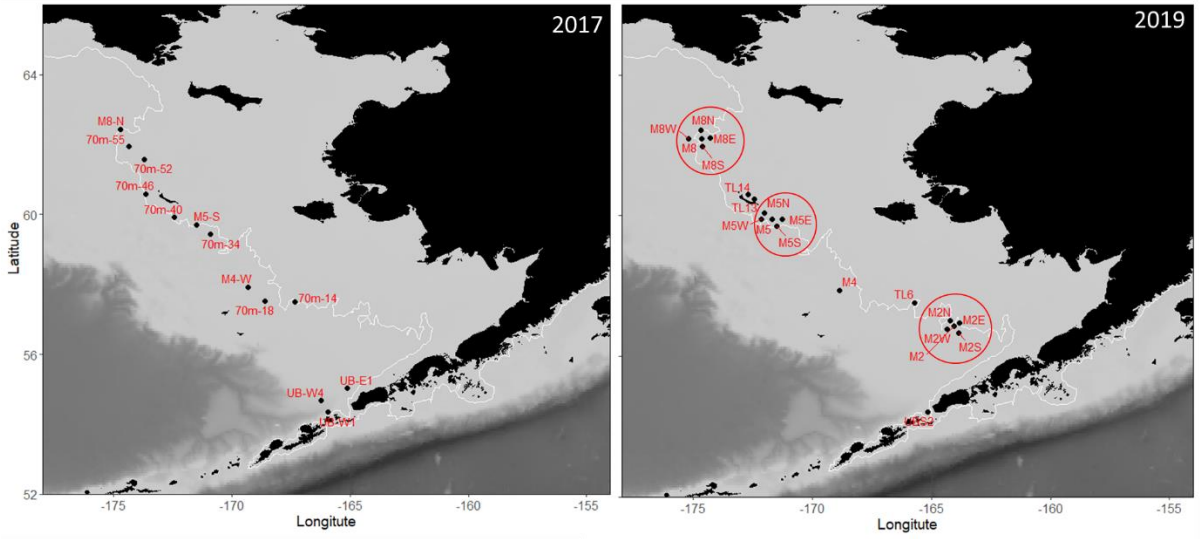

Fig 3.2. Map of the eastern Bering Sea (EBS) showing locations and station labels for 18S sequencing samples taken during the fall mooring cruises (EcoFOCI Program, NOAA) in 2017 and 2019. Although 18S sequencing samples were not taken at the same locations across years, CTD cast and bottle data at consistent sampling locations allowed for comparisons of physical and chemical variables at moorings 2 (M2), 5 (M5), and 8 (M8) between 2017 and 2019 by treating in-situ measurements taken at each mooring station and the 4 surrounding stations (N, E, S, W; see 2019 station locations surrounded by circles) as replicates and conducting statistical tests. The white line represents the 70 m isobath and the grey shading displays the bathymetry of the EBS.

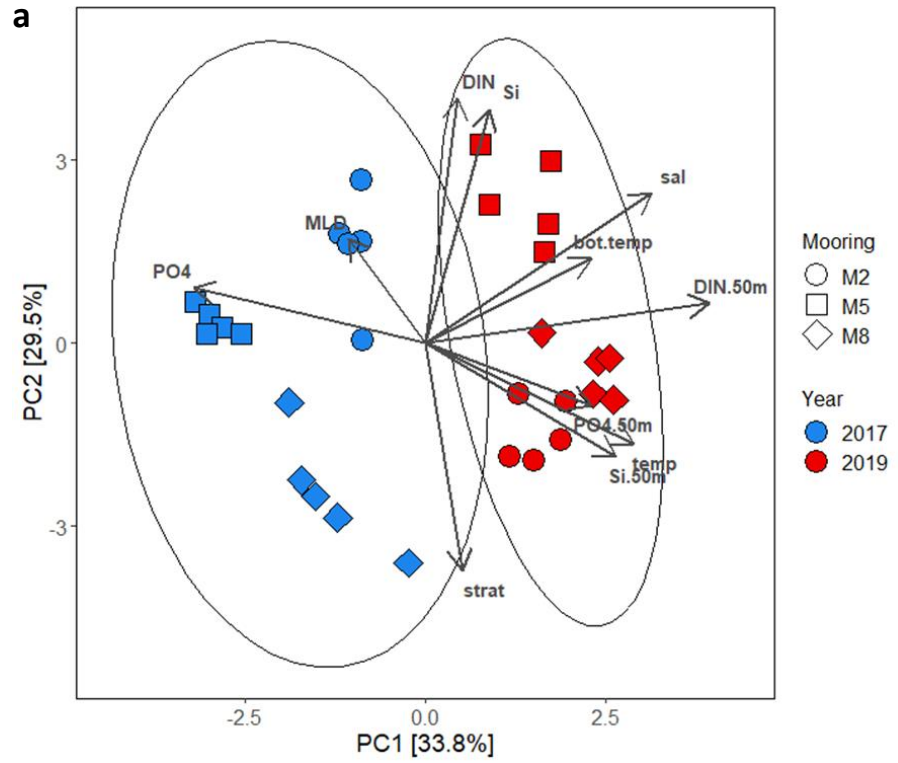
a
DIN
Si
sal
MLD
bot.temp
PO4
DIN.50m
PO4.50m
temp
Si.50m
strat
Mooring
M2
M5
M8
Year
2017
2019
PC2 [29.5%]
PC1 [33.8%]
3
0
-3
-2.5
0.0
2.5

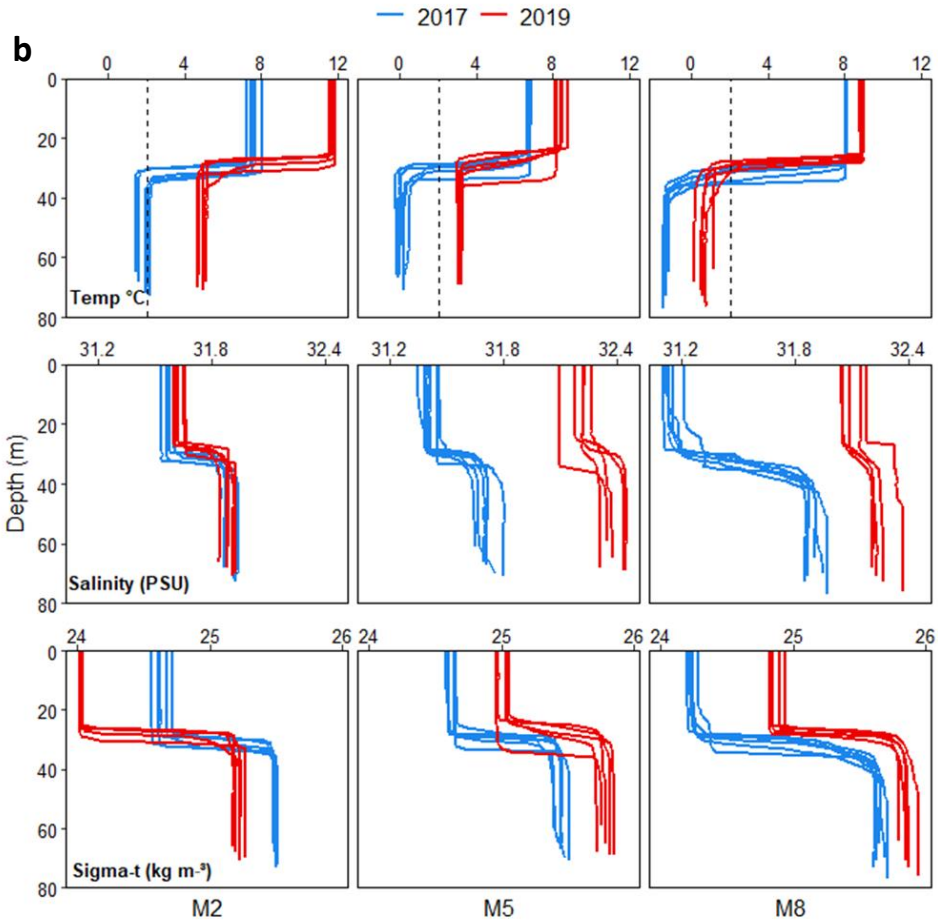
b
2017
2019
Temp °C
Salinity (PSU)
Sigma-t (kg m-3)
Depth (m)
M2
M5
M8

Fig. 3.3. a. Principal component analysis (PCA) of site-specific environmental conditions measured at sampling locations surrounding moorings 2 (M2; circles), 5 (M5; squares), and 8 (M8; diamonds) during fall cruises in 2017 (blue) and 2019 (red). The arrows denote the eigenvectors of each environmental variable associated with the first two principal component axes. The environmental variables included in the ordination are surface and bottom temperature (temp and bot.temp), mixed layer depth (MLD), stratification strength (strat), surface salinity (sal), dissolved inorganic nitrogen concentration at the surface (DIN) and at 50 m depth (DIN.50m), phosphate concentration at the surface (PO4) and at 50 m depth (PO4.50m), silicic acid concentration at the surface (Si) and at 50 m depth (Si.50m). b. Depth profiles of temperature, salinity, and sigma t for stations surrounding each mooring during the 2017 and 2019 cruises. Significant differences in surface temperature and salinity and bottom water temperatures between 2017 and 2019 were detected at each mooring (BH adjusted $p < 0.05$).

Table 3.1. Summary table showing the mean values (n = 5) and results of pairwise t-tests for surface salinity, temperature (temp), bottom temp, turbidity, and stratification strength around 3 mooring stations (M2, M5, and M8) in 2017 and 2019. Darker red colors represent larger values within each set of variables. Adjustment of p-values for multiple testing was conducted using the Benjamini-Hochberg method and significant differences are bolded. *p<0.05, **p<0.01, ***p<0.001

	Mooring	2017	2019	F Ratio	Prob > F	BH adjusted p-value	
Salinity	M2	**31.57**	**31.63**	9.99	0.0134	0.0182	*
(PSU)	M5	**31.41**	**32.20**	485.25	<0.0001	<0.0001	***
	M8	**31.14**	**32.10**	876.92	<0.0001	<0.0001	***
Temp	M2	**7.62**	**11.69**	739.71	<0.0001	<0.0001	***
(°C)	M5	**6.77**	**8.41**	185.64	<0.0001	<0.0001	***
	M8	**8.10**	**8.91**	494.67	<0.0001	<0.0001	***
Bottom temp	M2	**1.86**	**4.90**	333.51	<0.0001	<0.0001	***
(°C)	M5	**0.04**	**3.14**	1516.71	<0.0001	<0.0001	***
	M8	**-1.40**	**0.62**	125.36	<0.0001	<0.0001	***
Turbidity	M2	0.29	0.36	1.18	0.3130	0.3130	
(FNU)	M5	**0.28**	**0.36**	5.59	0.0457	0.0527	
	M8	**0.13**	**0.47**	12.83	0.0072	0.0108	*
Stratification	M2	**0.86**	**1.19**	103.29	<0.0001	<0.0001	***
(kg m^{-3})	M5	**0.84**	**0.77**	7.37	0.0265	0.0331	*
	M8	1.27	1.00	4.30	0.0716	0.0767	

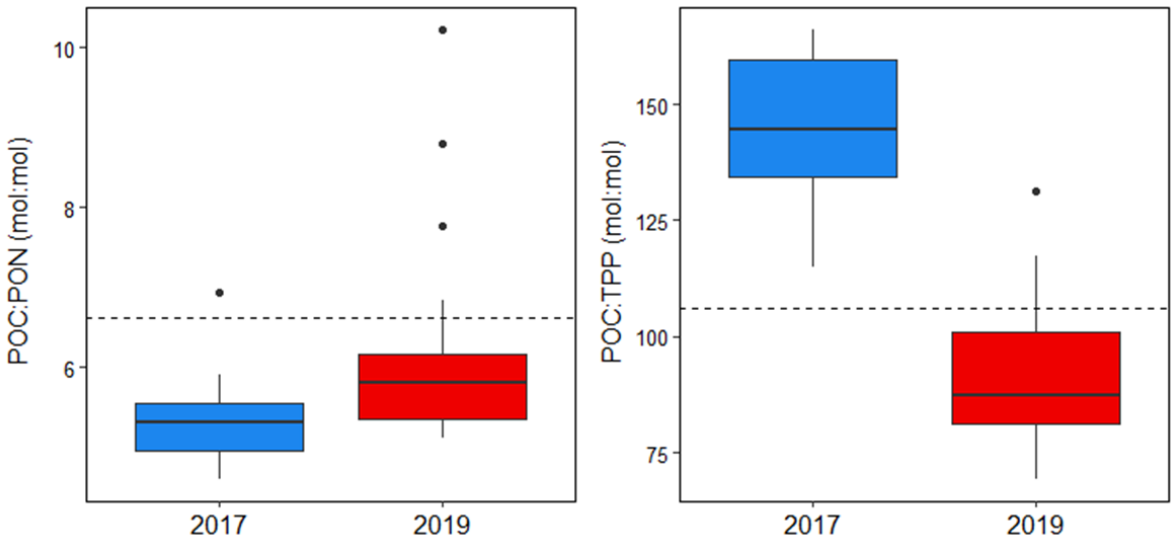

Fig. 3.4. Particulate organic carbon (POC) to particulate organic nitrogen (PON) (left) or total particulate phosphorus (TPP) (right) ratios in 200 μm pre-filtered samples measured at stations shown in Fig 2 for 2017 (n=11 (POC:PON) or 9 (POC:TPP); measurements below limits of detection not included; blue) and 2019 (n=20; red). Significant differences in the median POC:PON (Wilcoxon exact test, BH adjusted $p < 0.05$) and the mean POC:TPP (Welch's t-test, BH adjusted $p < 0.05$) were detected across years. Dashed lines represent molar Redfield ratios of C:N (106:16) or C:P (106:1).

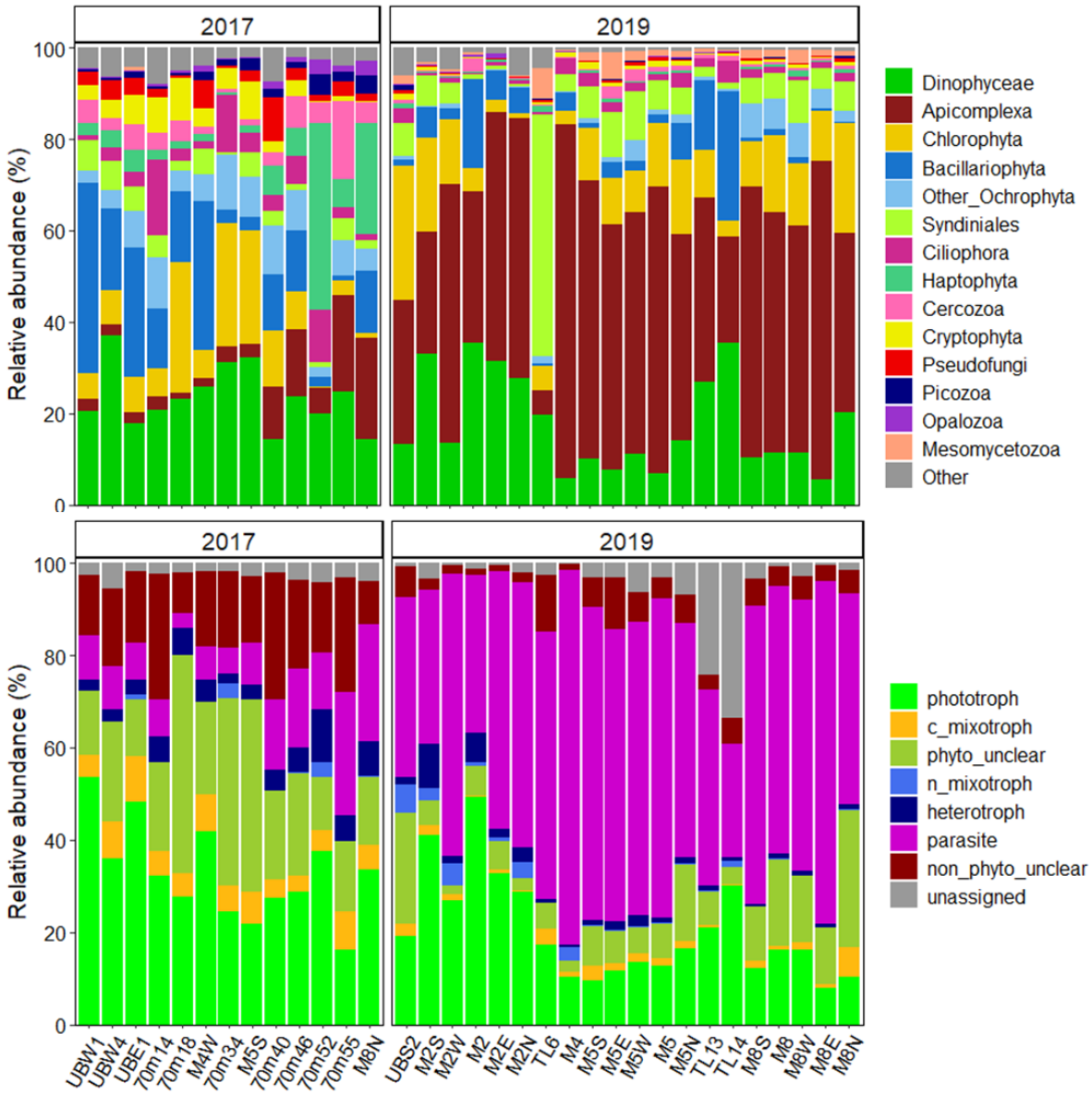

Fig. 3.5. Relative abundances of ASVs grouped by Division or Class (top) or by trophic position (bottom) across all stations sampled in 2017 and 2019 ordered by increasing station latitude and labeled as in Fig 3.2. Division Dinoflagellata has been divided to show the relative abundance of Classes Dinophyceae and Syndiniales while Division Ochrophyta has been divided to show Bacillariophyta and other Ochrophyta Classes. The "Other" group represents ASVs from less abundant Divisions/Classes including Radiolaria, Katablepharidophyta, Telonemia, Sagenista, Choanoflagellida, Centroheliozoa, Discoba, Lobosa, Apusomonadidae, Foraminifera, unassigned Alveolata, unassigned Stramenopiles, and other Dinoflagellata Classes. Trophic assignments for individual ASVs were determined to be phototrophs, constitutive mixotrophs (c_mixotroph), non-constitutive mixotrophs (n_mixotroph), heterotrophs, parasites following guidelines by Mitra et al. 2016. If an ASV

could not be defined to one of these assignments (either due to lack of taxonomic resolution or unclear trophic status) then an ASV was classified as a phytoplankton (photosynthetic but not known whether it is obligate autotrophic or a constitutive mixotrophic) (phyto_unclear; green/yellow colors), non-phytoplankton (not inherently capable of photosynthesis, could be a non-constitutive mixotroph, parasitic, or heterotrophic) (non_phyto_unclear; blue/red colors), or unassigned (grey). Note: colors represent different classifications, either taxonomic (top) or trophic (bottom), in the two panels and specific taxonomic groups do not necessarily correlate to a trophic group.

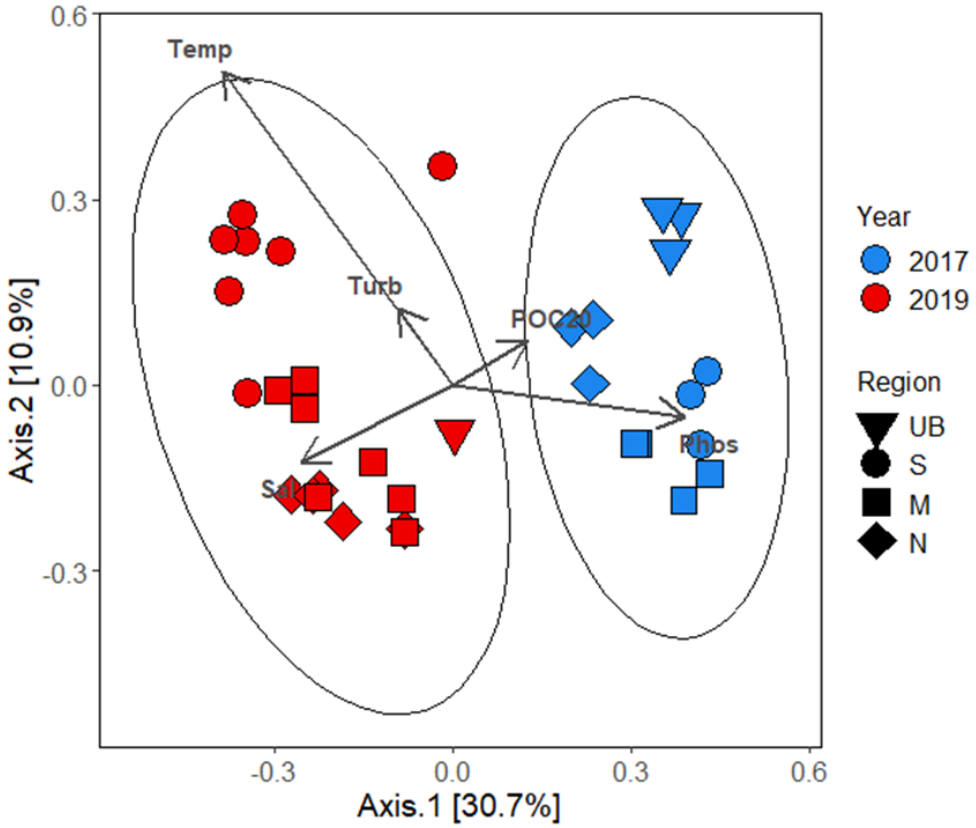

Fig. 3.6. Principal coordinates analysis (PCoA) based on Bray-Curtis dissimilarities of the POC scaled ASV RA between samples taken in 2017 (blue) and 2019 (red) at stations around Unimak Pass (UB; <56 latitude) and along the southern (S; 56-59 latitude; same region as MS), middle (M; 59-61 latitude; same region as M5), and northern (N; >61 latitude; same region as M8) portions of the 70 m isobath. Arrows show the best subset of environmental factors (measured at all stations) with maximum correlation with community dissimilarities (bioenv function) and their magnitude and direction represent their correlation with the first two principal coordinate axes (envfit function). Permutational multivariate analysis of variance (PERMANOVA) detected significant differences across years ($p = 0.001$; adonis function).

Table 3.2. Taxonomic assignments of the top 10 POC-scaled ASVs for each year separately ordered from top to bottom as largest to smallest average POC concentration across all samples. Bold ASVs were within the top 10 ASVs for both years.

	ASV	Division	Class	Order	Family	Genus	Species
2017	**sv3**	**Chlorophyta**	**Trebouxiophyceae**	**Chlorellales**	**Chlorellales_X**	**Nannochloris**	**Nannochloris_sp.**
	sv6	Ochrophyta	Bacillariophyta	Bacillariophyta_X	Polar-centric-Mediophyceae	Minidiscus	Minidiscus_sp.
	sv4	Dinoflagellata	Dinophyceae	Gymnodiniales	Kareniaceae	NA	NA
	sv7	Ochrophyta	Bacillariophyta	Bacillariophyta_X	Polar-centric-Mediophyceae	Arcocellulus	Arcocellulus_cornucervis
	sv1	**Apicomplexa**	**Gregarinomorphea**	**Eugregarinorida**	**Cephaloidophoridae**	**Cephaloidophoridae_X**	**Cephaloidophoridae_X_sp.**
	sv2	Dinoflagellata	Dinophyceae	Prorocentrales	Prorocentraceae	Prorocentrum	Prorocentrum_micans
	sv9	Dinoflagellata	Dinophyceae	Peridiniales	Heterocapsaceae	Heterocapsa	NA
	sv26	Ochrophyta	Bacillariophyta	Bacillariophyta_X	Polar-centric-Mediophyceae	NA	NA
	sv87	Haptophyta	Prymnesiophyceae	Phaeocystales	Phaeocystaceae	Phaeocystis	NA
	sv45	Ochrophyta	Bacillariophyta	Bacillariophyta_X	Radial-centric-basal-Coscinodiscophyceae	Proboscia	Proboscia_alata
2019	**sv1**	**Apicomplexa**	**Gregarinomorphea**	**Eugregarinorida**	**Cephaloidophoridae**	**Cephaloidophoridae_X**	**Cephaloidophoridae_X_sp.**
	sv5	Apicomplexa	Gregarinomorphea	Eugregarinorida	Cephaloidophoridae	Cephaloidophora	Cephaloidophora_sp.
	sv13	Dinoflagellata	Dinophyceae	Suessiales	Suessiaceae	Protodinium	Protodinium_simplex
	sv8	Chlorophyta	Prasino-Clade-V	Pseudoscourfieldiales	Pycnococcaceae	Pseudoscourfieldia	Pseudoscourfieldia_marina
	sv3	**Chlorophyta**	**Trebouxiophyceae**	**Chlorellales**	**Chlorellales_X**	**Nannochloris**	**Nannochloris_sp.**
	sv12	Dinoflagellata	Dinophyceae	Dinophyceae_X	Dinophyceae_XX	Dinophyceae_XXX	Dinophyceae_XXX_sp.
	sv18	Dinoflagellata	Syndiniales	Dino-Group-I	Dino-Group-I-Clade-1	Dino-Group-I-Clade-1_X	Dino-Group-I-Clade-1_X_sp.
	sv10	Apicomplexa	Gregarinomorphea	Eugregarinorida	Cephaloidophoridae	Cephaloidophoridae_X	Cephaloidophoridae_X_sp.
	sv31	Ochrophyta	Bacillariophyta	Bacillariophyta_X	Polar-centric-Mediophyceae	Chaetoceros	Chaetoceros_socialis
	sv58	Mesomycetozoa	Ichthyosporea	NA	NA	NA	NA

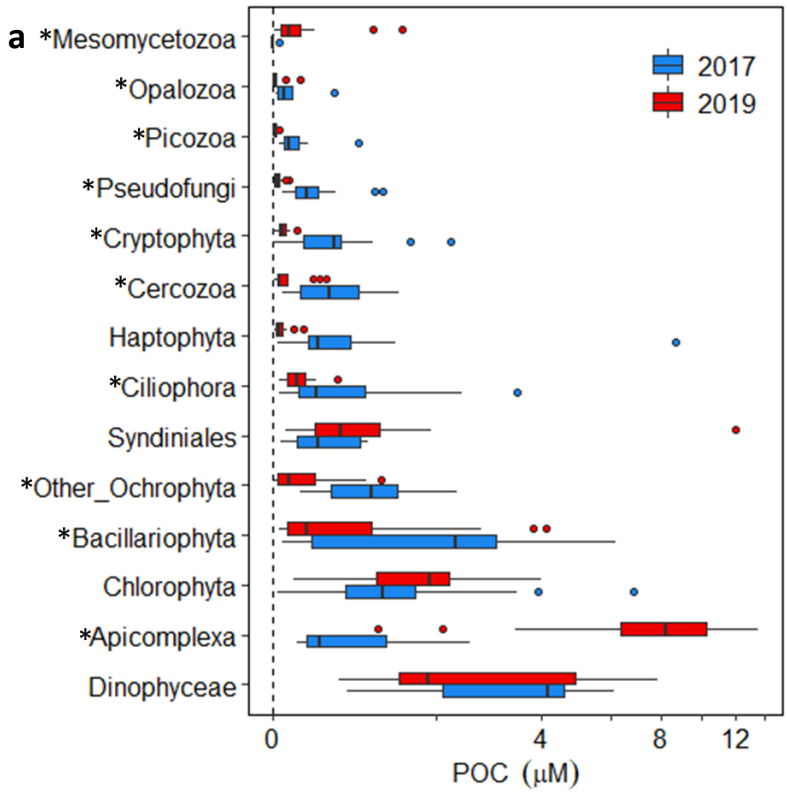
a
*Mesomycetozoa
*Opalozoa
*Picozoa
*Pseudofungi
*Cryptophyta
*Cercozoa
Haptophyta
*Ciliophora
Syndiniales
*Other_Ochrophyta
*Bacillariophyta
Chlorophyta
*Apicomplexa
Dinophyceae
2017
2019
0
4
8
12
POC (µM)

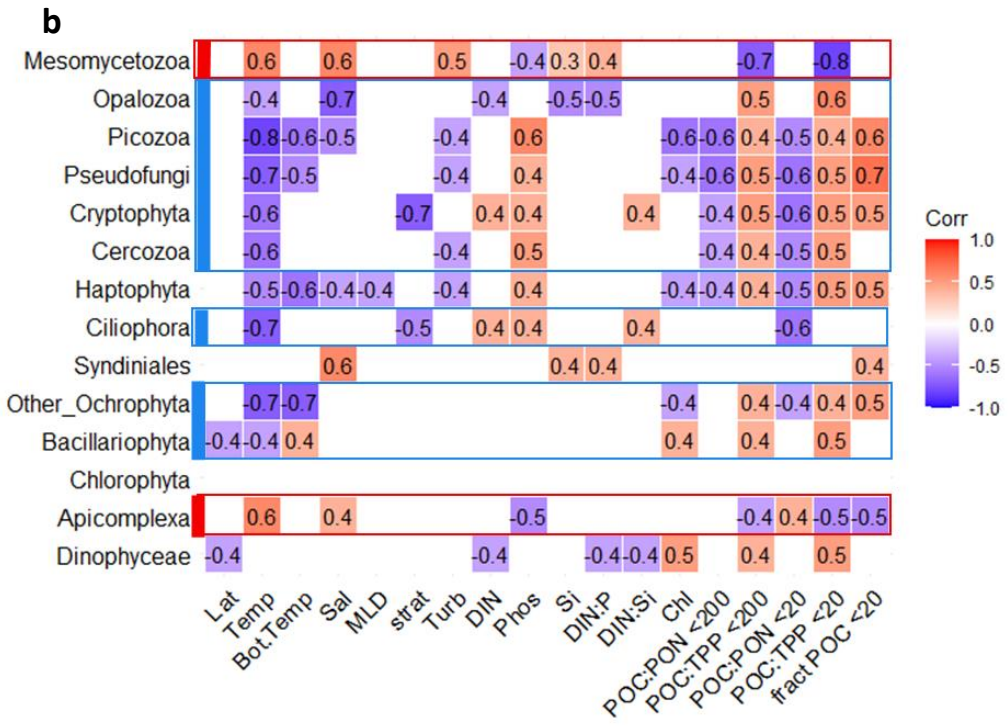
b
Mesomycetozoa 0.6 0.6 0.5 -0.4 0.3 0.4 -0.7 -0.8
Opalozoa -0.4 -0.7 -0.4 -0.5 -0.5 0.5 0.6
Picozoa -0.8 -0.6 -0.5 -0.4 0.6 -0.6 -0.6 0.4 -0.5 0.4 0.6
Pseudofungi -0.7 -0.5 -0.4 0.4 -0.4 -0.6 0.5 -0.6 0.5 0.7
Cryptophyta -0.6 -0.7 0.4 0.4 0.4 -0.4 0.5 -0.6 0.5 0.5
Cercozoa -0.6 -0.4 0.5 -0.4 0.4 -0.5 0.5
Haptophyta -0.5 -0.6 -0.4 -0.4 -0.4 0.4 -0.4 -0.4 0.4 -0.5 0.5 0.5
Ciliophora -0.7 -0.5 0.4 0.4 0.4 -0.6
Syndiniales 0.6 0.4 0.4 0.4
Other_Ochrophyta -0.7 -0.7 -0.4 0.4 -0.4 -0.5 0.4 0.5
Bacillariophyta -0.4 -0.4 0.4 0.4 0.4 0.5
Chlorophyta
Apicomplexa 0.6 0.4 -0.5 -0.4 0.4 -0.5 -0.5
Dinophyceae -0.4 -0.4 -0.4 -0.4 0.5 0.4 0.5
Lat
Temp
Bot.Temp
Sal
MLD
strat
Turb
DIN
Phos
Si
DIN:P
DIN:Si
Chl
POC:PON <200
POC:TPP <200
POC:PON <20
POC:TPP <20
fract POC <20
Corr
1.0
0.5
0.0
-0.5
-1.0

Fig. 3.7. a. Particulate organic carbon (POC) concentrations associated with the 12 most abundant taxonomic Divisions across 2017 (blue) and 2019 (red). Division Dinoflagellata has been divided to show the POC of Classes Dinophyceae and Syndiniales while Division Ochrophyta has been divided to show Bacillariophyta and other Ochrophyta Classes. Note that the x-axis has been transformed with a pseudo-log transformation to more clearly display the range of POC associated with the various Divisions/Classes. Significant differences in POC across years were detected for several Divisions/Classes and are denoted by asterisks next to the group labels (Bootstrap test for differences in the mean; BH adjusted $p < 0.05$). b. Pairwise spearman correlation coefficients among taxonomic group POC and associated environmental variables for all samples in both 2017 and 2019. Only significant correlations ($p < 0.05$; rcorr asymptotic p-values) are shown. The red and blue boxes correspond to taxonomic groups that had significantly higher biomass in 2017 (blue) or 2019 (red).

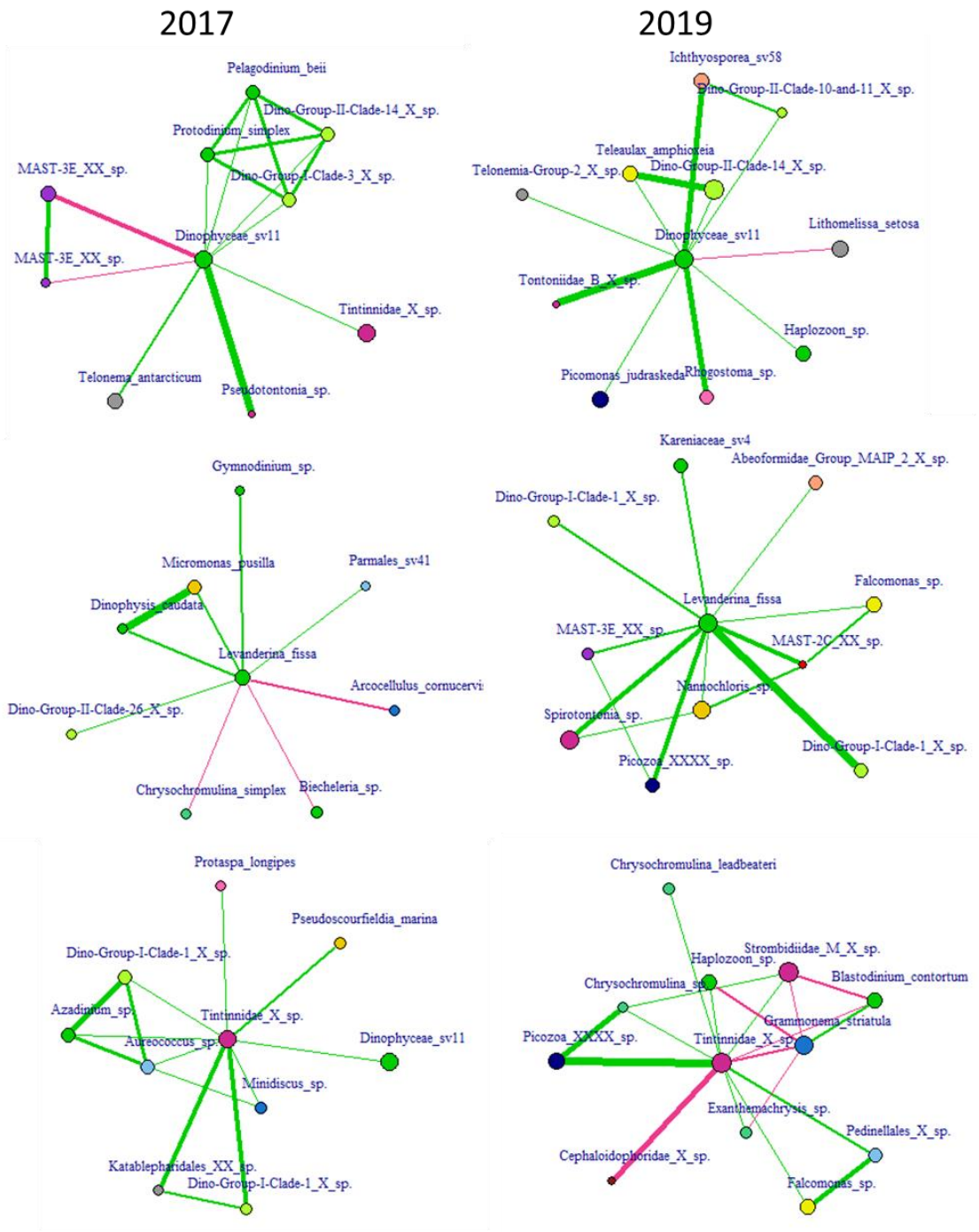

Fig 3.8. Network diagrams for the 3 ‘hub species’ that were consistent across years showing direct positive (green) or negative (red) interactions with other ASVs (colored by taxonomic Division/Class as in Fig 3.5). The size of each node (circle) is proportional to the ASVs degree and the width of the edge (line) is proportional to the interaction strength.

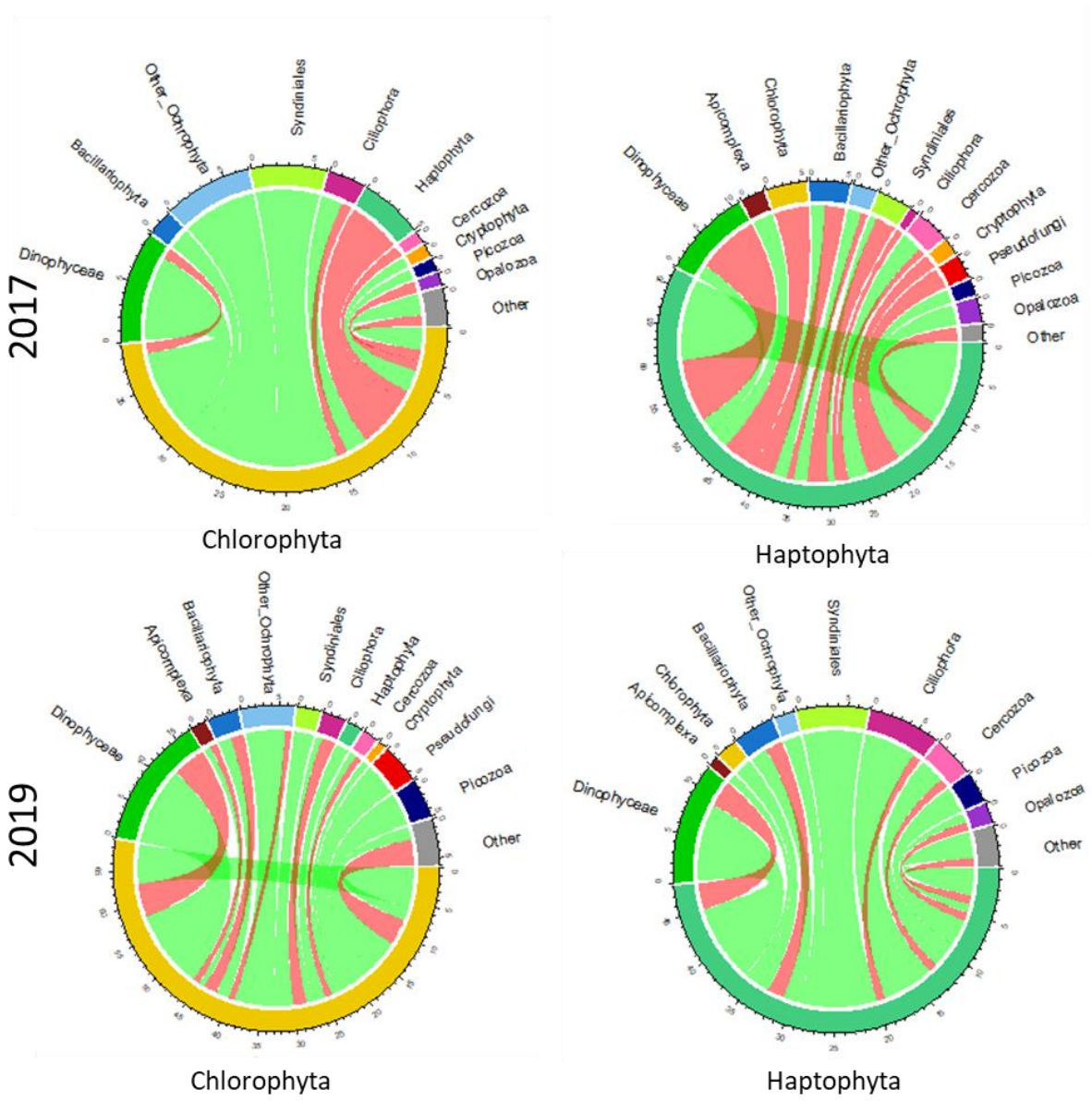

Fig. 3.9. The number of positive (green) or negative (red) interactions between ASVs belonging to the Division Chlorophyta (left) or Haptophyta (right) and ASVs in all other major protist Divisions/Classes in either 2017 (top) or 2019 (bottom). The width of each connection represents the number of interactions between ASVs belonging to the connecting taxonomic groups but it does not show how many distinct ASVs were involved in the interactions. Since total numbers of interactions changed across years, the takeaway from this plot is how the proportions and directions of interactions change between chlorophytes and haptophytes with other taxonomic groups in the two years.

Appendix A

Supplementary material for Chapter 1

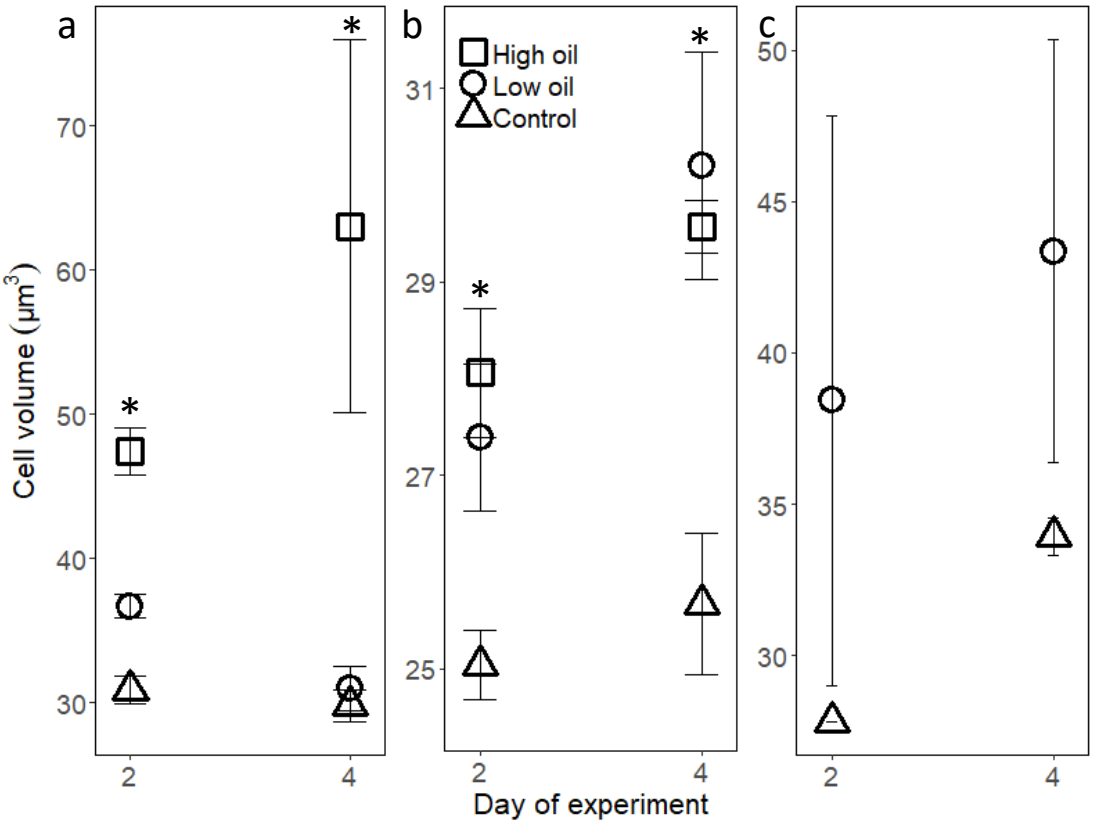

Fig. A1. *E. huxleyi* cell volumes measured during days 2 and 4 of experiments 1 (a), 2 (b), and 4 (c). Asterisks represent significant differences between treatments at each time point ($\alpha = 0.05$). Error bars are ± 1 standard deviation from the mean (n = 3).

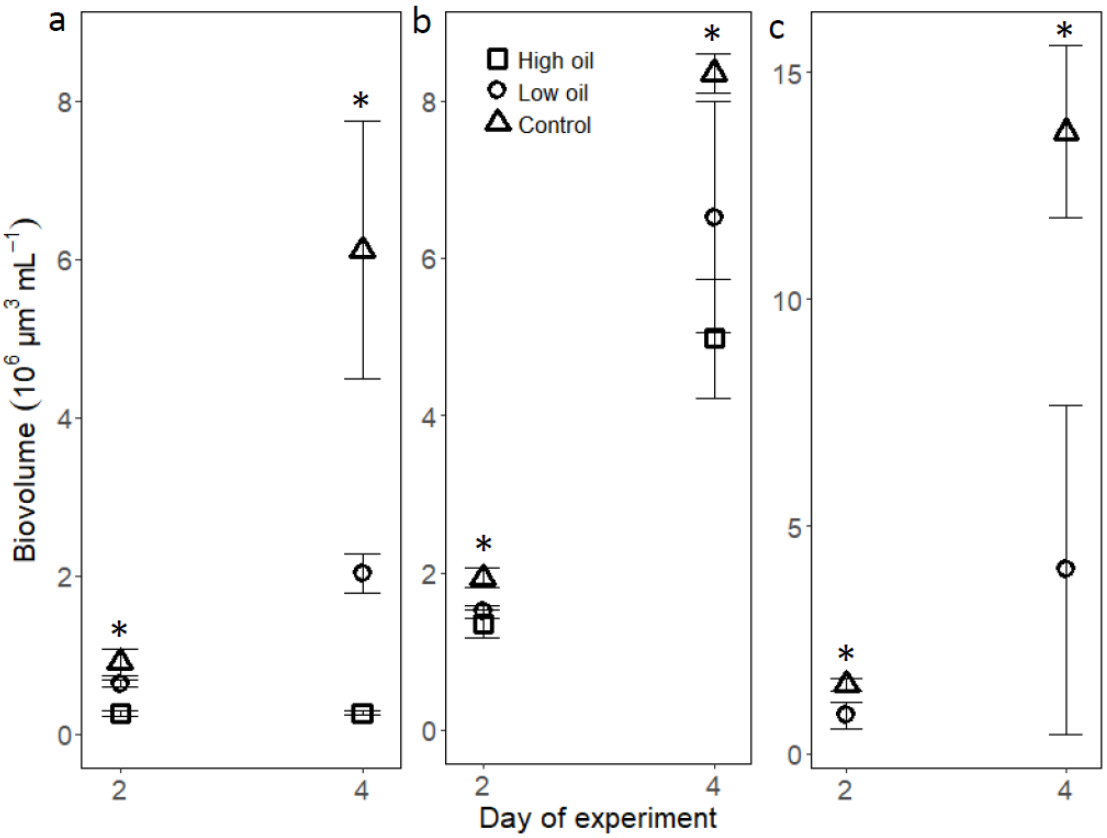

Fig. A2. Biovolume measurements from *E. huxleyi* cultures in experiments 1 (a), 2 (b), and 4 (c). Asterisks represent significant differences between treatments at each time point (α = 0.05). Error bars are ± 1 standard deviation from the mean (n = 3).

Table A1. Mean ± standard deviation (n = 3) of the initial and final measured nutrient concentrations for each independent experiment.

Exp ID	Species (strain)	Growth media	Initial conc 100% WAF (µM) $[NO_3^-+NO_2^-]$ $[PO_4^{3-}]$ $[SiO_4^{4-}]$	Final conc 100% WAF (µM) $[NO_3^-+NO_2^-]$ $[PO_4^{3-}]$ $[SiO_4^{4-}]$	Initial conc 50% WAF (µM) $[NO_3^-+NO_2^-]$ $[PO_4^{3-}]$ $[SiO_4^{4-}]$	Final conc 50% WAF (µM) $[NO_3^-+NO_2^-]$ $[PO_4^{3-}]$ $[SiO_4^{4-}]$	Initial conc control (µM) $[NO_3^-+NO_2^-]$ $[PO_4^{3-}]$ $[SiO_4^{4-}]$	Final conc control (µM) $[NO_3^-+NO_2^-]$ $[PO_4^{3-}]$ $[SiO_4^{4-}]$
1	*E. huxleyi* (150604 A9)	mod f	98.2 ± 0.3 5.48 ± 0.03 NA	96.6 ± 0.9 3.21 ± 0.08 NA	98.1 ± 0.6 5.46 ± 0.03 NA	94.4 ± 0.1 3.0 ± 0.1 NA	97.6 ± 0.6 5.42 ± 0.06 NA	82 ± 4 2.1 ± 0.3 NA
2	*E. huxleyi* (150604 A9)	mod f	95.7 ± 0.5 5.50 ± 0.04 NA	94 ± 9 3.1 ± 0.8 NA	96.1 ± 0.3 5.58 ± 0.07 NA	83 ± 4 2.4 ± 0.1 NA	96.7 ± 0.3 5.6 ± 0.1 NA	60 ± 2 0.8 ± 0.2 NA
3	*P. australis* (HAB 207)	f/2	840 ± 14 30.4 ± 0.2 89.5 ± 0.3	844 ± 1 29.6 ± 0.1 99 ± 1	843 ± 3 30.7 ± 0.1 90.5 ± 0.1	844 ± 2 29.6 ± 0.1 97 ± 1	849 ± 1 30.7 ± 0.2 88 ± 2	837 ± 2 29.2 ± 0.1 86.6 ± 0.4
4	*E. huxleyi* (150604 A9)	f/2	--	--	856 ± 2 34.7 ± 0.3 97 ± 1	860 ± 11 31.5 ± 0.6 105 ± 1	866 ± 5 34.6 ± 0.4 99 ± 3	867 ± 8 29.1 ± 0.4 102 ± 3
4	*P. australis* (HAB 197)	f/2	--	--	868 ± 3 34.9 ± 0.1 96.6 ± 0.6	867 ± 9 31.7 ± 0.3 103.7 ± 0.5	865 ± 5 34.7 ± 0.2 94.7 ± 0.3	812 ± 5 28 ± 1 75 ± 3

Table A2. Statistical analyses (one-way ANOVA + FDR post hoc) of physiological parameters.

Variable	Exp #	Day	SS	Df	F	*p* -Value	FDR *q* -Value		
							H v C	L v C	H v L
Cell volume	1	**2**	**420.4**	**2**	**144.90**	**< 0.001**	**0.0011**	**0.0002**	**0.0002**
		4	**2135.0**	**2**	**18.80**	**0.0026**	**0.0030**	0.8537	**0.0030**
	2	**2**	**15.0**	**2**	**19.60**	**0.0023**	**0.0030**	**0.0053**	0.2376
		4	**36.1**	**2**	**27.12**	**0.0010**	**0.0017**	**0.0015**	0.3801
	4	2	168.5	1	3.80	0.1230			
		4	133.0	1	5.42	0.0804			
Biovolume	1	**2**	**6.3e11**	**2**	**30.63**	**0.0007**	**0.0006**	**0.0196**	**0.0054**
		4	**5.4e13**	**2**	**29.74**	**0.0008**	**0.0009**	**0.0029**	0.0645
	2	**2**	**5.6e11**	**2**	**16.10**	**0.0039**	**0.0048**	**0.0096**	0.2216
		4	**1.7e13**	**2**	**9.35**	**0.0143**	**0.015**	0.0858	0.0961
	4	**2**	**6.8e11**	**1**	**12.67**	**0.0236**			
		4	**1.4e14**	**1**	**16.69**	**0.0150**			
Dissolved DA	3	**1**	**6.2e-5**	**2**	**6.93**	**0.0276**	**0.0320**	**0.0320**	0.8127
		2	6.7e-6	2	1.16	0.3864	---	---	---
		3	**1.7e-5**	**2**	**77.02**	**0.0006**	**0.0009**	**0.0012**	0.1069
		4	**1.4e-4**	**2**	**12.89**	**0.0067**	**0.0101**	**0.0101**	0.5571
	4	**4**	**2.8e-5**	**1**	**53.14**	**0.0019**			
		5	**1.0e-4**	**1**	**54.01**	**0.0018**			

Variable	Exp #	Day	SS	Df	F	*p* -Value	FDR *q* -Value		
							H v C	L v C	H v L
Cellular DA	**3**	2	0.43	2	0.904	0.4538	---	---	---
		4	**33.2**	**2**	**5.42**	**0.0452**	0.053	0.053	0.8027
	4	3	0.37	1	0.24	0.6486			
		5	**9.4**	**1**	**14.01**	**0.0201**			
P. australis **TEP**	**3**	2	15.2	2	1.18	0.3706	---	---	---
		4	**195.2**	**2**	**10.14**	**0.0119**	**0.0153**	**0.0153**	0.7073
	4	**3**	**33.2**	**1**	**16.16**	**0.0159**			
		5	**227.1**	**1**	**37.66**	**0.0036**			
E. huxleyi **TEP**	**1**	**2**	**0.003**	**2**	**8.16**	**0.0194**	**0.0219**	0.2234	0.0596
		4	**0.014**	**2**	**10.26**	**0.0116**	**0.0129**	0.8672	**0.0129**
	2	**2**	**1.8e-11**	**2**	**6.03**	**0.0367**	**0.0408**	0.1281	0.2124
		4	3.8e-8	2	0.06	0.9411	---	---	---
	4	2	0.019	1	3.11	0.1524			
		4	0.007	1	2.06	0.2246			
$CaCO_3$	**1**	**2**	**92.4**	**2**	**62.78**	**<0.0001**	**0.0002**	0.2287	**0.0002**
		4	**246.4**	**2**	**38.72**	**0.0004**	**0.0005**	0.7704	**0.0005**
	2	**2**	**0.126**	**2**	**5.95**	**0.0377**	0.0524	0.0524	0.6437
		4	0.008	2	0.70	0.5351	---	---	---
	4	2	3.36	1	4.63	0.0977			
		4	1.02	1	2.55	0.1854			

Variable	Exp #	Day	SS	Df	F	*p* -Value	FDR *q* -Value		
							H v C	L v C	H v L
Coccolith:cell	1	**2**	**38.2**	**2**	**23.83**	**0.0014**	**0.0141**	**0.0203**	**0.0015**
		4	25.1	2	12.53	0.0612	---	---	---
	2	2	1.15	2	0.83	0.4806	---	---	---
		4	3.2	2	1.62	0.1185	---	---	---
	4	**2**	**41.2**	**1**	**11.79**	**0.0264**			
		4	**17.5**	**1**	**14.75**	**0.0184**			
E. huxleyi bacteria	1	0	4.4e11	2	3.40	0.1028	---	---	---
		1	3.1e11	2	0.62	0.5692	---	---	---
		2	2.3e10	2	1.34	0.3313	---	---	---
		3	7.8e10	2	1.01	0.4193	---	---	---
		4	8.9e10	2	1.31	0.3368	---	---	---
	2	0	1.3e9	2	0.09	0.9110	---	---	---
		1	2.0e8	2	0.11	0.9008	---	---	---
		2	4.7e8	2	0.83	0.4803	---	---	---
		3	1.3e7	2	0.003	0.9969	---	---	---
		4	2.3e9	2	0.59	0.5856	---	---	---
	4	**0**	**1.1e10**	**1**	**20.28**	**0.0108**			
		1	9.8e6	1	0.14	0.7310			
		2	3.8e8	1	0.66	0.4627			
		3	1.3e9	1	3.25	0.1458			
		4	1.3e10	1	2.12	0.2188			

Variable	Exp #	Day	SS	Df	F	*p* -Value	FDR *q* -Value		
							H v C	**L v C**	**H v L**
***P. australis* bacteria**	**3**	0	4.4e11	2	3.40	0.1028	---	---	---
		1	3.1e11	2	0.62	0.5692	---	---	---
		2	2.3e10	2	1.34	0.3313	---	---	---
		3	7.8e10	2	1.01	0.4193	---	---	---
		4	8.9e10	2	1.31	0.3368	---	---	---
	4	0	3.2e8	1	0.45	0.5382			
		2	6713	1	0.00	0.9993			
		3	1.3e10	1	0.59	0.4859			
		4	3.1e9	1	0.15	0.7169			
		5	6.7e8	1	0.01	0.9403			

Results from one-way ANOVA and, when applicable, FDR post hoc tests of treatment (high oil, low oil, control) on physiological parameters. *E. huxleyi* cell volume, *E. huxleyi* biovolume, *P. australis* dissolved domoic acid (DA), *P. australis* cellular DA, *P. australis* transparent exopolymer particles (TEP), *E. huxleyi* TEP, *E. huxleyi* $CaCO_3$, *E. huxleyi* coccolith:cell, *E. huxleyi* bacterial density, *P. australis* bacterial density. Values in **bold** represent significant effects ($p < 0.05$ or $q < 0.05$). Note, experiment 4 has only two treatments (low oil, control) so no post hoc tests are necessary.

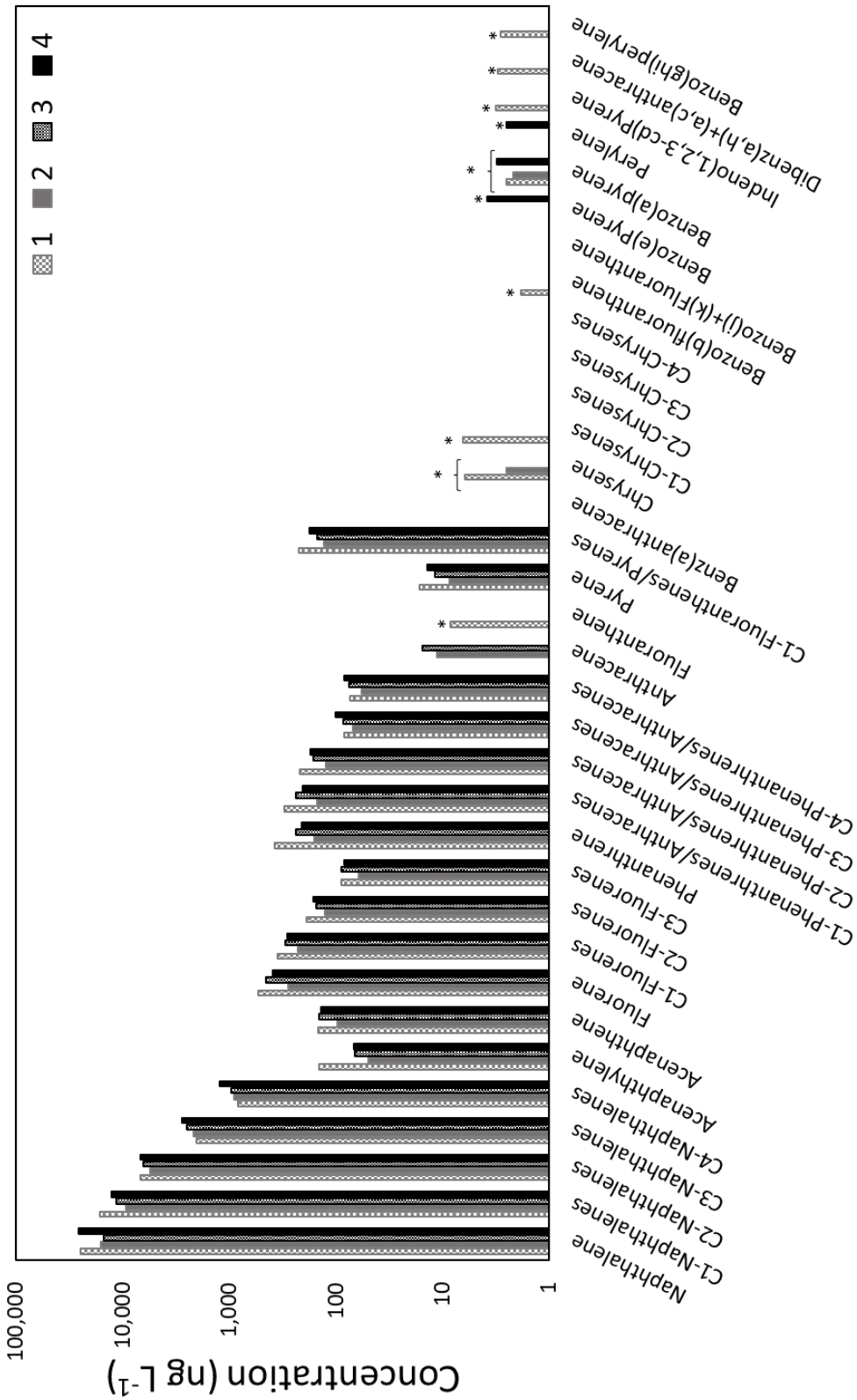

Fig. A3. Concentrations of measured polycyclic aromatic hydrocarbons (PAHs) in the four independent experiments conducted. Asterisks represent PAH concentrations that were below the quantitation limit but above the detection limit of the method and are considered estimated.

Fig. A4. Concentrations of measured saturated hydrocarbons (SHs) in the four independent experiments conducted. Asterisks represent SH concentrations that were below the quantitation limit but above the detection limit of the method and are considered estimated.

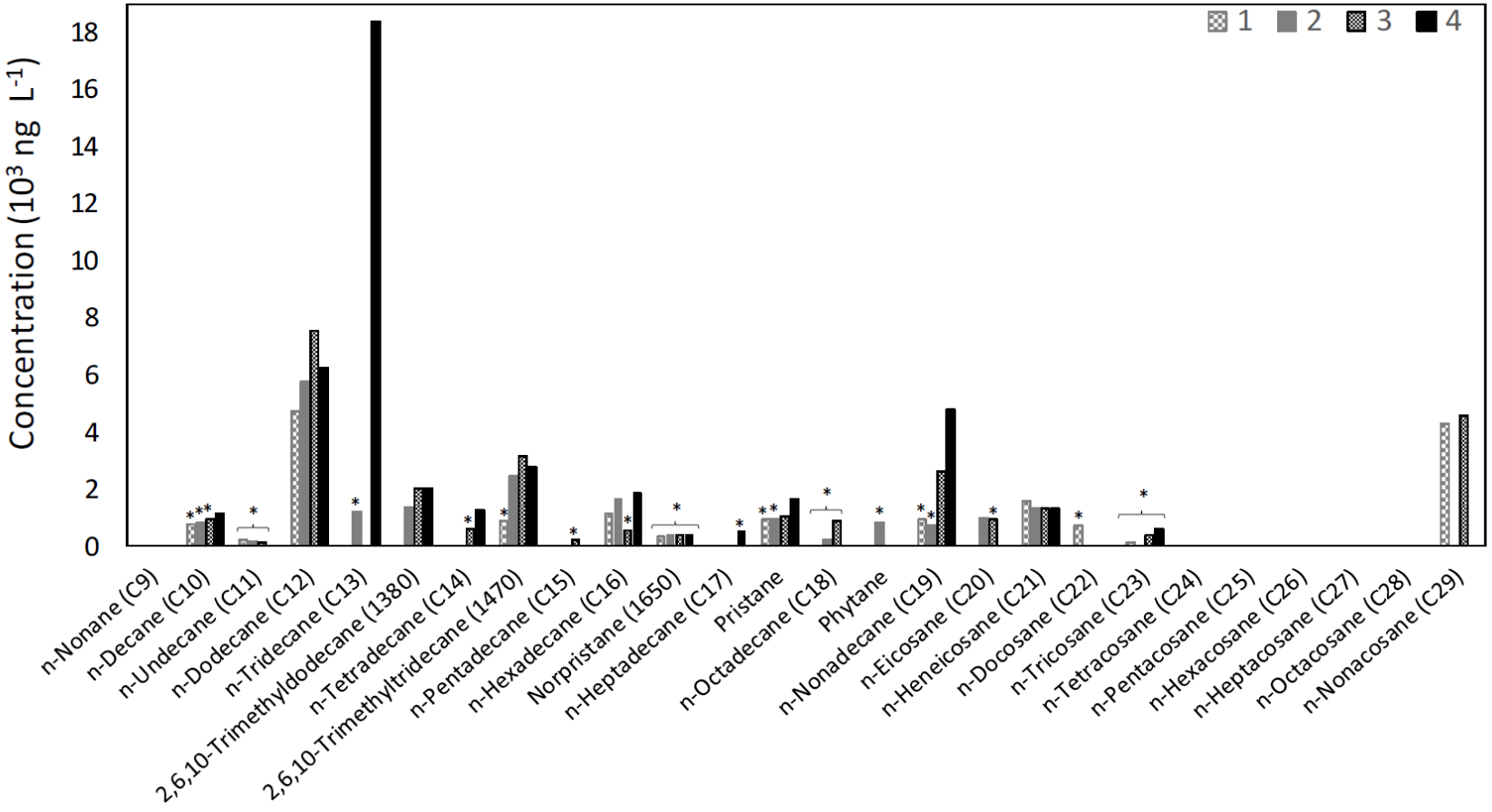

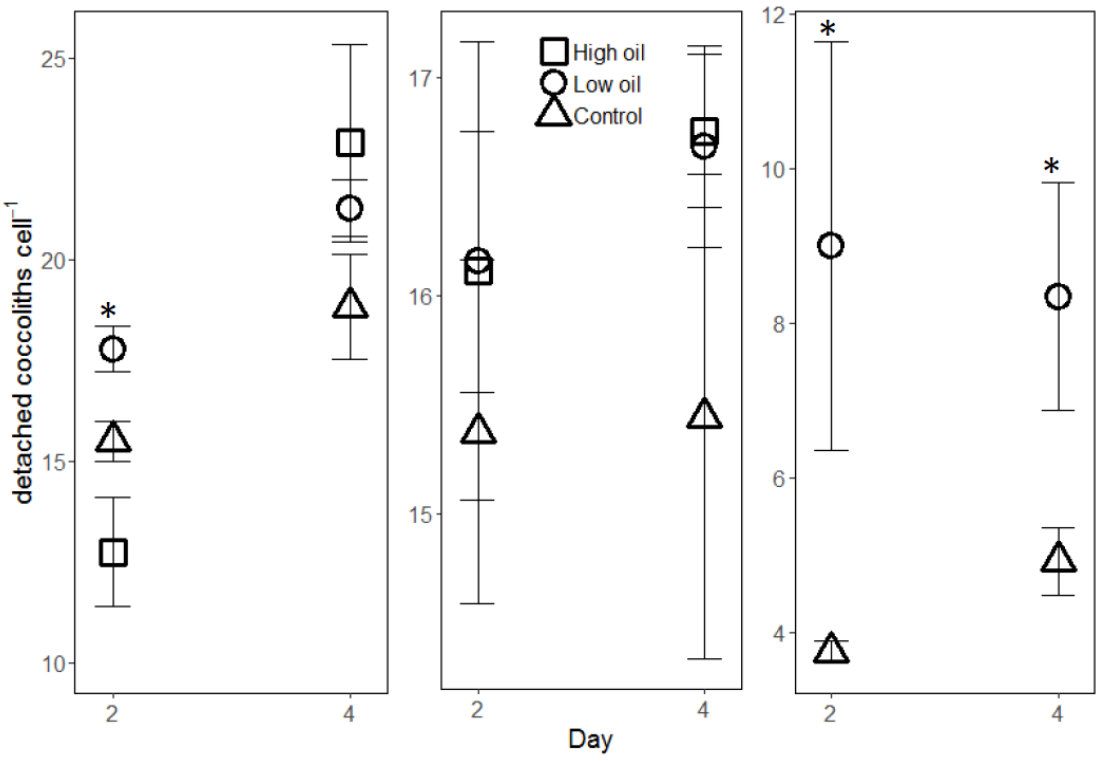

Fig. A5. Detached coccolith to cell ratios in *E. huxleyi* cultures in experiments 1 (a), 2 (b), and 4 (c). Asterisks represent significant differences among treatments at each time point ($\alpha = 0.05$). Error bars are ± 1 standard deviation from the mean (n = 3).

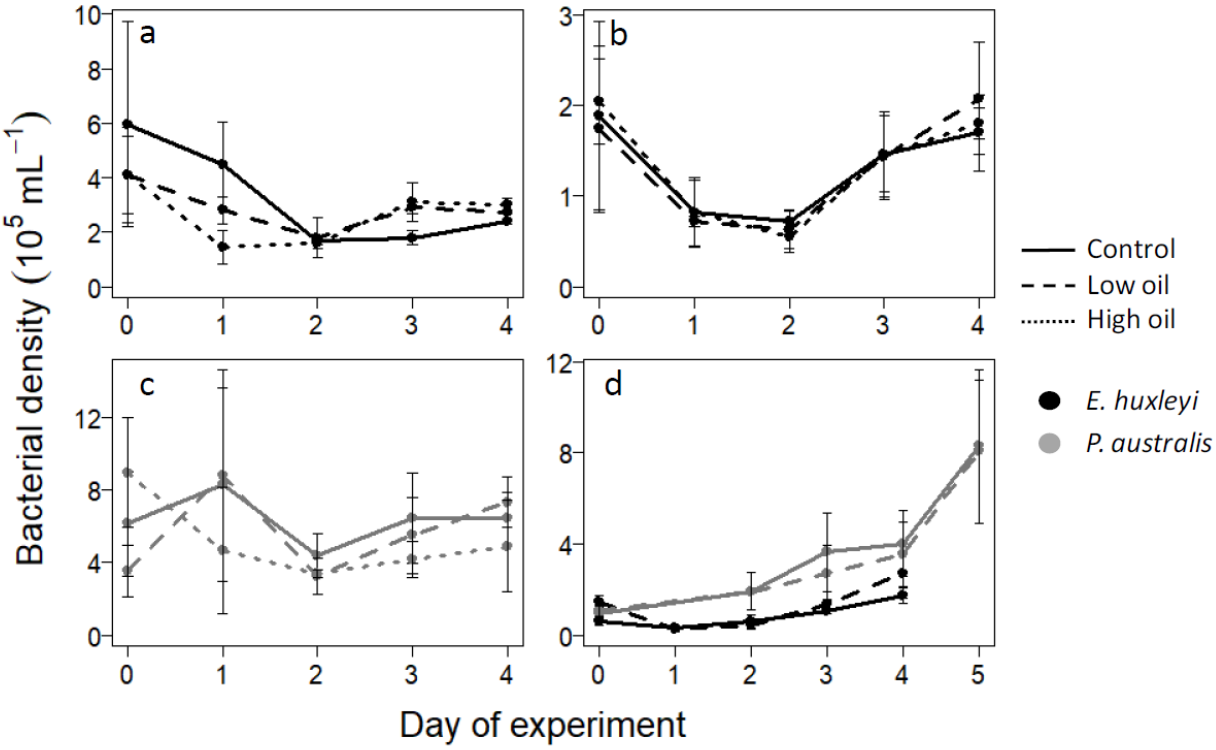

Fig. A6. Bacterial densities measured each day in experiment 1 (a), 2 (b), 3 (c), and 4 (d). Error bars are ± 1 standard deviation from the mean (n = 3).

Appendix B

Supplementary material for Chapter 2

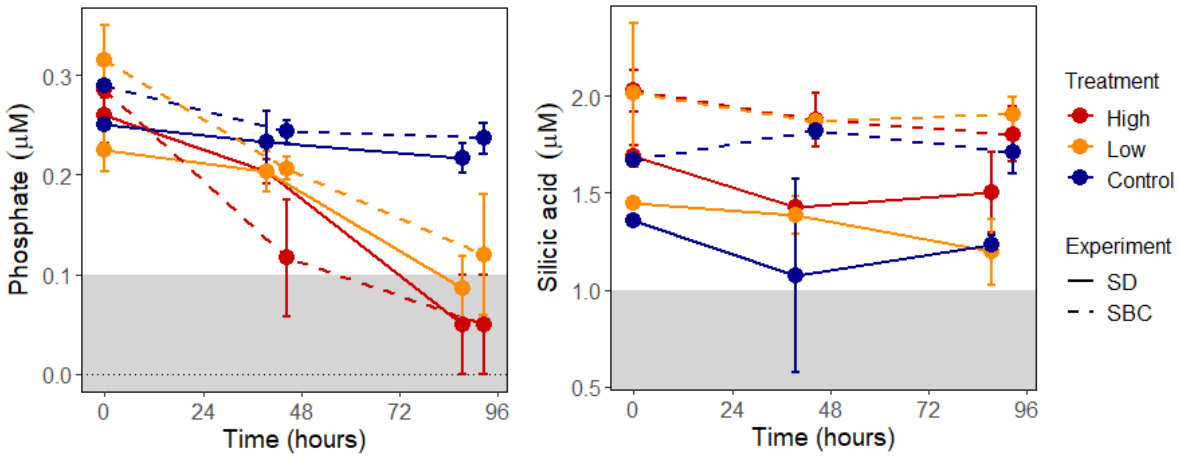

Fig. B1. Mean ± standard deviation (n=3, except at T0) concentrations of phosphate (PO_4^{3-}) and silicic acid ($Si(OH)_4$) over time in the ash and control treatments of both the SD and SBC incubations. At T0, values are from a single sample (control; n=1) or the average of a single sample and estimated concentrations from the leachate (ash treatments; n=2). Values in the shaded area represent measurements below the analytical limit of detection (0.1 µM PO_4^{3-}, 1.0 µM $Si(OH)_4$) and are not considered significantly different from zero.

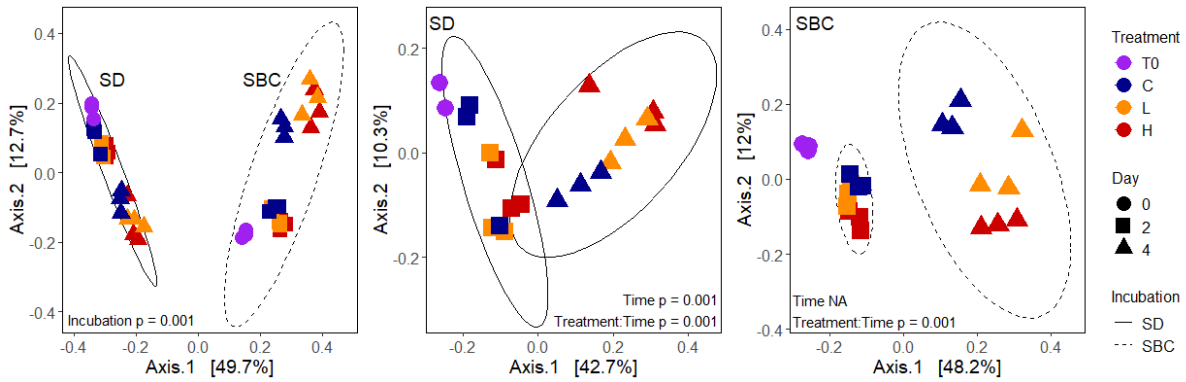

Fig. B2. Principle Coordinates Analysis (PCoA) ordination of Bray-Curtis community dissimilarity based on rarified ASV counts from the SD (solid line) and SBC (dashed line) incubations together and each incubation individually. Initial communities are represented by purple circles (T0) and communities at day 2 (squares) and day 4 (triangles) are colored by treatment: control (C) = blue, low ash (L) = orange, and high ash (H) = red. Ellipses represent 95% normal data ellipses (by incubation (left) or by time point (middle, right)) and p-values give the results of permutational multivariate analysis of variance (PERMANOVA) tests for the effects of incubation, sampling time (Time), or treatment while controlling for sampling time (Treatment:Time) on community dissimilarity. Pairwise comparisons between treatments at days 2 and 4 while controlling for time (pairwise.adonis2 function R) detected differences between both the high and low ash treatments compared to the control in the SD incubation (HvC: p = 0.011, LvC: p = 0.006, HvL: p = 0.147) while only the high ash treatment was significantly different from the control in the SBC incubation (HvC: p = 0.006, HvL: p = 0.003, LvC: p = 0.059).

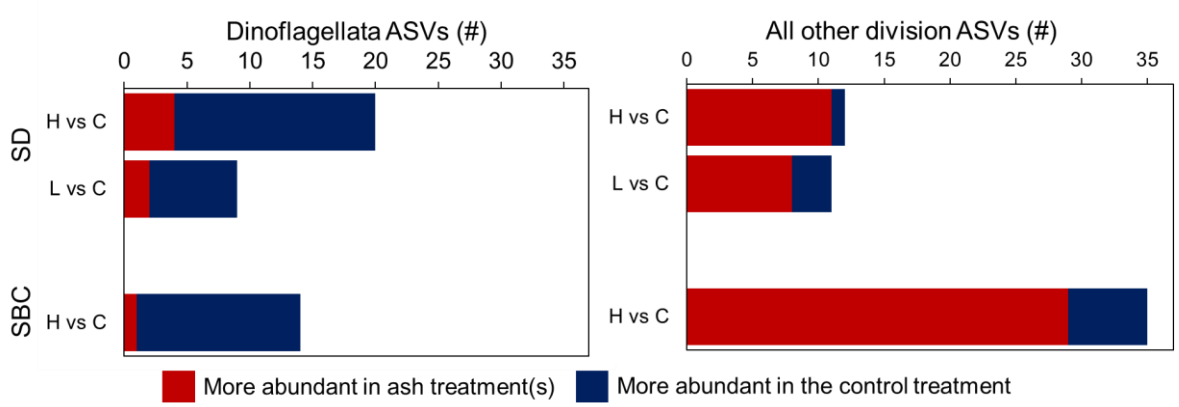

Fig. B3. The number of differentially abundant ASVs between ash (red) and control (blue) treatments separated by Dinoflagellata (right) and all other divisions (left) in both the SD and SBC incubations (DESeq2, padj < 0.05). Red bars represent the number of ASVs that were relatively more abundant in the high (H) or low (L) ash treatments compared to controls (C) while the blue bars represent the number of ASVs that were relatively more abundant in C versus either H or L treatments.

Table B1. Mean ± standard deviation additions of total dissolved nitrogen (TDN), dissolved organic nitrogen (DON), total dissolved phosphorus (TDP), dissolved organic phosphorus (DOP), and dissolved organic carbon (DOC) due to the leaching of ash in seawater. Significant differences between the background seawater and ash leachate as determined from paired t-tests are indicated in bold (* $p<0.05$, ** $p<0.01$, *** $p<0.0001$).

	Addition due to ash (μmol $g_{(ash)}^{-1}$) (n=4)	p-value
TDN	**24 ± 2**	**0.0001****
DON	**9 ± 1**	**0.0006****
TDP	0.1 ± 0.2	0.409
DOP	0.0 ± 0.2	0.540
DOC	**170 ± 10**	**<0.0001*****

Table B2. Mean ± standard deviation additions of iron, zinc, lead, nickel, cadmium, manganese, cobalt, and copper due to the leaching of ash in seawater. Significant differences between the background seawater and ash leachate as determined from paired t-tests are indicated in bold (* $p<0.05$, ** $p<0.01$, *** $p<0.0001$).

	Addition due to ash (nmol $g_{(ash)}^{-1}$) (n=4)	p-value
Iron	**0.3 ± 0.1**	**0.024***
Zinc	-0.2 ± 0.2	0.125
Lead	0.02 ± 0.01	0.107
Nickel	**1.2 ± 0.6**	**0.024***
Cadmium	-0.01 ± 0.02	0.309
Manganese	0.4 ± 0.3	0.104
Cobalt	**0.18 ± 0.03**	**0.001****
Copper	**12 ± 2**	**0.001****

Table B3. Initial inorganic nutrient concentrations measured in seawater collected from offshore San Diego (SD) and the Santa Barbara Channel (SBC) to be used for the incubation experiments. Bold values indicate that the measurement was below the limit of detection (LOD) and have been replaced with ½ LOD. LOD values are 0.2 µM nitrate + nitrite, 0.1 µM nitrite, 0.1 µM phosphate, and 1.0 µM silicic acid.

Experiment	Nitrate (µM)	Nitrite (µM)	Phosphate (µM)	Silicic Acid (µM)	N:P (mol:mol)
SD	0.21	**0.05**	0.25	1.36	1.0
SBC	0.38	**0.05**	0.29	1.67	1.5

Table B4. A subset of putative phototroph ASVs that had higher relative abundance in ash treatments compared to controls (DESeq padj < 0.05) in either the SD or SBC incubation, or both, that were identified to the Genus or Species level and were determined by various sources to be pico- or nano-phytoplankton.

Phototroph Identity (Division)	**Incubation**	**Approximate cell size**	**Source**
Micromonas commoda (Chlorophyta)	both	1-3 µm (pico/nano)	Simon et al. 2017
Micromonas bravo (Chlorophyta)	both	1-3 µm (pico/nano)	Simon et al. 2017
Bathycoccus prasinos (Chlorophyta)	SD	1-2.5 µm (pico/nano)	Eikrem & Throndsen 1990
Ostreococcus tauri (Chlorophyta)	SD	0.5-1.1 µm (pico)	Chretiennot-Dinet et al. 1995
Teleaulax sp. (Cryptophyta)	both	2- 25 µm (nano)	Hill 1991 Laza-Martínez et al. 2012
Triparma mediterranea (Ochrophyta)	SD	1-1.7 µm (pico)	Guillou et al. 1999 Ichinomiya et al. 2016
Skeletonemia menzellii (Ochrophyta)	SBC	2.7-7.0 µm (nano)	Guillard et al. 1974

Data S1. (separate file) Significantly differentially abundant ASVs and their taxonomic and trophic assignments (DESeq2, $p < 0.05$). Each incubation (SD and SBC) was analyzed separately for differences between ash and control treatments (high versus control = HC, low versus control = LC) while controlling for time point across days 2 and 4. (DataS1_DESeq_ASVs.csv)

Appendix C

Supplementary material for Chapter 3

Table C1. Summary table showing the median values (n = 5) and results of pairwise median tests for surface and 50 m dissolved inorganic nitrogen (DIN), phosphate, and silicic acid concentrations and surface and 50 m dissolved inorganic nitrogen to phosphate ratios (N:P) and dissolved inorganic nitrogen to silicic acid ratios (N:Si) around 3 mooring stations (M2, M5, and M8) in 2017 and 2019. All concentrations have units of µmol L-1 and nutrient ratios have units of mol:mol. Darker red colors represent larger values within each set of variables. Adjustment of p-values for multiple testing was conducted using the Benjamini-Hochberg method. *p<0.05, **p<0.01, ***p<0.001

	Mooring	2017	2019	S	Prob ≥ |S-Mean|	BH adjusted p-value	
DIN	M2	**2.42**	**0.03**	0	0.0079	0.0103	*
	M5	**0.81**	**2.75**	5	0.0079	0.0103	*
	M8	**0.09**	**0.77**	5	0.0079	0.0103	*
Phosphate	M2	**0.68**	**0.17**	0	0.0079	0.0103	*
	M5	0.69	0.50	1	0.2063	0.2063	
	M8	**0.75**	**0.31**	0	0.0079	0.0103	*
Silicic acid	M2	9.70	3.40	1	0.2063	0.2063	
	M5	**5.00**	**10.60**	5	0.0079	0.0103	*
	M8	**3.30**	**7.20**	5	0.0079	0.0103	*
N:P	M2	3.70	0.20	1	0.2063	0.2063	
	M5	**1.15**	**5.60**	5	0.0079	0.0103	*
	M8	**0.12**	**2.28**	5	0.0079	0.0103	*
N:Si	M2	**0.24**	**0.01**	0	0.0079	0.0103	*
	M5	**0.16**	**0.26**	5	0.0079	0.0103	*
	M8	**0.03**	**0.10**	5	0.0079	0.0103	*
DIN 50m	M2	**18.48**	**19.85**	5	0.0079	0.0103	*
	M5	**13.27**	**21.94**	5	0.0079	0.0103	*
	M8	**16.09**	**24.39**	5	0.0079	0.0103	*
Phosphate 50m	M2	1.82	1.79	1	0.2063	0.2063	
	M5	**1.67**	**2.00**	5	0.0079	0.0103	*
	M8	**2.12**	**2.38**	5	0.0079	0.0103	*
Silicic acid 50m	M2	**28.60**	**32.70**	5	0.0079	0.0103	*
	M5	**24.40**	**35.40**	5	0.0079	0.0103	*
	M8	38.10	41.60	4	0.2063	0.2063	
N:P 50m	M2	**9.95**	**11.12**	5	0.0079	0.0103	*
	M5	**8.11**	**10.71**	5	0.0079	0.0103	*
	M8	**7.60**	**10.11**	5	0.0079	0.0103	*
N:Si 50m	M2	0.65	0.61	1	0.2063	0.2063	
	M5	0.54	0.62	4	0.2063	0.2063	
	M8	**0.41**	**0.59**	5	0.0079	0.0103	*

Table C2. Summary table showing the mean values, sample sizes (n), and results of Welch's t-tests for chlorophyll-a (Chl), particulate organic carbon (POC), particulate organic nitrogen (PON), and total particulate phosphorus concentrations prefiltered at either 200 µm or 20 um and the ratios of POC to TPP in 200 or 20 µm prefiltered samples from 2017 and 2019. Samples were taken at stations shown in figure 2 with some samples removed in 2017 due to measurements below the limit of detection. Adjustment of p-values for multiple testing was conducted using the Benjamini-Hochberg method. *p<0.05, **p<0.01, ***p<0.001

	2017	n	2019	n	F Ratio	Prob > F	BH adjusted p-val
Chl (µg L^{-1})	1.56	13	2.42	20	9.05	0.0056	0.0115 *
POC <200 µm (µM)	15.4	13	16.7	20	0.61	0.4438	0.4807
PON <200 µm (µM)	3.07	11	2.72	20	1.47	0.2437	0.2880
TPP <200 µm (µM)	0.120	9	0.184	20	22.19	<0.0001	0.0004 ***
POC:TPP <200 µm (mol:mol)	144	9	92	20	58.96	<0.0001	<0.0001 ***
POC <20 µm (µM)	13.2	13	12.5	20	0.21	0.6508	0.6508
PON <20 µm (µM)	2.73	12	2.11	20	4.14	0.0563	0.0732
TPP <20 µm (µM)	0.100	10	0.131	20	7.56	0.0105	0.0171 *
POC:TPP <20 µm (mol:mol)	149	10	99	20	82.34	<0.0001	<0.0001 ***

Table C3. Summary table showing the median values, sample sizes (n), and results of Wilcoxon rank sum tests for particulate organic carbon (POC) to particulate organic nitrogen (PON) ratios prefiltered at either 200 µm or 20 um and the fraction of POC that was less than 20 µm in 2017 and 2019. Samples were taken at stations shown in figure 2 with some samples removed in 2017 due to measurements below the limit of detection. Adjustment of p-values for multiple testing was conducted using the Benjamini-Hochberg method. *p<0.05, **p<0.01, ***p<0.001

	2017	n	2019	n	S	Prob≥|S-Mean|	BH adjusted p-value
POC:PON <200 µm (mol:mol)	5.32	11	5.80	20	120	0.0202	0.0292 *
POC:PON <20 µm (mol:mol)	5.12	12	5.90	20	122	0.0023	0.0075 **
fract POC <20 µm	0.93	13	0.80	20	294	0.0062	0.0115 *

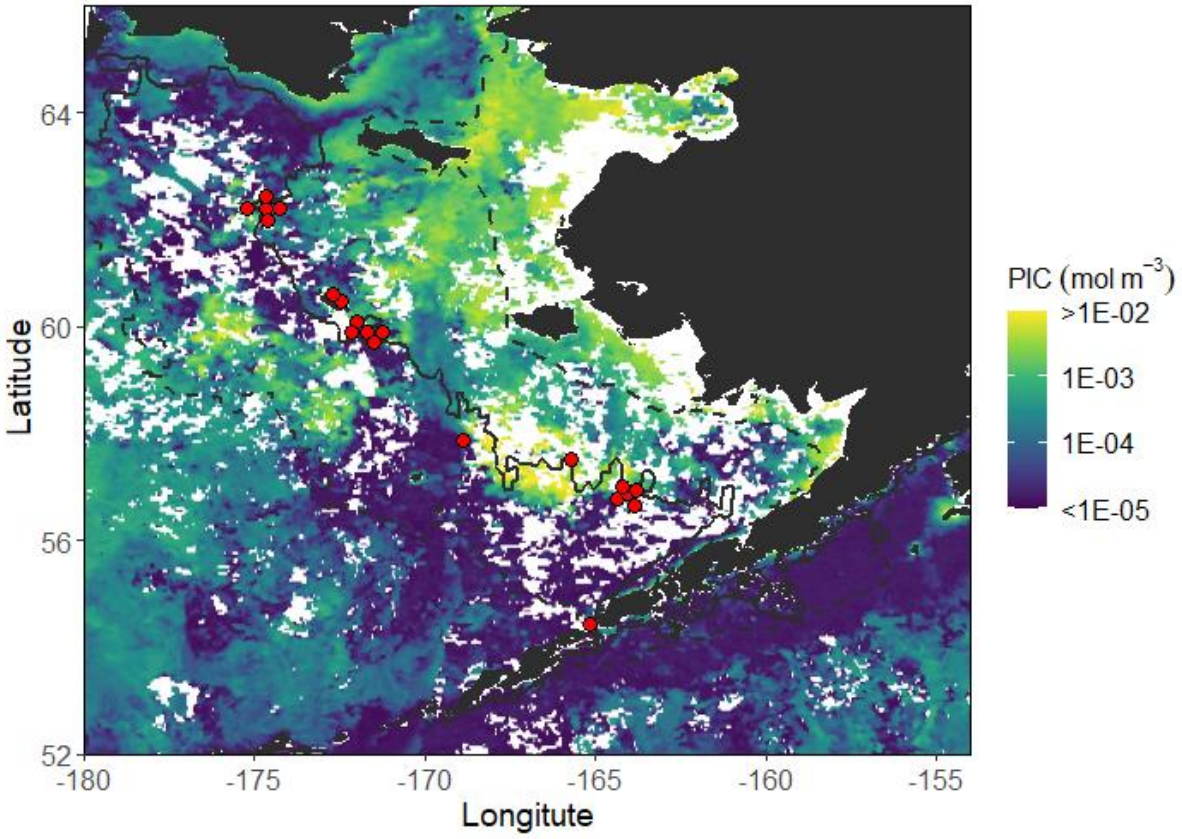

Fig. C1. September 2019 monthly composite satellite image of particulate inorganic carbon (PIC) concentrations (mol m-3) (NASA GSFC 2018) showing a coccolithophore bloom patch around ~ 57 °N and ~167 °W (bright yellow) in which sample “TL6” was taken.

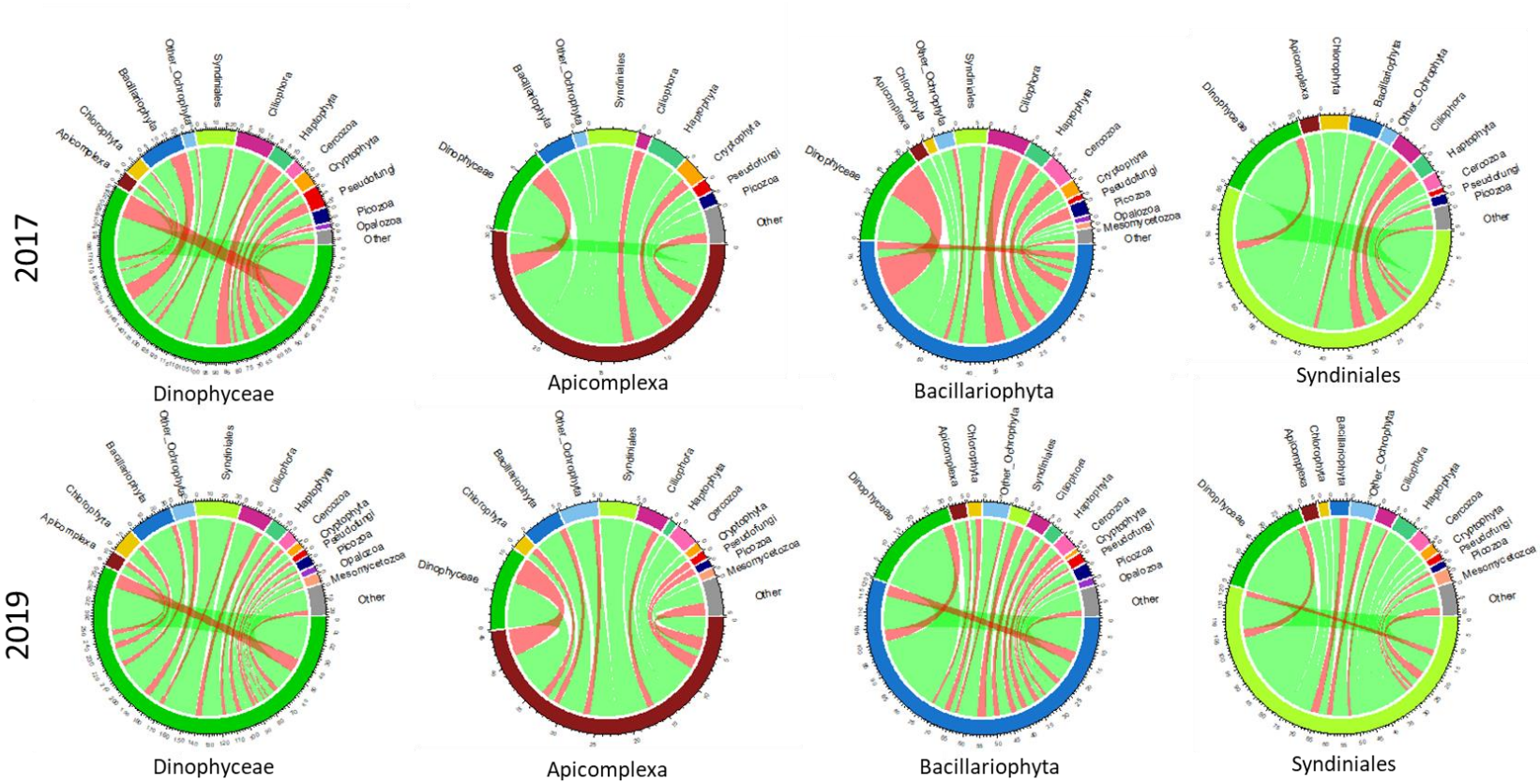

Fig. C2. The number of positive (green) or negative (red) interactions between ASVs belonging to the Divisions/Classes Dinophyceae, Apicomplexa, Bacillariophyta, and Syndiniales (from left to right) and ASVs in all other major protist Divisions/Classes in either 2017 (top) or 2019 (bottom).

Table C4. Taxonomic assignments of the top 15 most connected ASVs in the 2017 network (degree ≥ 8). Bold values represent ASVs that were within the top 15 most connected ASVs in both 2017 and 2019 networks.

	2017 Hubs					
	Division	**Class**	**Order**	**Family**	**Genus**	**Species**
sv9	Dinoflagellata	Dinophyceae	Peridiniales	Heterocapsaceae	Heterocapsa	---
sv11	**Dinoflagellata**	**Dinophyceae**	---	---	---	---
sv50	Picozoa	Picozoa_X	Picozoa_XX	Picozoa_XXX	Picomonas	Picomonas_judraskeda
sv81	**Ciliophora**	**Spirotrichea**	**Tintinnida**	**Tintinnidae**	**Tintinnidae_X**	**Tintinnidae_X_sp.**
sv83	Apicomplexa	Gregarinomorphea	Eugregarinorida	Cephaloidophoridae	Cephaloidophora	Cephaloidophora_communis
sv104	Ciliophora	Spirotrichea	Strombidiida	Strombidiidae_M	Strombidiidae_M_X	Strombidiidae_M_X_sp.
sv120	Haptophyta	Prymnesiophyceae	Prymnesiales	Chrysochromulinaceae	Chrysochromulina	Chrysochromulina_sp.
sv127	Dinoflagellata	Syndiniales	Dino-Group-I	Dino-Group-I-Clade-1	Dino-Group-I-Clade-1_X	Dino-Group-I-Clade-1_X_sp.
sv138	Haptophyta	Prymnesiophyceae	Prymnesiales	Chrysochromulinaceae	Chrysochromulina	Chrysochromulina_leadbeateri
sv160	Telonemia	Telonemia_X	Telonemia_XX	Telonemia-Group-2	Telonema-Group-2	Telonema_antarcticum
sv188	**Dinoflagellata**	**Dinophyceae**	**Gymnodiniales**	**Gymnodiniales_X**	**Levanderina**	**Levanderina_fissa**
sv224	Opalozoa	MAST-3	MAST-3E	MAST-3E_X	MAST-3E_XX	MAST-3E_XX_sp.
sv249	Telonemia	Telonemia_X	Telonemia_XX	Telonemia-Group-2	Telonemia-Group-2_X	Telonemia-Group-2_X_sp.
sv300	Haptophyta	Pavlovophyceae	Pavlovales	Pavlovaceae	Exanthemachrysis	---
sv379	Cercozoa	Filosa-Thecofilose	Cryomonadida	Protaspa-lineage	Protaspa	Protaspa_longipes

Table C5. Taxonomic assignments of the top 15 most connected ASVs in the 2019 network (degree ≥ 10). Bold values represent ASVs that were within the top 15 most connected ASVs in both 2017 and 2019 networks.

	2019 Hubs					
	Division	**Class**	**Order**	**Family**	**Genus**	**Species**
sv6	Ochrophyta	Bacillariophyta	Bacillariophyta_X	Polar-centric-Mediophyceae	Minidiscus	Minidiscus_sp.
sv10	Apicomplexa	Gregarinomorphea	Eugregarinorida	Cephaloidophoridae	Cephaloidophoridae_X	Cephaloidophoridae_X_sp.
sv11	**Dinoflagellata**	**Dinophyceae**	---	---	---	---
sv21	Dinoflagellata	Dinophyceae	Gymnodiniales	Gymnodiniaceae	Gyrodinium	Gyrodinium_fusiforme
sv27	Ochrophyta	Bacillariophyta	Bacillariophyta_X	Polar-centric-Mediophyceae	Thalassiosira	---
sv32	Dinoflagellata	Dinophyceae	Gonyaulacales	Ceratiaceae	Tripos	Tripos_fusus
sv81	**Ciliophora**	**Spirotrichea**	**Tintinnida**	**Tintinnidae**	**Tintinnidae_X**	**Tintinnidae_X_sp.**
sv95	Ciliophora	Spirotrichea	Strombidiida	Strombidiidae_M	Strombidiidae_M_X	Strombidiidae_M_X_sp.
sv99	Ciliophora	Spirotrichea	Strombidiida	Tontoniidae_A	Spirotontonia	---
sv105	Dinoflagellata	Dinophyceae	Dinophyceae_X	Dinophyceae_XX	Dinophyceae_XXX	Dinophyceae_XXX_sp.
sv132	Cercozoa	Filosa-Imbricatea	Filosa-Imbricatea_X	Novel-clade-2	Novel-clade-2_X	Novel-clade-2_X_sp.
sv188	**Dinoflagellata**	**Dinophyceae**	**Gymnodiniales**	**Gymnodiniales_X**	**Levanderina**	**Levanderina_fissa**
sv221	Ochrophyta	Bacillariophyta	Bacillariophyta_X	Araphid-pennate	Grammonema	Grammonema_striatula
sv306	Dinoflagellata	Syndiniales	Dino-Group-II	Dino-Group-II-Clade-14	Dino-Group-II-Clade-14_X	Dino-Group-II-Clade-14_X_sp.
sv338	Dinoflagellata	Syndiniales	Dino-Group-II	Dino-Group-II-Clade-10-and-1	Dino-Group-II-Clade-10-and-11_	Dino-Group-II-Clade-10-and-11_X_sp.